

BULGARIAN CHEMICAL COMMUNICATIONS

2010 Volume 42 / Number 3

*Journal of the Chemical Institutes
of the Bulgarian Academy of Sciences
and of the Union of Chemists in Bulgaria*

Pyrolyzed Co-phtalocyanine as a catalyst for the oxidation of sulphur dioxide

K. Petrov*, Iv. Nikolov, T. Vitanov, D. Uzun, V. Ognjanov¹

Institute of Electrochemistry and Energy Systems, Bulgarian Academy of Sciences (IEES-BAS), G. Bonchev Str., Bl 10, 1113 Sofia Bulgaria;

¹*Institute of Organic Chemistry, Bulgarian Academy of Sciences G. Bonchev Str., Bl 9, 1113 Sofia Bulgaria*

Received March 2, 2010, Revised March 17, 2010

The catalytic activity of pyrolyzed Co-phtalocyanine, deposited onto active carbon "Norit-NK" for oxydation of sulphur dioxide in sulphuric acid media was investigated. The optimum phtalocyanine content and the best pyrolysis temperature of this catalyst were determined. It was shown that gas diffusion electrodes (GDE), catalyzed with Co-Phtalocyanine, pyrolyzed at 700°C ensure 500 hours operation at current density of 60 mA.cm⁻² with increase of polarization approximately of 50 mV.

Keywords: sulphur dioxide, pyrolyzed Co-phtalocyanine

INTRODUCTION

Sulphur dioxide oxidation has been used for production of hydrogen and sulphuric acid under very favourable energy saving conditions [1]. An original approach was proposed in our laboratory (IEES) [2]. This approach is based on use of GDE which utilize gases containing SO₂. In such a way the production of hydrogen can be combined with purification of waste gases form SO₂. GDE developed in IEES are catalyzed with pyrolyzed metal chelate complexes: dibenzo-cobalt-tetra-azaanulene (CoTAA), cobalt tetra-methoxy-phenyl-porphirine (CoTMPP), and modified active carbon (MC) [3, 4]. Although the initial characteristics were quite promising, the long-term tests of electrodes modified with the above catalysts, revealed that their activity decreased rapidly. On the other hand, the synthesis of these chelate complexes proved to be rather expensive and labour-consuming. These shortcomings stimulated the research to find a catalyst which is more stable in sulphuric acid solutions, easily available, and cost-efficient.

Literature data provide evidence that the metal complexes of phtalocyanines and their pyrolyzed products display catalytic activity toward several electrochemical processes, including the oxidation of SO₂ [5-11]. According to Bagotski et al [6], the activity of metal chelate complexes and their pyrolysis products at 800°C with respect to this reaction diminish in the following order: CoTAA >> CoTMPP > CoTPP > CoPc (Co-phtalocyanine).

Probably this is the reason why the last compound in this row, as well as its pyrolytic derivatives, has attracted less attention in the investigations in this field. Since CoPc is more available and less expensive [12, 13] than CoTAA and CoTMPP, we have decided to study the behaviour of GDE catalyzed with pyrolyzed products of this compound with respect to the oxidation of SO₂.

EXPERIMENTAL

The catalyst is prepared by heating phtalodinitrile together with cobalt nitrate according to a method described in [14]. The product is dissolved in 96 %wt. H₂SO₄, followed by precipitation onto active carbon "Norit-NK" (specific surface 650 m².g⁻¹, according to BET), and cooling the solution in an ice-water mixture [5]. The next steps are drying and subjecting to pyrolysis in argon atmosphere for 5 hours at temperatures within the range between 600 and 900°C. Thus active carbon, catalyzed with 1 – 20 % wt. pyrolyzed phtalocyanine, is obtained, and further on, used for the preparation of GDE. The later are of double-layer type: a porous gas supplying layer and a porous catalytic layer. The binder is PTFE which was previously precipitated upon acetylene black [15].

The electrochemical characteristics of the electrodes are determined by tracing the stationery galvanostatic voltage-current relationships (E-i), and by long term tests. The measurements are carried out in a specially designed electrolytic cell, comprising a cathode, prepared from tungsten carbide, PTFE and Na₂SO₄ [16]. 4.5 N H₂SO₄ is used as electrolyte. The

* To whom all correspondence should be sent:
E-mail: kpetrov@bas.bg

ΔE - i curves are traced under the condition that the electrodes are supplied either with pure SO_2 or with gas mixture of $\text{SO}_2 + \text{Ar}$. The gases are fed to the gas supplying layer without overpressure. The potential of the electrodes is recorded vs. $\text{Hg}/\text{Hg}_2\text{SO}_4$ reference, recalculating data vs. NHE in the same electrolyte. The results from these measurements are used for plotting of the E - i curves in normal and semi-logarithmic coordinates as well as the ΔE - i relationships. ΔE is defined as difference between the stationary potentials at identical current densities from polarization curves of the same electrode, traced in pure SO_2 (E_{SO_2}), and in gas mixture, $\text{Ar} + 20\% \text{ vol. SO}_2$ ($E_{\text{Ar}+\text{SO}_2}$), so $\Delta E = E_{\text{SO}_2} - E_{\text{Ar}+\text{SO}_2}$. The former are used for evaluation of the activity of the catalyst, while the later provide a criterion for the transport hindrances in the electrodes [17].

RESULTS AND DISCUSSION

The composition of the catalyst is optimized with respect to the parameters which determine its activity, the amount of CoPc and the temperature of pyrolysis [5, 18]. The voltage – current relationships of a set of electrodes, containing different quantities of CoPc are shown on Fig. 1. It can be noted that the characteristics of the electrode, containing 20 % wt. pyrolyzed catalyst, are practically identical to that of electrodes catalyzed with 10 % wt. This finding provides us with a foundation to continue further studies with electrodes prepared from “Norit-NK” + 10 % wt. pyrolyzed CoPc.

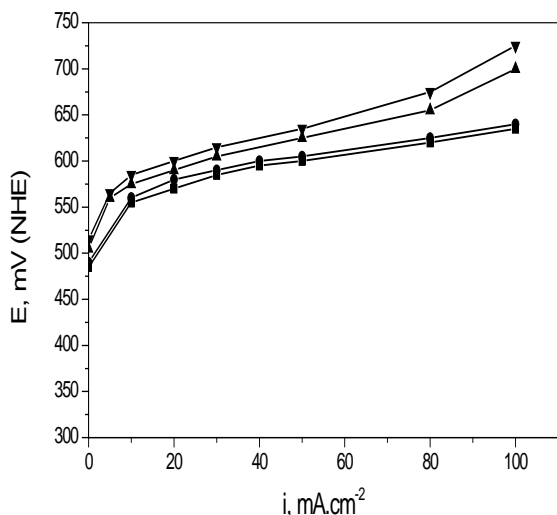


Fig. 1. Voltage – current characteristics of the GDE catalyzed with different amounts of CoPc, pyrolyzed at 900°C: (■) - 20mg/cm² catalyst “NORIT NK” + 1 wt. % CoPc; (◆) - 20 mg.cm⁻² catalyst “NORIT NK” + 5 wt. % CoPc; (▲) - 20 mg.cm⁻² catalyst “NORIT NK” + 10 wt. % CoPc; (▼) - 20 mg.cm⁻² catalyst “NORIT NK” + 20 wt. % CoPc ; 4.5 N H₂SO₄, T = 20°C.

The dependence of catalytic activity on pyrolysis temperature is studied with electrodes activated with the above mentioned amount of CoPc within the temperature range of $t^\circ = 600\text{--}900^\circ\text{C}$. The polarization curves of a set of electrodes with catalyst pyrolyzed at different temperatures are shown in Fig.2. The catalyst treated at 600°C is partially pyrolyzed [5] which explains the higher polarization of these electrodes. The best characteristics show the electrodes with CoPc pyrolyzed at 700°C in comparison with those, treated at higher temperatures. Similar dependence has been established for reduction of oxygen in sulphuric acid solutions [5]. In this case also, carbon catalysed with

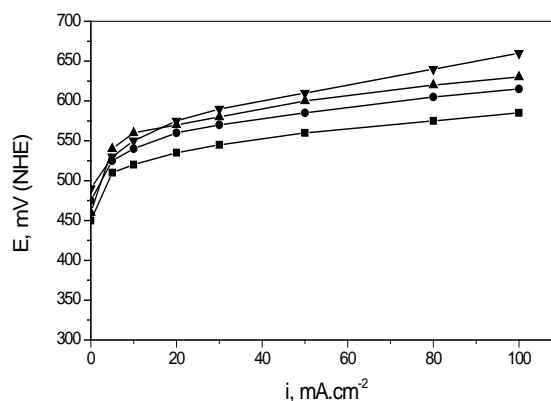


Fig. 2. Voltage – current characteristics of the GDE catalyzed with 20 mg.cm⁻² catalyst “NORIT NK” + 10 wt. % CoPc, pyrolyzed at different temperatures: (■) - $T_{\text{pyr.}} = 600^\circ\text{C}$; (●) - $T_{\text{pyr.}} = 700^\circ\text{C}$; (▲) - $T_{\text{pyr.}} = 800^\circ\text{C}$; (▼) - $T_{\text{pyr.}} = 900^\circ\text{C}$; 4.5 N H₂SO₄, T = 20°C.

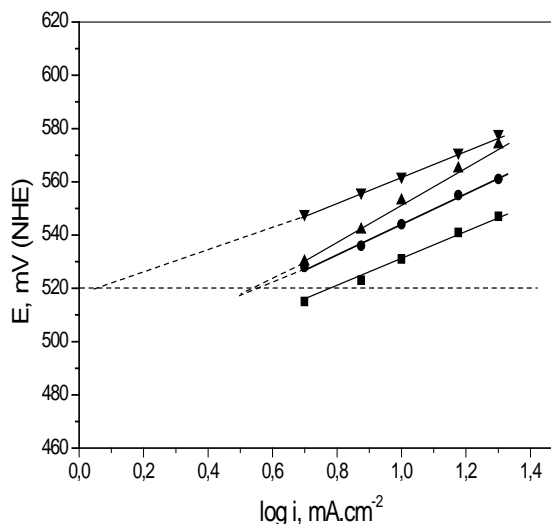


Fig. 3. Voltage – current characteristics in semi-logarithmic coordinates at low current densities of the electrodes in Fig. 2.

CoPc pyrolyzed at 700°C displays enhanced activity. The reasons for this temperature phenomenon could be two: a change in the activity of the catalyst

itself and/or alteration of the transport hindrances within the complex “Norit-NK” + pyrolyzed CoPc due to the different distribution of the catalyst in the pores of the carbon carrier. The effect exerted by each of these factors is estimated from the initial polarization curves at low current densities (up to $i = 20 \text{ mA}\cdot\text{cm}^{-2}$) and the ΔE - i relationships.

Fig. 3 shows the initial polarization curves. The Tafel plots provide evidence that transport hindrances in the electrodes are of minor importance within this current density range. The slopes of the straight lines are approximately 50 mV/dec in the case when CoPc is pyrolyzed at $t^{\circ}=700^{\circ}\text{C}$ or more elevated temperature. When CoPc is thermally treated at $t^{\circ} = 600^{\circ}\text{C}$ (temperature at which the pyrolysis of the chelate complex is not complete [5]) the Tafel slope is 75 mV/dec. Higher values of the Tafel slope (90–100 mV/dec) have been reported by Tarasevich and Radyushkina [7] for CoPc with no thermal treatment, deposited onto pyrographite.

The segments, cut by the Tafel plots, from the abscises at a given potential within the region of small polarizations ($E = +500 \text{ mV NHE}$) are a criterion for the activity of the complex “Norit-NK” + pyrolyzed CoPc in a real GDE [19]. Fig. 3 shows that the highest activity is reached with electrodes containing a catalyst pyrolyzed at $t^{\circ}=700^{\circ}\text{C}$. Higher pyrolysis temperature leads to reduced activity. The data are not relevant to the evaluation of the activity of the electrode catalyzed with CoPc pyrolyzed at $t^{\circ}=600^{\circ}\text{C}$ since the respective slope is different from the rest.

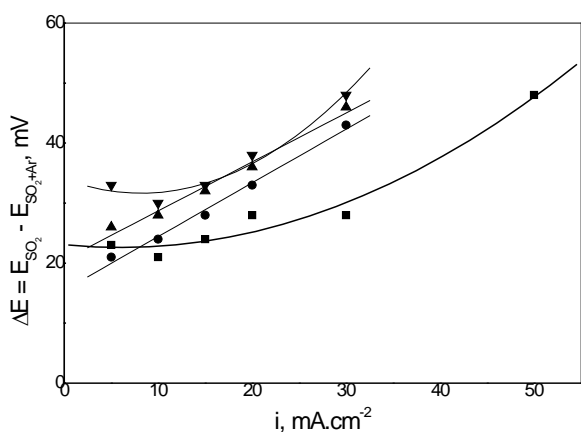


Fig. 4. ΔE - i curves of the electrodes in Fig. 2.

Fig. 4 shows the ΔE - i relationships. It can be noted that at all current densities the ΔE , hence the transport hindrances, in the electrode catalyzed with CoPc pyrolyzed at $t^{\circ}=700^{\circ}\text{C}$ are the least. Electrodes containing partially pyrolyzed catalyst ($t^{\circ}= 600^{\circ}\text{C}$) or thermally treated at temperatures exceeding 700°C display substantially more

pronounced hindrances. These variations probably are due to the different distribution of the pyrolyzed catalyst in the pores of the carbon carrier, respectively various structures and different hindrance patterns.

It can be concluded on the basis of the experimental results (Fig. 3 and 4) that the good characteristics of the electrodes catalyzed with CoPc pyrolyzed at $t^{\circ} = 700^{\circ}\text{C}$ are due to both: the high activity of the “NORIT NK” – pyrolyzed catalyst complex and the reduced transport hindrances for SO_2 in it.

Long term tests were carried out, using electrodes catalyzed with CoPc pyrolyzed at 700°C and 900°C . Fig. 5 shows the different pattern for the increase of polarization with time. The electrodes catalyzed with CoPc pyrolyzed at 700°C shows a deterioration of its characteristics during the initial 100 – 150 hours and further on the changes are slight. The other type of electrodes displays a continuous increase of polarization and at the end of the 500 hour test-run it reaches 200 mV, rendering them practically unusable. The periodically monitored voltage – current curves at low current densities and the ΔE – i relationship of these electrodes offer a possibility to explain the reasons which have led to the observed increase of polarization. Fig. 6 presents the initial and final Tafel curves for both types of electrodes. It can be noted that the segments cut on the abscissa for each type are slightly affected, hence the activity of the catalyst pyrolyzed at 700°C and 900°C shows only

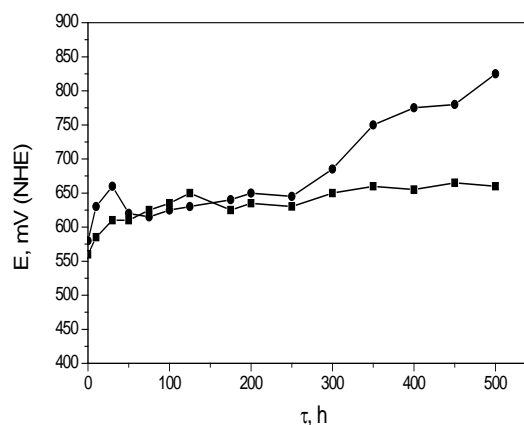


Fig. 5. Long term tests of GDE catalyzed with $20 \text{ mg}\cdot\text{cm}^{-2}$ catalyst “NORIT NK” + 10 wt. % CoPc, pyrolyzed at different temperatures: (■) - $T_{\text{pyr.}} = 700^{\circ}\text{C}$; (●) - $T_{\text{pyr.}} = 900^{\circ}\text{C}$; $i = 60 \text{ mg}\cdot\text{cm}^{-2}$, $4.5 \text{ N H}_2\text{SO}_4$, $T = 20^{\circ}\text{C}$

minor changes following 500 hour test operation at $60 \text{ mA}\cdot\text{cm}^{-2}$. The comparison of the ΔE - i relationship, however, provides evidence that the transport hindrances in both electrode types have

increased (Fig. 7). A close look at the figure reveals that: (i) for the electrode with the catalyst pyrolyzed at 700°C this increase is more substantial during the initial 125 hours; (ii) at the end of the 500 hour test the transport hindrances in electrodes with catalyst pyrolyzed at 900°C are more pronounced.

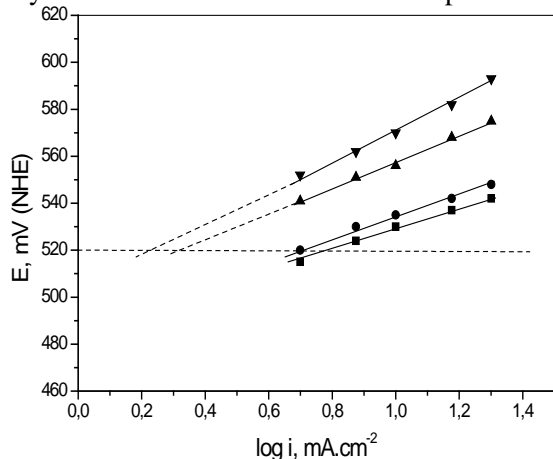


Fig. 6. Voltage – current characteristics in semi – logarithmic coordinates at low current densities of the electrodes subjected to long term tests: 1 -initial ; 2 - after 500 hours operation at $i = 60 \text{ mg.cm}^{-2}$.

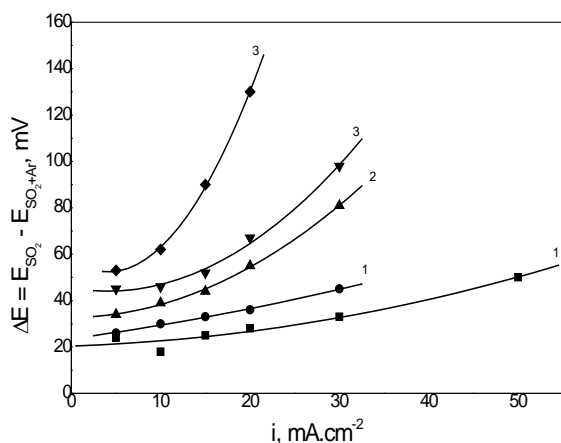


Fig. 7. $\Delta E - i$ curves of the electrodes subjected to long term tests: 1- initial; 2 - after 125 hours operation at $i = 60 \text{ mA.cm}^{-2}$; 3- after 500 hours operation at $i = 60 \text{ mg.cm}^{-2}$.

These experimental results explain the electrode behaviour during the long term tests. The conclusion, based on such results, is that the most suitable pyrolysis temperature for CoPc, used for preparation of a catalyst for the oxidation of sulphur dioxide, is $t^0 = 700^\circ\text{C}$.

A comparison with our previously reported results [2] shows that the long term characteristics of GDE, catalyzed with CoPc, pyrolyzed at 700°C, are superior to those of GDE, containing CoTAA and CoTMPP.

CONCLUSION

The investigated GDE, catalyzed with CoPc pyrolyzed at $t^0 = 700^\circ\text{C}$ provide adequate perfor-

mance and can be used as anodes for oxidation of sulphur dioxide in sulphuric acid solutions.

NOMENCLATURE

CoTAA – Dibenzo-cobalt-tetra-azaanulene
 CoTMPP – Cobalt tetra-methoxy-phenyl-porphirine
 MC – Modified active carbon
 CoTPP – Cobalt-tetra-phenyl-porphirine
 CoPc – Cobalt-phthalocyanine

REFERENCES

1. W. Lu and R. L. Ammon, *J. Electrochem. Soc.*, **127**, 2610 (1980).
2. K. 2. K.Petrov, I. Nikolov and T. Vitanov, *Int. J. Hydrogen Energy*, **9**, 901 (1984).
3. H. Hiller, H. Guthke and F. Beck, *D.O.S.*, **204**, 6334 (1970).
4. A.D. Adler, F. R. Longo, I. D. Finarelli, *J. Org. Chem.*, **32**, 476 (1967).
5. J. A. R. Van. Veen, G. Visser, *Electrochimica Acta*, **24**, 921 (1979).
6. М. Р. Тарасевич, К. А. Радюшкина, В. С. Боготцкий, В кн. Всесоюзная конференция по механизму металлических реакций. Тезисы докладов. М., Наука, т. 2. (1978) 265.
7. М. Р. Тарасевич, К. А. Радюшкина, Катализ и электрокатализ металлопорфиринам. М., Наука, (1982)
8. К. А. Радюшкина, М. Р. Тарасевич, *Электрохимия*, **22** (1986) 1155.
9. Q. Jiang, H. Ketamo, A.J. Niskanen, J. Suomi, M. Håkansson, S. Kulmala, *Electrochimica Acta*, **51**, 3332 (2006).
10. E.-G. Jäger, M. Rudolph, *J. Electroanal. Chem.*, **434**, 1 (1997).
11. Uehara, M. Kasuno, T. Okugaki, Y. Kitatsuji, O. Shirai, Z. Yoshida, S. Kihara, *J. Electroanal. Chem.*, **604**, 115 (2007).
12. M. Håkansson, Q. Jiang, M. Helin, M. Putkonen, A.J. Niskanen, S. Pahlberg, T. Ala-Kleme, L. Heikkilä, J. Suomi, S. Kulmala, *Electrochimica Acta*, **51**, 289 (2005).
13. S. Buchmann, H.A. Mayer, B. Speiser, M. Seiler, H. Bertagnolli, S. Steinbrecher, E. Plies, *Electrochimica Acta*, **46**, 3207 (2001).
14. F. Beck, W. Dammert, J. Heiss, H. Hiller, R. Rolster. *Z. Naturforsch.* **28a**, 1009 (1973)
15. E. Budevski, I. Iliev, S. Gamburgzev, A. Kaisheva, E. Vakanova, I. Mikhovski, *Commun. Dept. Chem. Bulg. Acad. Sci.*, **7**, 223 (1974).
16. Nikolov, K. Petrov, T. Vitanov, A. Gushev, *Int. J. Hydrogen Energy*, **8**, 437 (1983).
17. Iliev, S. Gamburgzev, A. Kaisheva, I. Mrha, *J. Appl. Electrochem.*, **5** 291 (1975).
18. Iliev, S. Gamburgzev, A. Kaisheva, *J. Power Sources*, **17**, 345 (1986).
19. A. Kaisheva, I. Iliev, S. Gamburgzev, *J. Power Sources*, **13**, 181 (1984).

ПИРОЛИЗИРАН СО-ФТАЛОЦИАНИН КАТО КАТАЛИЗАТОР ЗА ОКИСЛЕНИЕТО НА СЕРЕН ДИОКСИД

К. Петров, Ив. Николов, Т. Витанов, Д. Узун, В. Огнянов¹

Институт по електрохимия и енергийни системи, Българска академия на науките, ул. Акад. Г. Бончев, бл. 10, 1113 София, България

¹*Институт по органична химия с Център по фитохимия, Българска академия на науките, ул. Акад. Г. Бончев, бл. 9, 1113 София, България*

Постъпила на 2 март, 2010 г. Преработена на 17 март, 2010 г.

Изследвана е каталитичната активност на пиролизен Со-фталоцианин, отложен върху активен въглен “Norit-NK” за окисляването на серен диоксид в сярно-кисела среда. Определени са оптималното съдържание на Со-фталоцианин и най-подходящата температура за катализатора. Показано е, че газово-дифузионите електроди с катализатор от Со-фталоцианин, получен при пиролиза при 700°C осигуряват работа в продължение на 500 часа при плътност на тока 60 mA.cm⁻² и свръхнапрежение около 50 mV.

The influence of small scale maldistribution in the vapor phase on the efficiency of the rectification in packed columns

K. Semkov*, S. Darakchiev

*Institute of Chemical Engineering, Bulgarian Academy of Sciences,
Acad. G. Bonchev St. Bl. 103, 1113 Sofia, Bulgaria*

Received November 2, 2009, Revised March 29, 2010

An analysis is made of the possibilities for accounting for small and large scale maldistribution in gas and liquid phases in packed columns. A stochastic parallel model is proposed for mathematical modeling of small scale maldistribution in gas (vapor) phase. It is assumed that the non-uniformity is normally distributed with standard deviation, equal to the maldistribution factor M_f . The reality of this assumption is confirmed by an analysis of previous experimental data for gas phase small scale maldistribution using modern random IMTP and RSRM packing. The model is tested for ethanol–water rectification using structured HOLPACK packing. Experimental data for seven types of modern packing (IMTP, Raschig Super-Ring (RSR) Metal and Plastic, and Ralu Flow Plastic) at high ethanol concentration are used to estimate the impact of vapor phase small scale maldistribution. It is found that its influence on mass transfer efficiency is quite different, and for various packing it is between 14 and 38 %. For comparison, this value for structured HOLPACK packing is 10-12 %. It is shown that a preliminary analysis of the efficiency reduction due to small scale maldistribution can provide information about the expedience of using a particular type of packing at particular operational conditions.

Keywords: Gas maldistribution, distillation, efficiency, packed columns

INTRODUCTION

In the last decades random packing of third and fourth generation have been developed and applied for industrial use. The examples are Nutter rings, Ralu Flow, IMTP, Raschig Super Rings (RSR), etc. Such packings are mainly made of metal using wasteless technology but there are also plastic varieties. They ensure high efficiency at low pressure drop and are very prospective for industrial heat and mass transfer processes. For this reason, it is necessary to develop reliable methods for determination of column efficiency when operating with these packings.

Up to now some basic parameters of these packings are investigated, such as pressure drop, effective surface, and mass transfer coefficients for processes, controlled by liquid or by gas phase. Also, for the reliable forecast of the efficiency, required is information about other substantial parameters which characterize important events in the packed columns, related to the hydrodynamic and mass transfer mechanisms, and are used in mathematical models. Important events are for example the axial mixing, the liquid phase

distribution, the redistribution of gas (vapor) phase, the influence of packing discrete structure. There are studies aiming at determination of liquid flow distribution coefficient for the considered packings [1], which coefficient is important for irrigation devices design. Also, the gas phase distribution is experimentally studied, and information is collected about the maldistribution due to discrete packing structure [2, 3].

It is known that a basic problem for the packed columns is the non-uniform flow distribution over the cross section. It changes the flow velocity and mass transfer intensity, and results in variable concentrations in radial direction and efficiency reduction. It is shown [4] that the negative effect depends not only on the rate of radial non-uniformity but also on the deviation between operational and equilibrium concentrations. If in some column sections these concentrations are rather close, the non-uniformity can provoke concentration ‘pinch’ and significantly reduction of mass transfer efficiency [4,7]. For this reason, strong effects are expected for rectification systems in a concentration zone of low relative volatility, as well as large number of theoretical stages.

The published studies on rectification with modern random packings are limited to a couple of systems, for example isobutene/n-butane, cyclo-

* To whom all correspondence should be sent:
E-mail: semkov@bas.bg

hexane/n-heptane [8] and i-octane/toluene [9]. Recently thorough study has been published [6] dealing with an important industrial system, ethanol–water at different phase ratio in the high concentration zone, where equilibrium and operation line are very close.

The considered packings have low pressure drop due to their open structure. Hence, it is to expect higher minimal irregularity of the gas (vapor) phase in comparison with the traditional and especially with the structured packings. This conclusion is supported by experience. Therefore, more significant impact on the column efficiency has to be expected.

The aim of this paper is to study the influence of non-uniform vapor phase distribution and to develop a method for determination of this effect. Data are used from a case study using IMTP, Raschig Super Rings, and Ralu Flow packings, and the method is illustrated by the experimental results obtained from ethanol-water rectification.

PARALLEL COLUMN MODEL AND ITS APPLICATION

The parallel column model is often used for description of flow non-uniformity. A packed column is represented by a number of columns connected in parallel. Due to flow non-uniformity, the ratio of gas (vapor)/liquid [mol/mol] in each column is different.

According to the first model applications in rectification [4], the column is divided in two geometrical zones, wall and central zones, presented by two parallel columns. More often this concept is applied dividing a column in velocity zones instead of geometrical zones. For example, applying the two-column model, two zones with maximum deviation of gas-liquid ratio are formed, which provokes concentration pinch in the column ends [7]. Also, a scheme with three columns is proposed with two extreme and one mean value of the phase velocity ratio [10]. Models with even more columns are known [11]. Although some attempts to account on radial mixing by a two-column model [5], almost all parallel models neglect the radial mixing between the zones.

Generally, the parallel models treat liquid phase non-uniformity while the gas phase is assumed to be homogeneously distributed between the columns. The main shortcomings of these models are [7]: i) neglecting of radial mixing; ii) undefined number of parallel columns; iii) insufficient information about the real non-uniformity. For this reason the analyses are phenomenological, they show in general the

influence of process parameters on the efficiency, also they show that the efficiency should be reduced, plus the impact of the non-uniformity rate which results in efficiency reduction. However, the results cannot be used for apparatus design.

An additional disadvantage of the parallel model is the lack of differentiation, in terms of global treatment, between the large- and small scale maldistribution, although some comments are known about the eventual different influences of radial mixing on these two types of maldistribution [7]. On the other hand, the model is relatively simple and is well ground physically. A profound analysis of the conditions, at which it should be applied, can lead to improvement of its adequacy and extend its practical application.

Large-scale maldistribution is due to the initial phase distribution and formation of local flows as wall flow or bypass gas flows. They can be reduced or eliminated by technical devices. The initial distribution can be ameliorated by use of better inlet devices. Quick reduction of large-scale maldistribution is obtained after passing through relatively short packing layer due to its redistribution ability. Large-scale maldistribution is successfully modelled by radial dispersion model applying as main parameter spreading coefficient (for the liquid), and distribution coefficient (for the gas phase). We propose a relation to determine the redistribution layer height by multipoint irrigation devices with multiple orifices [12]. Also, we develop a method [14] for evaluation of gas distribution devices and for determination of penetration depth. The latter is defined as the height of packing layer necessary to attain minimal value of gas maldistribution factor [15, 16]. The wall flow can be limited with simple technical devices, i.e. wall flow deflecting rings [17] having less width than the characteristic width of a packing element. They are mounted horizontally on the column wall at relatively small distance and change the flow distribution in the wall zone. In case of rectification, a method is developed [18] for determination of the optimal distance between the rings, resulting in equal volume integral mean superficial velocity in wall zone and in the column bulk. It is mentioned [19] that these rings stop also the wall bypass gas (vapors) flow. It is to conclude that large-scale maldistribution can be eliminated except in short zones after the distribution devices.

Small scale maldistribution is due to the packing discrete structure and cannot be eliminated. Expressed by the value of maldistribution factor, it is manifested as a ‘noise’ which has specific value for each kind of packing [20, 25].

Small scale maldistribution provokes axial mixing in both phases which can be represented by the axial dispersion model. The packing is considered homogeneous in structure, and maldistribution is reflected by the axial mixing coefficients, i.e. by Peclet number which have to be determined experimentally. It is also necessary to identify the values of volume mass transfer coefficients that fit the dispersion model [21, 22, 24]. Regarding the liquid (dispersed) phase, the small scale maldistribution affects also the packing effective surface area but it is taken into account in the experimental determination of this surface. Significant impact of the liquid phase axial mixing on the mass transfer efficiency is registered, and it is rising at decreasing of the superficial velocity [22-24].

Considering the gas phase, the investigation of axial mixing goes through a relatively difficult and imprecise experiment due to faster transient process. However, relatively small axial mixing impact is found in the case of traditional random packings, about 19 %, which allows for using of relatively imprecise relations for its determination [21]. For some structured packings it is even admitted to neglect the gas phase axial mixing. There is no information about studies on the axial mixing in gas or liquid phase in columns with new highly efficient random packings. However, significant values of maldistribution factor after the penetration depth are experimentally determined which should be attributed to their open structure and existence of more than one characteristic geometrical dimension.

It can be concluded, resuming the existing information, that:

- Large-scale maldistribution can be limited to small zones in the column and can be successfully modeled by the dispersion model with radial mixing. Parallel model is not applicable to large-scale maldistribution because of large radial gradients and significant radial mixing.
- Small scale maldistribution in the liquid phase can be modeled with acceptable precision by the dispersion model with axial mixing. The packing can be regarded as homogeneous medium with uniform radial distribution. For this reason, it is not expedient to apply parallel model at these conditions.
- The experimental study of the gas phase axial mixing in the packing is difficult and relatively imprecise. There is no data on the modern random packings. However, detailed information is available about the maldistribution factor after

the penetration depth where the large-scale maldistribution is already eliminated. At these conditions radial velocity gradients are small and radial mixing is low. The parallel model can be applied.

THE STOCHASTIC PARALLEL MODEL

According to the above considerations, we propose to tighten the zone of parallel model application in order to ameliorate its adequacy. The model will be applied for evaluation of the impact of the gas (vapor) phase small scale maldistribution in packed columns. The following assumptions were taken:

- The liquid phase is uniformly distributed over the column cross-section;
- The radial mixing in the gas phase is negligible;
- Gas (vapors) velocity profile over the cross-section is described by normal random distribution law.

The last assumption eliminates the need to introduce undefined number of parallel columns. It corresponds well to the experiments, as it will be shown later.

The density of normal distribution is given by the expression

$$\phi(U) = \frac{1}{\sqrt{2\pi}} \exp\left(-\frac{1}{2}U^2\right), \quad (1)$$

where $U = \frac{z-\xi}{\sigma}$ is a standard normal variable.

The model solution is based on an approximate presentation of the Standard normal distribution with a mean 0 and standard deviation of 1 in nine specific intervals, when the center interval is within the quarter of a standard deviation of a mean, and each of the other intervals are a half standard deviation wide, except for the tails. This presentation is in terms of the so called stanines (standard nine intervals) [26], Fig. 1.

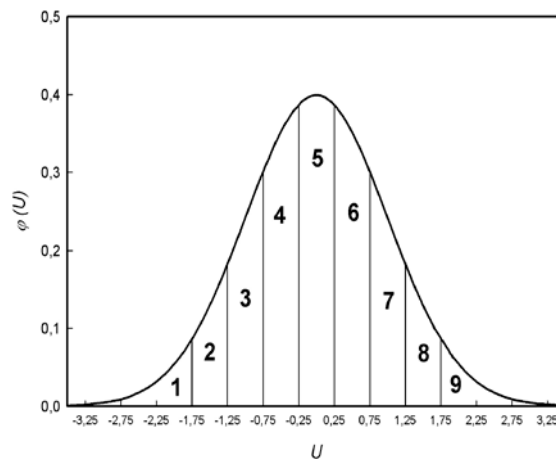


Fig. 1. Standard normal distribution in terms of “stanines” (standard nine intervals).

terms in Eq. (1) have the meaning

$$z \equiv G/G_0; \xi \equiv 1; \sigma \equiv M_f; U = \frac{G - G_0}{G_0 M_f} \quad (2)$$

For every stanine, the mean value of random variable is introduced

$$Sn_i \equiv (i - 5)0,5M_f \quad \text{for} \quad i = 2 \dots 8 \quad \text{and} \\ Sn_9 = -Sn_1 = 2,375M_f. \quad (3)$$

Then the mean density of the gas (vapor) molar flow in a particular stanine is

$$G_i = (1 + Sn_i)G_0, \quad i = 1, \dots, 9. \quad (4)$$

According to the first model assumption, the superficial velocity is the same for each stanine, i.e. $L_i = L_0$. Then the ratio of molar flows densities becomes

$$\frac{L_i}{G_i} = \frac{1}{(1 + Sn_i)} \frac{L_0}{G_0}, \quad i = 1, \dots, 9. \quad (5)$$

The partial flow for i^{th} stanine is given by the coefficient k_i (see Table 1).

Table 1. Part of the results for the stanines

i	1;9	2;8	3;7	4;6	5
k_i	0,04	0,07	0,12	0,17	0,20

Additionally, by definition

$$\sum_{i=1}^9 k_i = 1, \quad (6),$$

taking into account the symmetry of (3)

$$\sum_{i=1}^9 Sn_i = 0 \quad \text{and} \quad \sum_{i=1}^9 k_i Sn_i = 0. \quad (7)$$

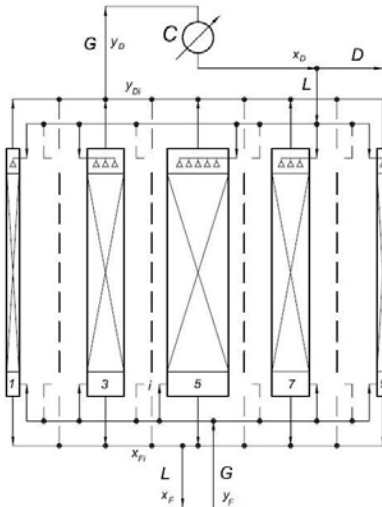


Fig. 2. Flowchart illustrating stochastic model with nine virtual parallel columns.

columns. In the present example the symbols, used in the model, are associated with the upper (enrichment) part of a rectification column with condenser C. In this case the model includes nine parallel columns, corresponding to nine stanines. The molar flow ratio is defined by (5) and the corresponding cross-sections are in the proportions, given in Table 1.

In the upper part of the parallel columns, a liquid flow (reflux) with concentration x_D is fed by the condenser C. In the lower part, vapor with concentration y_F comes from the column stripping part. As the ratio vapor/liquid is different for each parallel column, the corresponding outcome flows have different concentration – y_{Di} for vapors, and x_F for the liquid. The vapors are mixed to give a flow with concentration x_D . The liquid flows from the bottom of the columns are also mixed. The liquid with the resulting concentration x_N is used to feed the stripping part of the column. The material balance of the i^{th} column is

$$G_i(y_{Di} - y_F) = L_i(x_D - x_{Fi}), \quad (8)$$

For a given cross-section with operational concentrations x_i and y_i it is

$$G_i(y_i - y_F) = L_i(x_i - x_{Fi}). \quad (9)$$

After rearrangement of (8) and (9), an expression for the operating line of the i^{th} column is obtained

$$y_i = \frac{L_i}{G_i} x_i + \left(1 - \frac{L_i}{G_i}\right) x_D + (y_{Di} - x_D). \quad (10)$$

This operating line differs from the traditional line for the column upper part. In our case $x_D \neq y_{Di}$ for all stanines, including $i = 5$ when $L_5/G_5 = L_0/G_0$. Fig. 3 illustrates the operating lines for the

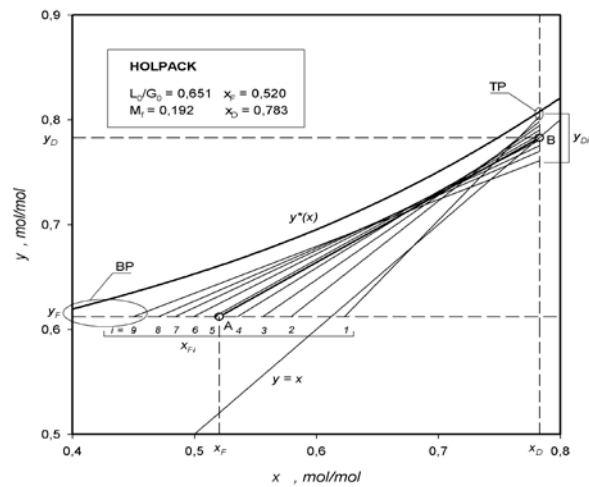


Fig.3. Operating lines for a given condition of ethanol-water rectification.

particular case of ethanol–water rectification using the HOLPACK packing [6]. Considering for the condition $L_i = L_0$ and from expression (4) the concentrations after mixing of outgoing flows become:

$$\text{-for the vapor phase} \\ y_D = \sum_i k_i (1 + Sn_i) y_{Di}, \quad (11)$$

$$\text{-and for the liquid phase} \\ x_N = \sum_i k_i x_{Fi}. \quad (12)$$

The correctness of Equations (11) and (12) can be easily confirmed as shown below. The concentration y_{Di} is obtained from Eq. (8) using (5):

$$y_{Di} = y_F + \frac{1}{1 + Sn_i} \frac{L_0}{G_0} (x_D - x_{Fi}) \quad (13)$$

Introducing Eq. (13) in (11) with regard to (6), (7) and (12), it is obtained

$$\begin{aligned} y_D &= y_F \sum_i k_i (1 + Sn_i) + \frac{L_0}{G_0} \sum_i k_i (x_D - x_{Fi}) = \\ &= y_F \sum_i k_i + \frac{L_0}{G_0} \left(x_D \sum_i k_i - \sum_i k_i x_{Fi} \right) = \\ &= y_F + \frac{L_0}{G_0} (x_D - x_N) \end{aligned} \quad (14)$$

As $y_D = x_D$, this expression represents the material balance of the column enriching part at mean vapor/liquid ratio, and the exit liquid concentration $x_N = x_F$.

The influence of the vapor phase maldistribution on the overall column efficiency can be evaluated by the number of transfer units, using HTU–NTU model. For a particular packing, defined operational conditions, including the L_0/G_0 ratio, and known column height, the concentrations $y_D = x_D$ and y_F can be measured. Then the number of transfer units in the vapor phase is

$$NTU^+ = \int_{y_F}^{y_D} \frac{dy}{y^* - y} \quad (15)$$

This expression can be interpreted as effective number of transfer units in the column at given degree of separation.

In our case the stochastic parallel model includes nine parallel columns with different vapor/liquid ratio, which depends on the model parameter, M_f . It is assumed for simplification that the mass transfer efficiency keeps constant value in the interval of vapor velocity changes due to small scale maldistribution. Hence, the same number of transfer units has to be placed in each column

$$NTU = NTU_i = \int_{y_F}^{y_{Di}} \frac{dy_i}{y^* - y_i} = const \quad (16)$$

where y_{Di} is determined via Eq. (13) which defines the relation between y_{Di} and x_{Fi} . Additionally, the conditions of the Equations (11) and (12) have to be satisfied. Eq. (16) represents the number of transfer units necessary to attain a preset separation in the presence of gas phase radial maldistribution. The impact on mass transfer efficiency can be expressed by the efficiency coefficient

$$\eta = \frac{NTU^+}{NTU} \leq 1 \quad (17)$$

This expression can also be regarded as the reduction rate of the driving force due to the vapor phase maldistribution.

MODEL SOLUTION

At preset or experimentally measured concentrations x_F and x_D and the molar phase L_0/G_0 ratio, the concentrations y_F and $y_D = x_D$ can be determined from the operating line. Then NTU^+ can be directly derived from Eq. (15). Equilibrium dependence is also needed, and the integration is generally made by a proper numerical method.

The term NTU in Eq. (16), together with the conditions (11, 12) has to be determined by iterative procedures. We shall only mention without detailed description that after testing of different methods, type of functions, solution sensitivity and convergence velocity of the solution, we have developed a particular two-level iterative procedure. At the first (low) level the iterations are made for y_{Di} for every stanine until a predefined value of NTU is attained. Then x_F is determined by Eq. (13). The values of y_D and x_N are obtained by summing the stanine concentrations, Equations (11 and 12). At the second (high) level the iterations are made for NTU until the condition $x_N = x_F$ is satisfied. At both levels the new approximations are defined by the secant method, a numerical version of the Newton-Raphson method. The integration is made by the method of Simpson. The convergence velocity depends strongly on initial approximations of y_D , especially for $i=1$ and $i=9$, where top (TP) and bottom pinch (BP) are obtained (see Fig. 3). For these cases the initial approximations have been chosen according to the pinch with small (0.5%) reserve in the safe side. In regards to the other stanines, the result for the previous stanine has been used as initial approximation for the next one. The software program developed is very stable and fast with relative deviation of $1 \cdot 10^{-4}$, attained with 3-8 iterations for y_{Di} and 3-5 iterations for NTU .

EXPERIMENTAL STUDY

The studies on gas phase distribution [2,3] have been carried out in a column of 0.47 m in diameter with random Raschig Super-Ring, IMTP and Ralu Flow packings, and a structured HOLPACK packing has been used for comparison [27, 16]. Thermoanemometry has been applied to measure the gas velocity profile (single phase with no countercurrent liquid flow) throughout the cross-section. The measuring device has been connected to a computer. A hundred values in each point have been taken and a mean value has been determined. The measurement points have been placed over two perpendicular diameters in 22 points on each of them. In some cases, when it has been technically possible (for example at the end of a column section with height 0.8 m), gas velocity has been measured in 112 points, regularly distributed throughout the cross-section. These results, considered to be more reliable, are used in this paper. Measurements for different packing height have been carried out, too. The results have been presented as maldistribution factor:

$$M_f = \frac{1}{w_0} \sqrt{\frac{\sum_{j=1}^n (w_j - w_0)^2}{n-1}}, n = 112 \quad (18)$$

Fig. 4 represents the experimental gas velocity distribution of IMTP 25 at 0.8 m packing height.

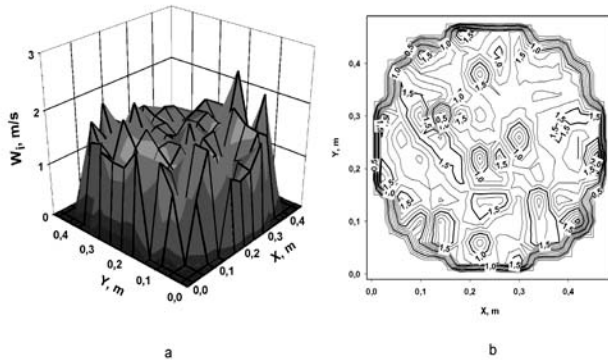


Fig. 4. Experimental gas velocity distribution for IMTP 25 at 0.8 m packing height: a) 3D representation; b) contour plot.

Fig. 5 illustrates the results for the IMTP 25 packing at different packing height. This is a typical graph for most of the modern random packings. In the beginning the maldistribution factor descends sharply, passes through a minimum, and then begins slowly to rise. The first zone corresponds to the large-scale maldistribution, produced by the inlet gas distribution device. The minimum is attained at packing height of only 0.2 m. It is the so called

‘uniformity limit’ or the ‘noise’, which expresses the small scale maldistribution due to the packing discrete structure. The rising part of M_f represents a new development of relatively small large-scale maldistribution, which can be attributed to the formation of wall gas flow. It is typical for the random packings and can be attributed to the different geometrical structure of the wall and bulk zones. In the case of block or package packings with regular cell structure (Honeycomb [14] or HOLPACK [27, 16]), this effect is not pronounced.

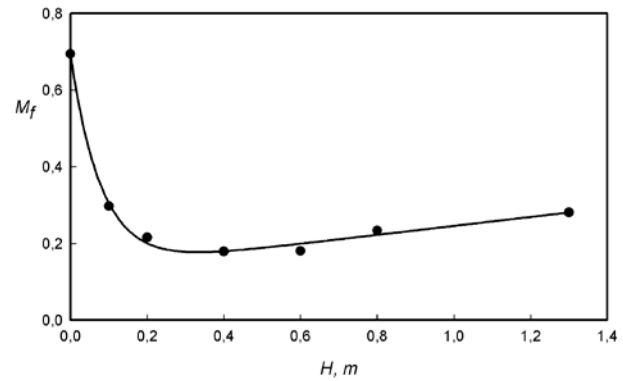


Fig. 5. Maldistribution factor vs. packing height for IMTP 25-typical graph for most of the modern random packings.

The assumption for existence of normal standard distribution, Eq. (1) is verified by the test of Kolmogorov-Smirnov [28]. It is based on the determination of the maximal difference D_c between the cumulative frequencies of the empirical and theoretical distribution

$$D_c = \max |F_n(U) - F(U)|, \quad (19)$$

where F/U is a theoretical probability integral

$$F(U) = \Phi(U) = \frac{1}{\sqrt{2\pi}} \int_0^U \exp\left(-\frac{t^2}{2}\right) dt. \quad (20)$$

The value, derived by (19), is to be compared to a tabulated value. In case the latter is smaller, the hypothesis for normal distribution is not valid. When the number of points is larger than 35, the tabulated value at significance level of 0.05 is calculated by the expression [27]

$$D_{c|0.05} = \frac{1.36}{\sqrt{n}}. \quad (21)$$

For our experiments $n = 112$ and $D_{c|0.05} = 0.1285$.

Fig. 6a shows a comparison between corresponding cumulative frequencies for 20 intervals (IMTP 25 packing, 1.3 m in height). Fig. 6b represents a comparison of theoretical and experimental distribution of nine stanines. The

values, derived from Eq. (19), are $D_C = 0.055 < D_{C|0.05} = 0.1285$, i.e. the hypothesis for normal distribution is approved. The same value of D_C is obtained for packing of 0.8 m height. For the RSRM 2, RSRM 3 and RSRP 2 packings at 0.8 m height, the corresponding values of D_C are respectively 0.073; 0.068 and 0.045. Hence, the hypothesis of normal distribution is applicable in these cases, too.

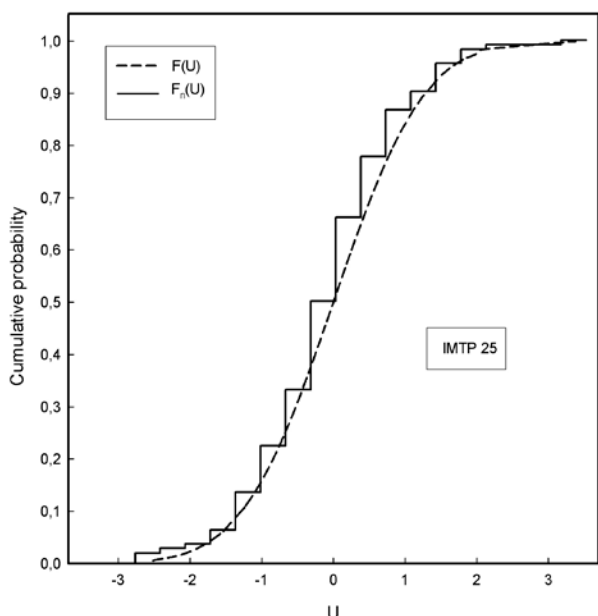


Fig. 6(a)

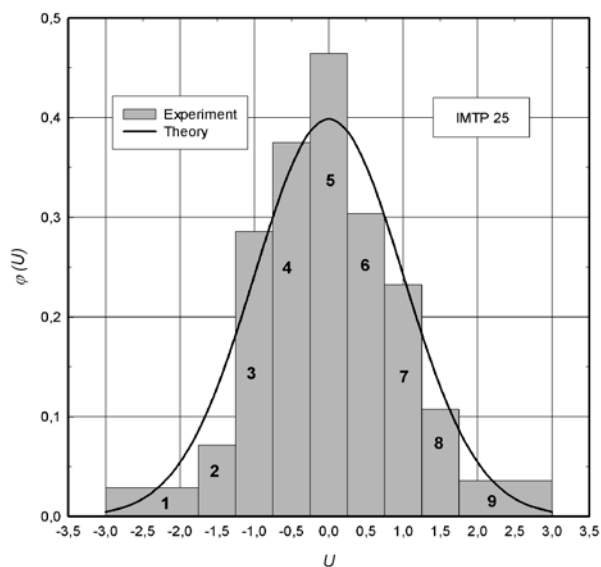


Fig. 6(b)

Fig. 6. Standard normal distribution representation of the gas velocities for IMTP 25 at 1.3 m packing height: a) comparison of corresponding cumulative frequencies for 20 intervals; b) comparison of theoretical and experimental distribution in terms of stanines.

The study on ethanol–water system rectification [6] has been carried out in the zone of high ethanol concentration, which corresponds to the common case for the main part of the industrial rectification columns. The experimental column is of 0.213 m diameter with packing layer of 2.8 m. Wall flow deflecting rings (WFDR) [17] are mounted on the inner wall surface at 200 mm distance. They serve to eliminate the liquid wall flow and its harmful impact [18]. Obviously, the rings also

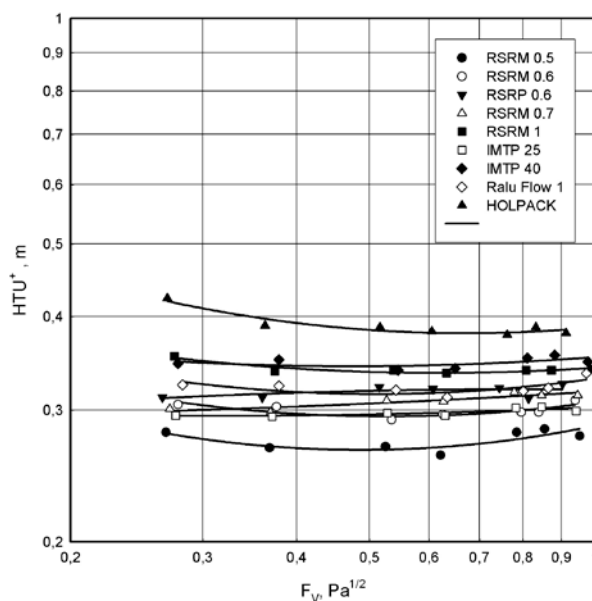


Fig. 7. Experimental (effective) height of transfer units vs. F -factor at full reflux.

hamper the development of gas wall flow. The column can operate at constant or variable reflux.

Seven types of modern random packings are studied: four metal Raschig Super – Rings with characteristic sizes of 0.5; 0.6; 0.7 and 1”, one plastic – 0.6”, two types of IMTP, and one plastic Ralu Flow. For comparison, a structured metal HOLPACK packing, used currently in the ethanol production, is also tested under identical conditions. The experiments are carried out at vapor flow velocity of 0.253 – 0.936 m/s and liquid superficial velocity of $4.44 \cdot 10^{-4} \text{ m}^3/(\text{m}^2 \cdot \text{s}) - 1.63 \cdot 10^{-3} \text{ m}^3/(\text{m}^2 \cdot \text{s})$ at full and variable reflux, attained at constant liquid superficial velocity and variable vapor velocity, as well as at constant vapor velocity and variable liquid velocity. Fig. 7 illustrates the results, obtained at full reflux.

Table 2 contains the values of the gas phase maldistribution factor for the relevant rectification column conditions, using the available experimental results from different authors. In all cases, the values refer to the zone beyond the penetration depth where mainly small scale maldistribution is pronounced.

Table 2. Gas maldistribution factor and packing specific surface area.

Packing	M_f [-]	a , m^2/m^3
RSRM 0.5	0.260 [2]	236 [29]
RSRP 0.6	0.270 [2]	206 [1]
RSRM 0.7	0.241 [2]	176 [29]
RSRM 1	0.245 [2]	156 [29]
IMTP 25	0.181 [3]	243 [30]
IMTP 40	0.263 [3]	172 [30]
Ralu Flow 1	0.197 [3]	177 [30]
HOLPACK	0.192 [27, 16]	56 [6]

Table 2 includes also data on the packing specific surface area, a , in order to allow an approximate comparison of their efficiencies.

RESULTS AND DISCUSSION

The stochastic model is applied to our previous experimental results for the ethanol–water rectification [6]. Preliminary check of the model performance was done using the rectification results for the structured HOLPACK packing. This packing is thoroughly investigated. The packing parameters are determined by unified method for modeling of heat and mass transfer processes [31, 32, 23] because of the lack of experimental data. These parameters are: mass transfer coefficients in both boundary layers [33, 34], effective surface area [35], liquid phase axial mixing (Peclet number) [36], and the impact of Marangoni effect [13, 23]. Only the influence of vapor phase axial mixing is not taken into account because of lack of experimental data. It is admitted [23] that the HOLPACK packing (perforated and extended metal sheets placed horizontally) ensures uniform distribution of vapors, and they have plug-flow structure.

Fig. 8 shows the results of the stochastic model application using data, obtained by a mathematical modeling. A comparison between the experimental results is also shown. The term HTU_m is the height of a transfer unit, determined by the abovementioned unified method, which neglects the vapor phase maldistribution. After applying the stochastic model and considering the vapor phase maldistribution, the effective height of transfer unit HTU_m^+ is calculated. The corresponding experimental data for HTU_m^+ are determined from Eq. (15). Obviously, the description is significantly improved when vapor phase small scale maldistribution is taken into account. The efficiency reduction for HOLPACK packing at the particular experimental conditions is about 10-11%.

Fig. 9 illustrates the results at full reflux, presented as influence of F -factor, F_v , on the efficiency coefficient, η , Eq. (17). The upper line

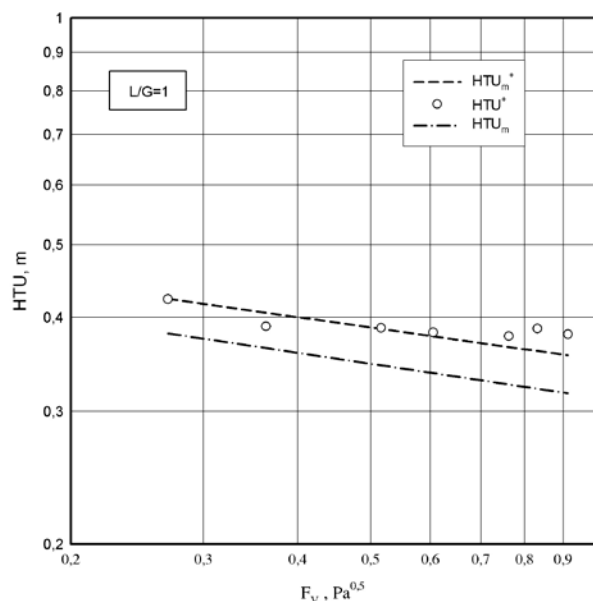


Fig. 8a

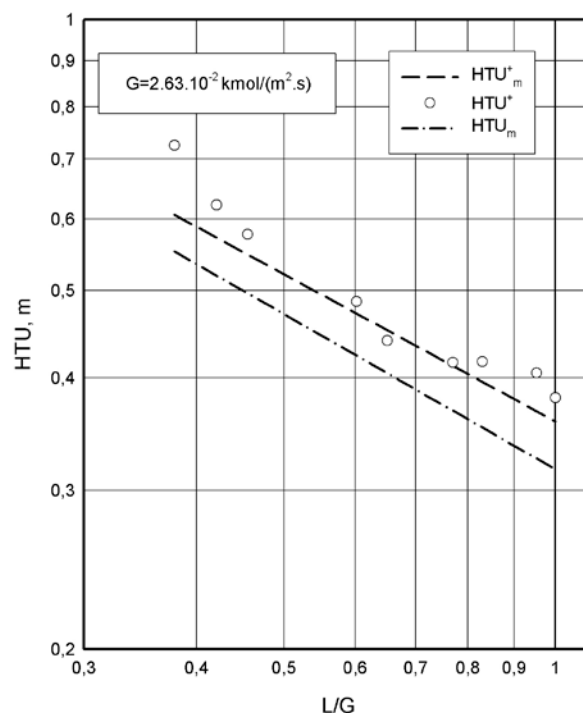


Fig. 8b

Fig. 8. Comparison between experiment (NTU^+), and models without NTU_m and with (NTU_m^+) taking into account vapor phase maldistribution for HOLPACK: a) at full reflux; b) at constant vapor load.

refers to the structured HOLPACK packing. Significant difference of efficiency coefficients is seen. It is to stress upon the strong impact of vapor phase maldistribution – up to 37% for the RSRM 0.5 packing. Nevertheless, the efficiency of this packing is the best, see Fig. 7.

Similar results are obtained at variable reflux. The result analysis of the results, as well as

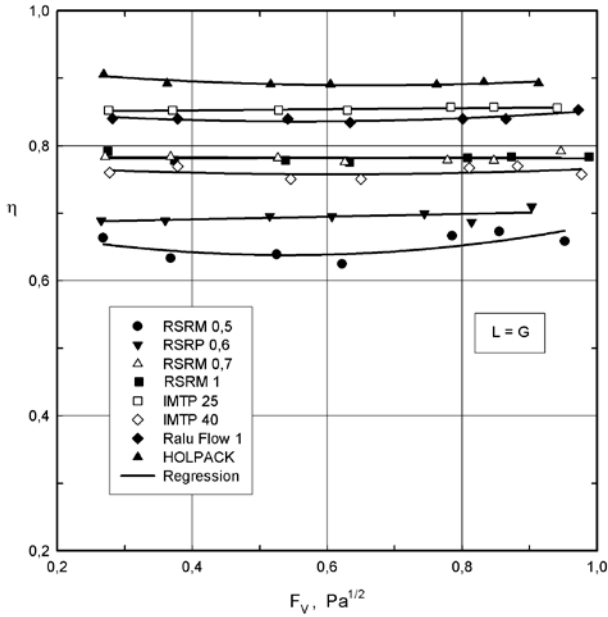


Fig. 9. Efficiency coefficient vs. F-factor at full reflux.

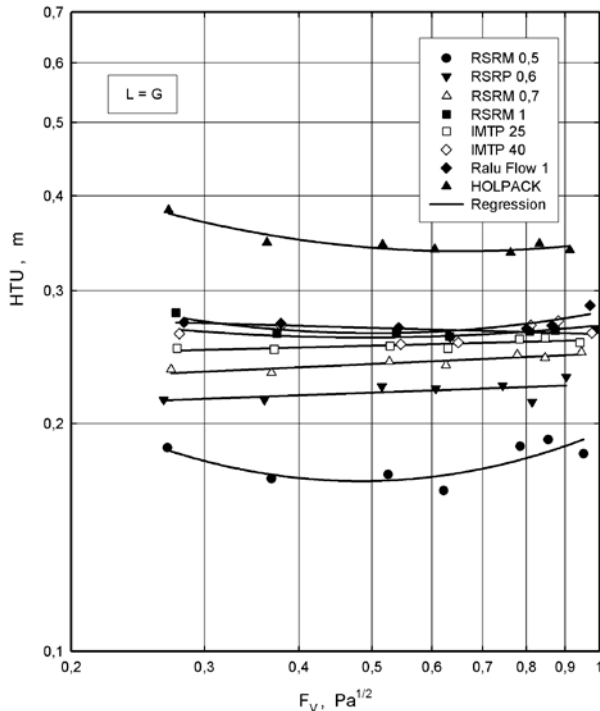


Figure 10. HTU neglecting the vapor phase maldistribution vs. F-factor at full reflux.

simulation results, show that the influence of the vapor phase maldistribution is stronger for more efficient packings and at a higher value of the maldistribution factor. The relative efficiency of random packings might be estimated in relation with their specific surface area, Table 2. Although it is a rough comparison, it might be done because the effective surface/specific surface area ratio does not practically depend on the specific surface [29]. This ratio values are between 0.72 and 0.89 in these particular experimental conditions. The same is true

for the IMTP and Ralu Flow packings [30] because of their similar structure. However, it is not applicable to the HOLPACK packing which has a completely different structure. Correspondingly, the value of the above mentioned ratio is about 1.5, i.e. the effective surface is significantly larger than the specific surface. The vapor phase maldistribution affects most strongly the packing with the largest specific surface and highest maldistribution factor, i.e. the RSRM 0.5. For IMTP 25 which has similar specific surface but small maldistribution factor, the impact is twice smaller, 15-16%. The smallest influence is registered in the case of the HOLPACK packing, which has small specific surface and small maldistribution factor.

Fig. 10 illustrates the height of transfer unit, neglecting vapor phase maldistribution. In this case more pronounced difference between the efficiency of different packages is observed. The ratio best/worst efficiency is about 2, while it is not greater than 1.4 in the case of experimental efficiency determination (Fig. 7).

CONCLUSION

A stochastic model is proposed which allows for quantitative evaluation of the influence of the vapor phase maldistribution on the packing efficiency based on data on the maldistribution factor. Using modern random packings, significant reduction of packing efficiency, between 16 -38 %, is found for the ethanol–water rectification in the zone of high ethanol concentration. Such a strong impact should not be neglected and has to be taken into account when selecting the type of packing. It is necessary to improve the accuracy of the experimental determination of the maldistribution factor because of its essential influence on the efficiency.

Acknowledgements This study has been carried out with the financial support of the Grant scheme № BG051PO001-3.3.04/30 /28.08.2009 under the Operational Program “Human Resources Development” 2007-2013, co-financed by European Social Fund of European Community.

NOMENCLATURE

Symbols used

- a specific surface area of the packing, m^2/m^3
- F cumulative frequencies, [-]
- F_v F-factor ($F_v = w_0 \sqrt{\rho}$), $Pa^{1/2}$
- D_M molar flow of the distillate, mol/s
- D_C term in Eq. (19), [-]

G	density of the gas (vapor) phase molar flow, mol/(m ² s)
G_M	vapor molar flow, mol/s
H	height of the packing layer, m
k	weight coefficient, Table 1, [-]
L	density of the liquid phase molar flow, mol/(m ² s)
L_M	molar flow of the reflux, mol/s
M_f	maldistribution factor, Eq. (18), [-]
n	number of experiments, [-]
Sn	mean value of the random variable U , [-]
w	gas (vapor) flow velocity, m/s
x	liquid phase molar concentration, mol/mol
y	vapor phase molar concentration, mol/mol
H	height of the packing layer, m
HTU	height of the transfer unit, m
NTU	number of transfer units, [-]
t	current value, Eq. (20), [-]
U	standard normal random variable, [-]
z	random variable, [-]

Greek letters

η	efficiency coefficient, Eq. (17), [-]
ρ	gas (vapor) density, kg/m ³
σ	standard deviation, [-]
ξ	mathematical expectation, [-]
$\Phi(U)$	probability integral, [-]
$\varphi(U)$	probability density, [-]

Subscripts

i	for i^{th} stanine (parallel column)
j	for j^{th} point
m	model
n	experimental for n^{th} interval, Eq. (19)
0	mean value
D	in/out at column top
F	in/out at column bottom
N	summing value at the bottom exit

Superscripts

+	effective value including maldistribution impact
*	equilibrium value

REFERENCES

1. D. Dzhonova-Atanasova, N. Kolev, S. Nakov, *Chem. Eng. Technol.*, **30**, 202, (2007).
2. R. Darakchiev, T. Petrova, S. Darakchiev, *Chem. Eng. Process.*, **44**, 827, (2005).
3. S. Darakchiev, T. Petrova, R. Darakchiev, *Chem. Biochem. Eng. Q.*, **19**, 147, (2005).
4. J.W. Mullin, *Ind. Chem.*, **33**, 408, (1957).
5. M. Huber, R. Hiltbrunner, *Chem. Eng. Sci.*, **21**, 819, (1966).
6. S. Darakchiev, Kr. Semkov, *Chem. Eng. Technol.*, **31**, 1039, (2008).
7. J. F. Billingham, M. J. Lockett, *Trans. IChemE*, **80**, Part A, 373, (2002).
8. M. Schultes, *Trans. IChemE.*, **81**, Part A, 48, (2003).
9. IMTP High Performance Packing, *Bulletin KGIMTP-2 2MI303E*, KOCH-GLITSCH, (2003).
10. M. Schultes, *Ind. Eng. Chem. Res.*, **39**, 1381, (2000).
11. Stichlmair J., A. Stemmer, *IChemE Symp. Ser.*, **104**, B213, (1987).
12. Kr. Semkov, *Chem. Eng. Sci.*, **46**, 1393, (1991).
13. N. Kolev, Kr. Semkov, *Chem. Eng. Process.*, **29**, 77, (1991).
14. T. Petrova, Kr. Semkov, Ch. Dodev, *Chem. Eng. Process.*, **42**, 931, (2003).
15. D.P.Edwards, K.R.Krishnamurthy, R.W.Potthoff, *Trans IChemE*, **77**, 656, (1999).
16. R. Darakchiev, Ch. Dodev, *Chem. Eng. Process.*, **41**, 385, (2002).
17. N. Kolev, R. Darakchiev, Bulg. Patent No. 18018, (1972).
18. Kr. Semkov, N. Kolev, V. Stanek, *Coll. Czech. Chem. Commun.*, **52**, 2438, (1987).
19. I.E. Idel'chik, *Aerodynamics of contact, filtering and adsorption apparatuses with a layer of granulated materials*, Moscow, 1982, 37
20. Kr. Semkov, T. Petrova, *1-st South East European Congress of Chem. Eng.*, Belgrade, Serbia and Montenegro, September 2005, Book of Abstracts, 55.
21. N. Kolev, Kr. Semkov, *Commun. Dep. Chem., Bulg. Acad. Sci.*, **12**, 299, (1979).
22. N. Kolev, Kr. Semkov, *Chem. Eng. Process.*, **19**, 175, (1985).
23. N. Kolev, Kr. Semkov, *Chem. Eng. Process.*, **29**, 83, (1991).
24. N. Kolev, Kr. Semkov, *Vt "Verfahrenstechnik"*, **17**, 474, (1983).
25. T. Petrova, *PhD Thesis*, Institute of Chemical Engineering, Bulgarian Academy of Sciences, 2008.
26. *Webster's New Millennium™ Dictionary of English, Preview Edition (v 0.9.7) Copyright © 2003-2008 Dictionary.com, LLC.*
27. R. Darakchiev, *Chem.Eng.Process.*, **18**, 317, (1984).
28. P. Hoel, *Introduction to Mathematical Statistic*, 3th Ed., John Wiley&Sons, 1962.
29. N. Kolev, Sv. Nakov, L. Ljutzkanov, D. Kolev, *Chem.Eng.Process.*, **45**, 429, (2006).
30. Sv. Nakov, N. Kolev, L. Ljutzkanov, D. Kolev, *Chem.Eng.Process.*, **46**, 1385, (2007).
31. N. Kolev, Kr. Semkov, R. Darakchiev, *New developments in separation processes associated with processes industries, biotechnology and environmental protection*, European Federation of Chemical Engineering, Warsaw 29-31 May 1996, 32.
32. Kr. Semkov, *PhD Thesis*, Centr. Lab. Chem. Process. Fund., Bulg. Acad. Sci., 2008.

33. R. Darakchiev, N. Kolev, G. Chapkanova, *Chem.- Eng. Techn.*, **46**, 31, (1974). 34. Kr. Semkov, N. Kolev, *Commun. Dep. Chem., Bulg. Acad. Sci.*, **22**, 329, (1989).
35. N. Kolev, *Vt Verfahrenstechnik*, **8**, 145, (1974).

ОТЧИТАНЕ ВЛИЯНИЕТО НА ДРЕБНО-МАЩАБНАТА НЕРАВНОМЕРНОСТ В ПАРОВАТА ФАЗА ПРИ РЕКТИФИКАЦИЯ С МОДЕРНИ ВИСОКО-ЕФЕКТИВНИ НЕНАРЕДЕНИ ПЪЛНЕЖИ

К. Семков, С. Даракчиев

*Институт по инженерна химия, Българска академия на науките,
Ул. "Акад. Г. Бончев", бл. 103, 1113, София*

Постъпила на 2 ноември, 2009 г., преработена на 29 март 2010 г.

(Резюме)

Направен е анализ на възможностите за отчитане на дребно- и едромашабните неравномерности в двете фази при колони с пълнеж. Но тази основа е предложен стохастичен паралелен модел за математично моделиране на дребно-машабната неравномерност в газовата (паровата) фаза. При него се приема, че неравномерностите се подчиняват на нормално случайно разпределение със стандартно отклонение равно на фактора на неравномерност M_f . Правомерността на това допускане е показана на основата на анализ на получени по-рано експериментални данни за дребно-машабната неравномерност в газовата фаза при съвременни ненаредени пълнежи IMTP и Raschig Super-Ring (RSR). Възможностите на модела са проверени и доказани при ректификация на система етанол-вода със структурен пълнеж HOLPACK. Обработени са експериментални данни по ректификация на същата система при високи концентрации на етанола с осем вида съвременни пълнежи от сериите IMTP, Raschig Super-Ring (метални и пластмасови), и Ralu Flow. Показано е, че при конкретните условия влиянието на дребно-машабните неравномерности в паровата фаза върху ефективността на масообмена силно се различава за отделните пълнежи и варира между 14 и 38%. При използвания за сравнение структуриран пълнеж HOLPACK това влияние е 10-12%. Посочено е, че предварителният анализ на понижаването на ефективността вследствие на споменатата неравномерност може до голяма степен да реши целесъобразността на използването на даден вид пълнеж при конкретни условия на процеса.

An experimental study of spiral-plate heat exchanger for nitrobenzene-water two-phase system

S. Sathiyar^{1,*}, M. Rangarajan², S. Ramachandran³

^{1,2} Department of Chemical Engineering and Materials Science, Amrita School of Engineering, Amrita Vishwa Vidyapeetham, Coimbatore, Tamil Nadu, 641 105, India.

³ Department of Chemical Engineering, Erode Sengunthar Engineering College, Erode, Tamil Nadu, 638 057, India.

Received February 5, 2010, Revised April 23, 2010

This paper presents the results of two-phase (immiscible liquids) heat transfer studies, conducted using a spiral plate heat exchanger. Experimental studies were conducted using hot water as the service fluid. The two-phase system of nitrobenzene-water in different mass fractions and flow rates was studied as a cold process fluid. The two phase heat transfer coefficients were correlated with Reynolds numbers, Prandtl number, and by the following equation $Nu = a \cdot (Re)^b \cdot (Pr)^c \cdot (X)^d$, adopting an approach available in the literature for the two-phase flows. The data obtained from the experimental study are compared with the theoretical predictions. The predicted coefficients showed a spread of $\pm 15\%$ in the laminar range. This new correlation for predicting Nusselt number may be used for practical applications.

Keywords: Spiral plate heat exchanger, two- phase flow, single-phase heat transfer coefficients, two-phase heat transfer coefficients, Nusselt number, Reynolds number

INTRODUCTION

The heat exchanger is a device where energy is transferred from one fluid to another across a solid surface. With rising equipment costs and increasingly stringent space constraints, compact heat exchangers are gaining a larger portion of the heat exchanger market. Spiral plate heat exchangers are extremely compact, fitting a large heat transfer surface area into a small volume, have higher heat transfer rates, less fouling, operational flexibility, and are easy to maintain. An important feature of spiral plate exchangers is its capacity to handle high viscosity and highly suspended liquids, exhibiting lower tendency to fouling. This type of exchanger is common in the paper, petrochemical, food, and sugar industries with applications in evaporation and condensation.

Simultaneous flow of two or more immiscible fluids is one of the different types of multiphase flows that occur widely in the industry, in environmental, chemical and biochemical processes. Heat transfer in liquid-liquid systems is frequently encountered in metal processing, the petrochemical and other industries. For improved heat exchanger designs, it is critical to gain better

understanding of the momentum and heat transferring in the multiphase flow processes where fluids of different thermophysical properties are involved.

Jha and Rao [1] have studied the outside-film and inside-film heat transfer coefficients in an agitated vessel. They have derived an equation to predict the Nusselt number based on the geometry of the helical coil and the location of the agitator. Kalb and Seader [2] have performed numerical studies for uniform wall heat flux with peripherally uniform wall temperature for Dean numbers in the range of 1-1200, Prandtl numbers of 0.005-1600, and curvature ratios of 10 to 100 for fully developed velocity and temperature fields. Yao and Berger [3] have studied the effects of buoyancy forces on fully developed laminar flow with constant heat flux. Their studies have been based on the Boussinesq approximation for the buoyancy forces and analyzed for both horizontally and vertically oriented curved pipes. The heat transfer to a helical coil in an agitated vessel has been studied by Havas *et al.* [4], and a correlation has been developed for the outer Nusselt number based on a modified Reynolds number, Prandtl number, viscosity ratio, and the tube diameter to the vessel diameter ratio.

Lemenand and Peerhossaini [5] have developed a correlation for Nusselt number based on the Reynolds number, Prandtl number, and the number of bends in the pipe. Their study shows that

*To whom all correspondence should be sent:
E-mail: E-mail: ssathiyar78@gmail.com;
Phone: + (91) 422 2685557

the Nusselt number slightly drops off with the increase of bend number. Gut *et al.* [6] have developed a parameter estimation procedure for plate heat exchangers that handles experimental data from multiple configurations. Hemamalini *et al.* [7] have developed correlations for the prediction of the pressure drop in a two-phase flow based on pure component density, gas and liquid flow rates in a horizontal pipe and a control valve, in series for an air/palm oil two-phase flow. Shah [8] has summarized the advances in compact heat exchangers related to two-fluid exchanger effectiveness, NTU results for highly complex flow arrangements, heat transfer, pressure drop analyses, CFD role in the design, analysis of header and manifold design, recuperator design procedure, design data for compact heat exchanger, and thermodynamic modeling and analysis.

Paisarn and Jamnean [9] have experimentally investigated the effect of curvature ratios on the heat transfer and flow development in horizontal spirally coiled tubes. In their work, the turbulence flow and the heat transfer have been simulated by using the $k-\varepsilon$ standard turbulence model. The centrifugal force is seen to have significant effects on the enhancements of heat transfer and pressure drop. Marchitto *et al.* [10] have carried out experiments on a horizontal cylindrical two-phase flow header supplying sixteen vertical channels and have analyzed the effects of nozzles and of orifices placed upstream of the header and connecting it to the channels. Their experimental results show that the operating conditions exert a strong influence on the structure of the two-phase flow pattern inside the header, and therefore on the flow distribution to the channels.

In this study, heat transfer investigations were carried out using a spiral plate heat exchanger with water as the hot fluid, and nitrobenzene and two-phase mixtures of nitrobenzene-water immiscible liquid mixture as the cold fluids. Single- and two-phase heat transfer coefficients were obtained for the cold side from the experiments. Predictive correlations were developed for the cold-side (two-phase fluid) heat transfer coefficient.

EXPERIMENTAL

Experimental set-up and procedure

A schematic diagram of the experimental setup is shown in Fig. 1. The heat exchanger, used in the experiment, was a spiral plate heat exchanger, manufactured by Alfa Laval (India) Ltd., Pune,

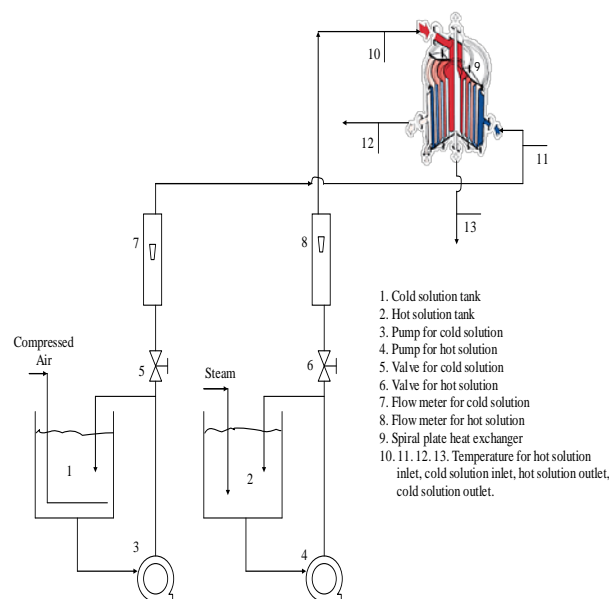


Fig. 1. Schematic diagram of the experimental set-up.

India, Type 1V, with a heat transfer area of 2.24 m^2 , and a channel spacing of 5 mm.

The service fluid used was water, heated in a stainless steel vessel by steam purging. A temperature controller was used to maintain the inlet temperature to the heat exchanger. The process (cold-side) fluid was stored in a separate stainless steel tank. Weighed quantities of nitrobenzene and demineralized water were charged into this tank to obtain the experimental range of nitrobenzene mass fractions (0, 20, 40, 60, 80 and 100%). The agitation in the tank was maintained by air bubbling. Centrifugal pumps were used for the circulation of the two streams of fluids. The two-phase rotameters were calibrated for each experimental mass fraction before the experimental run. Online calibrated resistance temperature detectors with digital indicators were used for temperature measurements of the inlet and outlet streams of the service and process fluids.

The service-fluid-side inlet temperature and the flow rate were kept steady. The two-phase side flow rate was varied and for each selected flow rate observations of all four temperatures and two flow rates were recorded after steady state was reached. Experimental runs with pure liquids in the process side were also carried out. The service and process fluid flow paths of heat exchanger are shown in Fig. 2. The heat-transfer performance of the spiral plate heat exchangers mainly depends on mass flow rate of the fluid, flow area and logarithmic temperature difference between entering and leaving fluid streams.

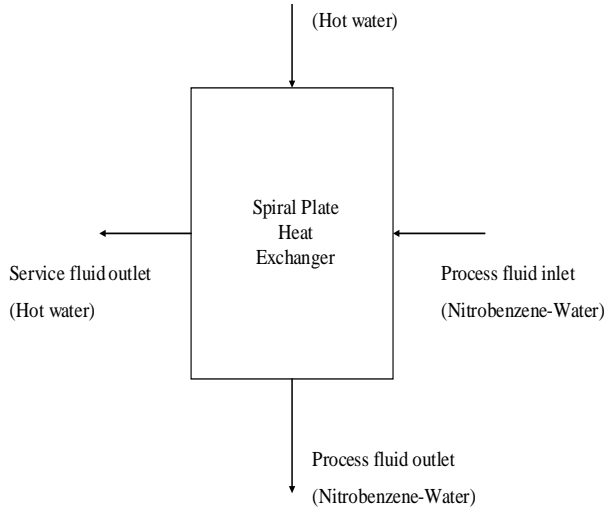


Figure 2: Service and process fluid flow paths of the heat exchanger

Calculation methodology

The heat load is calculated using the expression:

$$Q = M_h C_{p_h} (\Delta T)_h; \quad (1)$$

M_h – Mass flow rate of the hot fluid, kg/s
 C_{p_h} – Specific heat of the hot fluid, J/kg K
 $(\Delta T)_h$ – Temperature drop of the hot fluid, K.

Using equation (1), the overall heat transfer coefficient is obtained from the relation:

$$U = \frac{Q}{A(\Delta T)_{lm}}; \quad (2)$$

U – Overall heat transfer coefficient, W/m² K
 A – Area of heat transfer, m²
 $(\Delta T)_{lm}$ – Logarithmic mean temperature difference, K.

The hot-fluid-side heat-transfer coefficient (h_h) is calculated using the following equation [11]:

$$Nu = 0.0315(Re)^{0.8}(Pr)^{0.25}; \quad (3)$$

Nu is the Nusselt number, given by

$$Nu = \frac{h_h d_e}{k_h}; \quad (4)$$

h_h – Hot-side heat-transfer coefficient, W/m² K
 d_e – Equivalent diameter of the flow channel, m
 k_h – Thermal conductivity of the hot fluid, W/m K

The cold-fluid-side (two-phase side) heat-transfer coefficient ($h_{2\phi}$) is estimated using the expression, where the results from Eqs. (2) to (4) are used.

$$\frac{1}{U} = \frac{1}{h_h} + \frac{t}{k_{ss}} + \frac{1}{h_{2\phi}}; \quad (5)$$

t – wall thickness of the spiral plate, m
 k_{ss} – thermal conductivity of the wall, W/m K

$h_{2\phi}$ – heat transfer coefficient of the two-phase fluid, W/m² K.

The experimental Nusselt number, for the two-phase cold fluid, is estimated based on the two-phase heat-transfer coefficient from Eq. (5) using the expression

$$Nu_{experimental} = (h_{2\phi})_{hotside} (d_e/k)_{cold side}. \quad (6)$$

In developing a predictive correlation for the cold-side two-phase heat-transfer coefficient, $h_{2\phi}$, d_e , $k_{2\phi}$, $\rho_{2\phi}$, $\nu_{2\phi}$, $\mu_{2\phi}$, $C_{p_{2\phi}}$ and X are the eight relevant variables, assuming average properties assigned to the two-phase system. There are four fundamental dimensions. That is why, four is the number of the dimensionless groups involved. These groups are the Nusselt number (Nu), Reynolds number (Re), Prandtl number (Pr), and the mass fraction (X). Therefore, the general form of the correlations developed is

$$Nu_{predicted} = a(Re)^b(Pr)^c(X)^d, \quad (7)$$

where a , b , c , and d are constants, obtained from linear regression using MS Excel. The thermo-physical properties of the pure substances were calculated based on the correlations given in Yaws [12]. The two-phase properties were obtained using a linear mixing rule.

RESULTS AND DISCUSSION

Single-phase flow

The experimental results of single-phase studies are presented in the form of a plot between Reynolds Number and $h_{1\phi}$ in Fig. 3. The relation between Re and $h_{1\phi}$ (heat transfer coefficient for pure nitrobenzene, W/m² K) were correlated by regression analysis in the form given in Eq. (7). For pure water, equation (3) was used to predict $h_{1\phi}$.

Two-phase flow

Two-phase studies were carried out with different mass fractions of nitrobenzene in water (20%, 40%, 60% and 80%). Fig. 4 represents the two-phase heat transfer coefficients, $h_{2\phi}$ as a function of Reynolds number for various compositions. For two-phase systems, the Reynold's number is based on the weighted-average thermophysical properties of the fluids at the respective mean bulk temperatures. The obtained data are fitted by regression to the correlation given in equation (7), and the values of a , b , c , and d are given in Eq. (8):

$$Nu_{predicted} = 1.7311 \times 10^{-6} (Re)^{1.6947} (Pr)^{1.1767} (X)^{-0.6860} \quad (8)$$

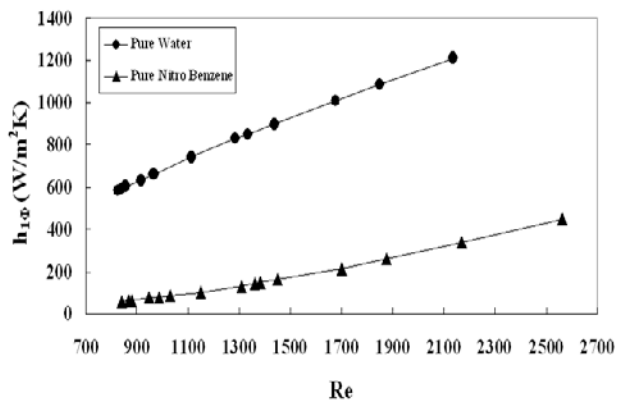


Fig. 3. Variation of heat transfer coefficient with Re for single phase system.

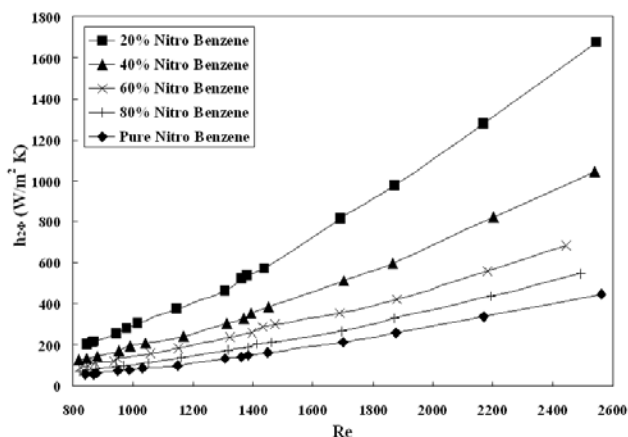


Fig. 4. Variation of Heat Transfer Coefficient with Re for Nitrobenzene -Water System

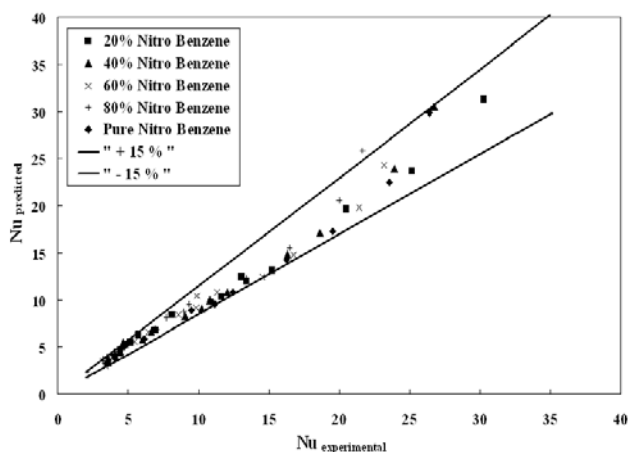


Fig. 5. Comparison of $Nu_{\text{experimental}}$ with $Nu_{\text{predicted}}$ for nitrobenzene-water system.

The developed correlations were tested against new experimental data of the same system (comparison of the results from equations 6 and 8). The calculated values of $h_{2\phi}$, based on these constants, agreed with the experimental data within an error of $\pm 15\%$. Table 1 shows the ranges of Reynolds and Prandtl numbers for which the correlations are valid.

Table 1 Ranges of Re and Pr.

System	Re	Pr
Water	826 < Re < 2135	4.68 < Pr < 5.64
Nitrobenzene/ Water	819 < Re < 2561	6.59 < Pr < 17.42

Fig. 5 shows the comparison between the Nusselt numbers, obtained from the conducted experiments and the numbers, calculated from the developed correlations. The predicted Nusselt numbers are within $\pm 15\%$ of the experimental values. Observed discrepancies between the measured data and the calculated results may be due to the uncertainties of the correlation and also due to the assignment of average properties for the two-phase mixtures. Further studies are needed to develop better correlations for two-phase convective transfer of polar systems, aromatics, and highly viscous liquids.

CONCLUSIONS

This paper presents experimental data from measurement of the heat transfer coefficient of a mixture of water and nitrobenzene in a spiral plate heat exchanger. The obtained data from the experimental study are compared with the theoretical prediction. New correlations are proposed based on the experimental data, which may be used for practical applications. Further work at higher Reynolds number and for different two-phase systems is in progress.

REFERENCES

1. R.K. Jha, M.R. Rao, *Int. J. Heat Mass Transfer*, **10**, 395 (1967).
2. C.E. Kalb, J.D. Seader, *Int. J. Heat and Mass Transfer*, **15**, 801 (1972).
3. L.-S. Yao, S.A. Berger, *J. Fluid Mech.*, **88** (2), 339 (1978).
4. G. Havas, A. Deak, J. Sawinsky, *The Chem. Eng. J.*, **35**, 61 (1987).
5. T. Lemenand, H. Peerhossaini, *Appl. Therm. Eng.*, **22**, 1717 (2002).
6. J.A.W. Gut, R. Fernandes, P.M. Jose, C.C. Tadani, *Chem. Eng. Sci.*, **59**, 4591 (2004).
7. R.R. Hemamalini, P. Partheeban, J. S.C. Babu, S. Sundaram, *Int. J. Heat Mass Transfer*, **48**, 2911 (2005).
8. R.K. Shah, *Heat Transfer Engineering*, **27**, 3 (2006).
9. N. Paisarn, S. Jamnean, *Int. J. Heat Mass Transfer*, **50**, 444 (2007).
10. A. Marchitto, F. Devia, M. Fossa, G. Guglielmini, C. Schenone, *Int. J. Multiphase Flow*, **34**, 128 (2008).
11. R.H. Perry, D.W. Green, J.O. Maloney, *Perry's Chemical Engineers' Handbook*, Seventh Edition, McGraw-Hill, New York, 1998, pp. 11, 55.
12. C.L. Yaws, *Chemical Properties Handbook*, McGraw-Hill Inc., New York, 1999.

ЕКСПЕРИМЕНТАЛНО ИЗСЛЕДВАНЕ НА РАБОТАТА НА ТОПЛООБМЕННИК СЪС
СПИРАЛНИ ПЛАСТИНИ ПРИ ДВУ-ФАЗНАТА СИСТЕМА ВОДА-НИТРОБЕНЗЕН

С. Сатиян¹, М. Рангараджан², С. Рамачандран³

^{1,2} Департамент по инженерна химия и материалознание, Колеж по инженерство “Амрита”,
Амрита Вишва Видяпетвам, Коимбатор, Тамил Наду, 641 105

³ Департамент по инженерна химия, Колеж по инженерство Ерод Сенгунтхар, Ерод, Тамил Наду,
638057, Индия

Постъпила на 5 февруари, 2010 г., преработена на 23 април, 2010 г.

(Резюме)

В работата са представени резултати от изследване на топлообмена в топлообменник със спирални пластини за дву-фазна система от две несмесващи се течности. Като носещ флуид при изследванията е използвана гореща вода. Като студен флуид е използвана сместа от вода и нитробензен при различни масови съотношения и дебити. Коефициентите на топлообмен за двете фази са корелирани с числата на Рейнолдс и Прандтл по уравнението $Nu = a \cdot (Re)^b \cdot (Pr)^c \cdot (X)^d$. Получените експериментални резултати показват, че при ламинарни режими опитните данни са в съгласие с изведеното уравнение в границите на разсейване от $\pm 15\%$. Тази нова зависимост позволява изчисляването на числото на Нуселт за практически важни случаи.

Effective catalytic synthesis of substituted flavones and chromones using Preyssler and heteropolyacids (HPAs) as catalysts

A. Gharib^{A,B*}, M. Jahangir^A, M. Roshani^A, J. (Hans) W. Scheeren^C

^ADepartment of Chemistry, Islamic Azad University, Mashhad, IRAN

^BAgricultural Research and Service Center, Mashhad, IRAN

^CCluster for Molecular Chemistry, Department of Organic Chemistry, Radboud University, Nijmegen, The Netherlands

Received September 17, 2009; Revised March 5, 2010

We report on the use of Preyssler's anion and heteropolyacids catalysts for obtaining substituted flavones and chromones for the cyclization of 1-(2-hydroxyphenyl)-3-aryl-1,3-propanediones. The reactions were performed using chloroform as solvent at reflux temperature conditions and in the absence of solvent, at 110 °C. We had excellent yields and high selectivity at these conditions. The presented synthetic method is a simple, clean and environmentally friendly alternative for synthesizing substituted flavones and chromones.

Keywords: Catalyst; Chromones; Flavones; Heteropolyacid; Preyssler

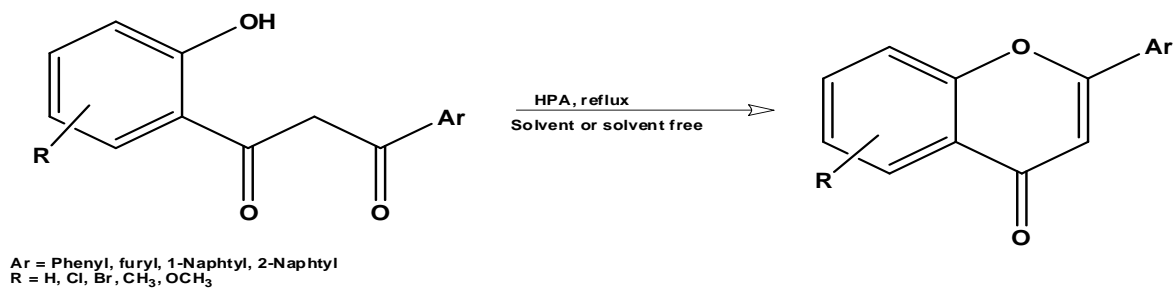
INTRODUCTION

The flavonoid family has chromone structure (4*H*-benzopyran-4-one), found in nature, and the chromones are part of the flavonoid family [1]. Then flavones and chromone compounds have been reported to exhibit multiple biological properties, for example anti-HIV [2], antibacterial, antifungal, anticancer [2–4] and antitumor [5] ones. Some flavonoids inhibit the histamine release from human basophils and rat mast cells [6]. There are some methods for synthesis of the flavones and chromones, such as: the Allan-Robinson strategy, from chalcones, and via the intramolecular Wittig strategy [7, 8]. One of the most common methods involves acylation of *o*-hydroxyacetophenone with aromatic acid chloride, and it yields an aryl ester. Some reaction conditions employed were: the use of the excess sulfuric acid in glacial acetic acid, [8] cationic exchange resins in isopropanol, [9] glacial acetic acid-anhydrous sodium acetate or aqueous potassium carbonate [10]. The most interesting compounds are those that bear an aromatic ring, e.g. phenyl or substituted phenyl group in the oxygenated ring of chromone at C₂ (flavones) or at C₃ (isoflavones). The use of applicable industrial catalyst that is eco-friendly, green and simply recycled in the reaction mixtures, has been under attention in the recent decade. Thus, green chemistry has been defined as a set of principles that reduces or eliminates the use or generation of hazardous substances throughout the entire life of the chemical materials [11]. If we compare technology with

medical care, Green/Sustainable Chemistry (GSC) focuses on precaution (or prevention) rather than on diagnosis and cure [11]. Heteropolyacids (HPAs) are more active catalysts than the conventional inorganic and organic acids for various reactions in solutions [12, 13]. A variety of organic reactions, that are catalyzed by Brønsted acids, such as H₂SO₄, HCl, and other protonic acids, or Lewis acids such as AlCl₃, FeCl₃, etc., proceeded, in the presence of solid heteropolyacids or polyoxometalates, more efficiently, under milder conditions, with greater selectivity, better yields, shorter reaction times, etc. HPAs are widely applicable in the production of fine chemicals such as fragrances, pharmaceuticals, and food [13]. HPAs have been studied extensively as an efficient solid acid catalyst due to their unique advantages such as strong Brønsted acidity, structure alterability and environmental friendliness [13, 14]. Nowadays, most of the studies focus on the catalytic behaviour of the Keggin structured heteropolyacids, [15] among which the 12-tungstophosphoric acid with the H₃PW₁₂O₄₀ formula is known to be a highly active catalyst for a variety of acid-catalyzed reactions [16, 17]. In contrast, the Preyssler-structured heteropolyacid does not attract much research attention. The Preyssler's anion [NaP₅W₃₀O₁₁₀]¹⁴⁻ consists of a cyclic assembly of five PW₆O₂₂ units and displays approximately D_{5h} symmetry (Fig. 1) [18].

The advantages of Preyssler heteropolyacid as a solid acid catalyst may include large number of balanced protons, strong acidity, high hydrothermal stability, and wide pH range stability in the solution

* To whom all correspondence should be sent:
E-mail: E-mail: aligharib5@yahoo.com



Scheme 1. Cyclocondensation Reaction

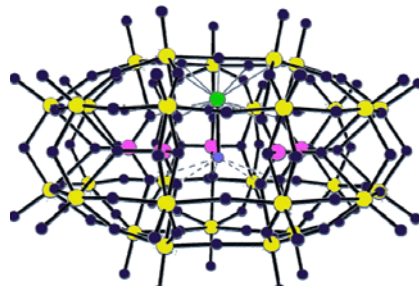


Fig. 1a

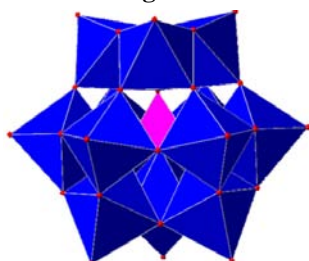


Fig. 1b

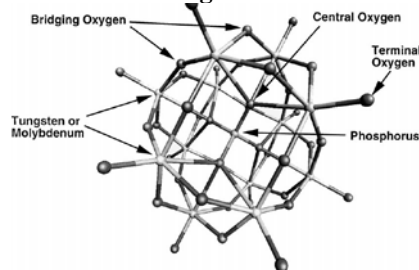


Fig. 1c

Figure. 1. In polyhedral notation, the center of each MO₆ unit is a metal nucleus, and each vertex is an oxygen nucleus. The representative POM structures in polyhedral notation:

1a) Ball-and-stick view of $[M(H_2O)P_5W_{30}O_{110}]^{n-}$, perpendicular to the C₅ axis, showing the position of the internal cation (green) and its associated water molecule (blue). The pink circles are the phosphorus atoms; **1b)** Keggin heteropolyanion structure $[PW_{12}O_{40}]^{3-}$; **1c)** The Keggin unit is the primary structure of the heteropolyacid and contains 12 transition metal atoms (normally tungsten or molybdenum), a central atom (usually phosphorus), and four types of oxygen atoms: central oxygens, terminal oxygens, and two types of bridging oxygens.

[19]. A few of the researchers have investigated the catalytic performances of Preyssler heteropolyacid

in a number of organic synthesis processes [20]. Heteropolyacids have many advantages that them economical and environmentally attractive in both, academic and industrial points of view; they are useful acids and oxidation catalysts in various reactions since their catalytic features can be varied at a molecular level [21]. Among the heteropolyacids, the Keggin type [22] HPAs have been known for a long to be good catalysts for oxidation reactions [23].

RESULTS AND DISCUSSION

Recently, we applied the heteropolyacid catalysts, the Preyssler's anion, the Preyssler mixed addenda, the Keggin and silica-supported Preyssler acid with a load from 10% to 50%, as a reusable, heterogeneous catalyst, to obtain substituted flavones and chromones for the cyclization of 1-(2-hydroxyphenyl)-3-aryl-1,3-propanediones (see Scheme 1 above).

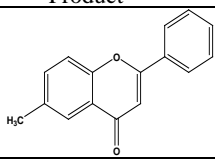
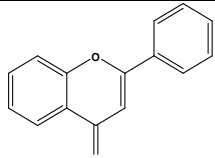
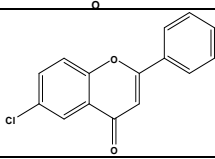
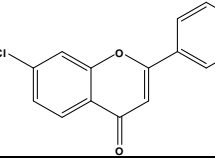
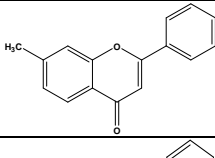
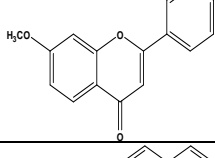
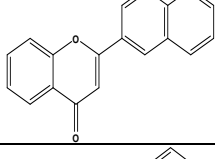
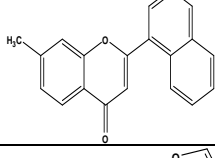
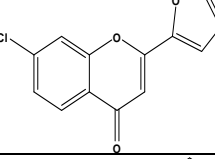
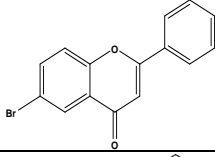
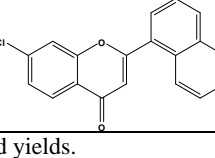
1-(2-hydroxyphenyl)-3-phenyl-1,3-propanedione was used as substrate. Different mole ratios, temperatures, and catalyst type to find the reaction optimum were tested. Cyclization reaction was not detected at room temperature. Heteropolyacid catalysts, used in diones cyclization reaction, were checked in two consecutives, and we obtained similar results and good yields in two consecutives.

Then, heteropolyacid catalysts showed almost constant activity. Also, the experiments performed in solvent-free conditions showed a substantial reduction of the reaction times. The yields of flavones were similar to those of chromones (see Tables 1 and 2 below).

This synthesis was carried out in the presence of solvent and without solvent. We obtained important results, and the yields with solvent and free solvent are very similar (Tables 1 and 2).

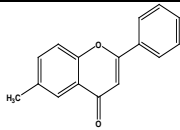
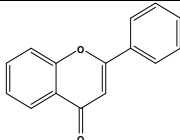
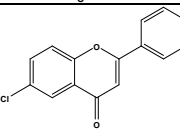
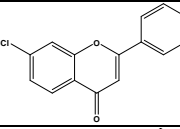
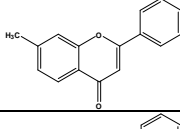
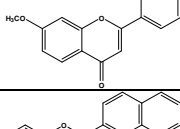
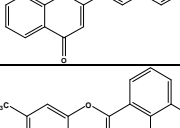
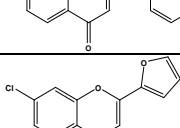
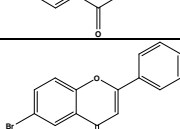
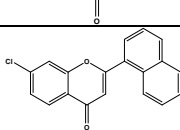
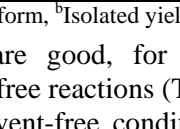
The catalyst mole ratio has not any effect on the improvement of the reaction and yields. In all the cases, the desired products were obtained at high selectivity, almost free of secondary products. We also carried out this synthesis in the presence of a solvent (Table 2). The reaction time is longer but the

Table 1. Preparation of flavones and chromones using heteropolyacid catalysts, Preyssler $H_{14}[NaP_5W_{30}O_{110}]$, $(H_{14}P_5)$, $H_{14}[NaP_5W_{29}MoO_{110}]$, $(H_{14}-P_5Mo)$, and Keggin $H_3[PW_{12}O_{40}]$ at reflux, solvent-free conditions

Entry	Product	^a Time(min)	^a Yield, %	^a Yield, % PW	^a Yield, % PW
1		30	94	92	87
2		30	96	94	88
3		30	95	92	86
4		30	94	90	86
5		30	95	90	87
6		45	91	88	84
7		45	96	92	87
8		50	97	93	89
9		50	95	90	87
10		50	91	88	86
11		50	90	80	84

^aSolvent-free, ^aIsolated yields.

Table 2. Preparation of flavones and chromones using supported Preyssler catalysts $H_{14}[NaP_5W_{30}O_{110}]$, ($H_{14}P_5/SiO_2$ 50%, $H_{14}P_5/SiO_2$ 40%, $H_{14}P_5/SiO_2$ 30%) at reflux, solvent conditions (Solvent = chloroform, Temperature = 62 °C)

Entry	Product	^b Time (min)	^b Yield(%)		
			$H_{14}P_5/SiO_2$ (50%)	$H_{14}P_5/SiO_2$ (40%)	$H_{14}P_5/SiO_2$ (30%)
1		150	91	89	82
2		150	94	91	83
3		180	91	88	82
4		180	90	88	81
5		120	91	87	80
6		120	86	83	76
7		210	93	91	83
8		210	93	89	82
9		210	91	89	80
10		120	85	83	74
11		210	84	82	74

^bIn chloroform, ^bIsolated yields.

yields are good, for both, using solvent and solvent-free reactions (Tables 1 and 2).

The solvent-free conditions are more suitable in the preparation of flavones and chromones because this system is green, clean, and environmentally friendly. All compounds were characterized by melting point, ^{13}C NMR and 1H NMR spectra (Table 3).

The characterisation of flavones provides an ideal application for NMR spectra with the typical skeleton, represented in Figure 2.

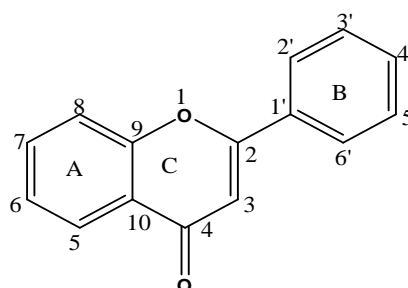
**Fig. 2.** Skeleton structure of the flavonoids, showing the numbering system.

Table 3. Spectral data for compounds of substituted flavones and chromones.

Entry	Compound	¹ H NMR δ (ppm)	Solvent (CDCl ₃)	M.p(°C)
2	6-Chloroflavone	6.85 (s, 1H), 7.54-7.57 (m, 4H), 7.66 (dd, 1H, J= 2.5, 8.8 Hz), 7.91-7.93 (m, 2H), 8.20 (d, 1H, J= 2.6 Hz)		185–186 Lit.27 (183–184)
3	7-Chloroflavone	6.83 (s, 1H), 7.42 (dd, 1H, J= 1.9, 8.4 Hz), 7.52-7.56 (m, 3H), 7.62 (d, 1H, J= 1.9 Hz), 7.90-7.92 (m, 2H), 8.23 (d, 1H, J= 8.4 Hz)		159–160 Lit.28 (156–157)
4	6-Methylflavone	2.46 (s, 3H), 6.83 (s, 1H), 7.46-7.54 (m, 5H), 7.92-7.94 (m, 2H), 8.04 (s, 1H)		120–121 Lit.29;(122–123)
5	7-Methylflavone	2.45 (s, 3H), 6.76 (s, 1H), 7.20 (d, 1H, J= 9.9 Hz), 7.30 (s, 1H), 7.40-7.54 (m, 3H), 7.91-7.97 (m, 2H), 8.10 (d, 1H, J= 9.9 Hz)		122–124 Lit.30(120)
6	7-Methoxyflavone	3.93 (s, 3H), 6.97 (s, 1H), 7.05 (dd, 1H, J= 2.4, 8.8 Hz), 7.34 (d, 1H, J= 2.4 Hz), 7.58-7.61 (m, 3H), 7.94 (d, 1H, J= 8.8 Hz), 8.05-8.10 (m, 2H)		109–110 Lit.30(110)
7	6-Bromoflavone	6.83 (s, 1H), 7.52-7.54 (m, 4H), 7.84 (dd, 1H, J= 2.4, 8.3 Hz), 7.89-7.93 (m, 2H), 8.35 (d, 1H, J= 2.4 Hz)		190–191 Lit.31 (189–190)
8	2-(2-Naphthyl)chromone	6.95 (s, 1H), 7.44 (ddd, 1H, J= 1.6, 6.6, 7.9 Hz), 7.54-7.59 (m, 2H), 7.64 (d, 1H, J= 8.0 Hz), 7.74 (ddd, 1H, J= 1.6, 6.6, 7.9 Hz), 7.87-8.05 (m, 4H), 8.22 (dd, 1H, J= 1.5, 7.9 Hz), 8.46 (s, 1H)		162–163 Lit.30 (164–165)
9	7-Methyl-2-(1-naphthyl)chromone	2.50 (s, 3H), 6.65 (s, 1H), 7.26 (d, 1H, J= 9.3 Hz), 7.33 (s, 1H), 7.54-7.60 (m, 3H), 7.75 (dd, 1H, J= 0.8, 6.7 Hz), 7.92-7.95 (m, 1H), 8.03 (d, 1H, J= 8.3 Hz), 8.11-8.15 (m, 1H), 8.16 (d, 1H, J= 8.1 Hz)		162–163
10	7-Chloro-2-(1-naphthyl)chromone	6.70 (s, 1H), 7.45 (dd, 1H, J= 1.9, 8.5 Hz), 7.58-7.64 (m, 4H), 7.78 (dd, 1H, J= 1.1, 7.2 Hz), 7.97-7.99 (m, 1H), 8.05 (d, 1H, J= 8.2 Hz), 8.12-8.15 (m, 1H), 8.27 (d, 1H, J= 8.6 Hz)		198–199 Lit.30(198-199)
11	2-(2-Furyl)chromone	6.58-6.60 (m, 1H), 6.73 (s, 1H), 7.12 (d, 1H, J= 3.4 Hz), 7.39 (s, 1H), 7.46 (d, 1H, J= 8.3 Hz), 7.61-7.67 (m, 2H), 8.21 (dd, 1H, J= 1.2, 7.5 Hz)		134–135 Lit.32(135)

Flavones are a class of natural substances which occur frequently in plants and which have 15 C atoms in their framework. The nine double-bond equivalents which are contained in the empirical formula, ¹H, signals in the region appropriate for shielded benzene ring protons (5.9-6.9 ppm). The ¹H NMR spectra of flavones showed a singlet at 6.55-6.8 due to 1H of 3H, i.e. pyrone ring; it is the characteristic singlet for flavones. The multiple at 7.1-7.9 is due to aromatic protons. The patterns of the aromatic protons reveal the nature of substitution of the various aromatic systems. The chemical shifts of the protons of rings A and B are independent one from another but are affected by ring C. Peaks arising from A occur upfield, and are easily recognised, therefore examination of an unfamiliar spectrum usually starts with recognition of these peaks. Remaining peaks in the aromatic region reveal the pattern of oxygenation of ring B and confirm the nature of ring C. The C-6 and C-8 resonances in flavones appear at between 92 and 100 ppm with C-6 downfield relative to C-8 resonance. The ¹H NMR spectrum shows that the presence of the double bond in ring C of flavones causes a marked downfield shift of the 6,8 protons, producing a two-doublet pattern. In flavones, the presence of the C-ring double bond causes shift of the 2',6'-protons and the spectrum shows the two complex multiplets, one centered at ¹H 8.0 (2',6') and the other at ¹H 7.6 (3',4',5'). In the reactions,

spectroscopic data (¹³C NMR) for authentic samples are as follows:

Flavone: ¹³C NMR (100 MHz, CDCl₃):

δ = 107.3 (C - 3), 117.9 (C - 8), 123.7 (C - 10), 124.9 and 125.5 (C - 6 or C - 5), 126.0 (C - 2' and C - 6'), 129.0 (C - 3' and C - 5'), 131.8 (C - 1' and C - 4'), 133.5 (C - 7), 155.9 (C - 9), 163.1 (C - 2), 177.9 (C=O).

7-methoxyflavone : ¹³C NMR (100 MHz, CDCl₃): δ= 56.3 (CH₃-O), 101.1 (C - 8), 106.9 (C - 3), 114.9 (C - 6), 117.3 (C - 10), 126.3 and 126.4 ((C - 2' and C - 6') or C - 5), 129.3 (C - 3' and C - 5'), 131.3 and 131.8 (C - 1' or C - 4'), 157.7 (C - 9), 162.3 (C - 2), 164.1 (C - 7), 176.6 (C=O).

6-Chloroflavone : ¹³C NMR (100 MHz, CDCl₃): δ = 107.5 (C - 3), 119.9 (C - 8), 125.0 (C - 5), 125.2 (C - 10), 126.3 (C - 2' and C - 6'), 129.1 (C - 3' and C - 5'), 131.2 and 131.4 (C - 6 or C - 1'), 131.9 (C - 4'), 134.0 (C - 7), 154.5 (C - 9), 163.6 (C - 2), 177.2 (C=O).

6-methylflavone : ¹³C NMR (100 MHz, CDCl₃): δ= 22.0 (CH₃), 107.5 (C - 3), 118.0 (C - 8), 122.0 (C - 10), 126.0 (C - 5), 127.2 (C - 2' and C - 6'), 129.0 (C - 3' and C - 5'), 131.7 and 132.0 (C - 4' or C - 1'), 135.2 (C - 6), 145.1 (C - 7), 156.3 (C - 9), 163.2 (C - 2), 178.2 (C=O).

CATALYST REUSABILITY

The catalyst could be recovered by a simple filtration at the end of the reaction. The recycled

catalyst could be washed with dichloromethane and used in a second run of the reaction process.

Catalyst preparations

All the chemicals were purchased from Merck Company. All the chemical compounds and Keggin type heteropolyacids were acquired from commercial sources. Preyssler, $H_{14}[NaP_5W_{30}O_{110}]$, ($H_{14}-P_5$), $H_{14}[NaP_5W_{29}MoO_{110}]$, ($H_{14}-P_5Mo$) and supported Preyssler on silica, $H_{14}P_5/SiO_2$ were prepared in accordance with the earlier reports [24-27].

EXPERIMENTAL

Instruments

The 1H -NMR spectra were recorded on an FT-NMR Bruker 250 MHz Aspect 3000 spectrometer, and 1H NMR and ^{13}C NMR spectra were recorded at 298°K. The melting points were recorded on an Electrothermal type 9100 melting point apparatus, and were uncorrected. Chemical shifts were reported in ppm (δ -scale) relative to the internal standard TMS (0.00 ppm); the solvent was used as a reference. TLC was carried out with E. Merck Silica gel GOF-254 (0.25 mm thickness) pre-coated tic plates. The column chromatography was carried out with the silica gel (Kieselgel 60, 70-230 mesh, E. Merck).

The progress of the reaction was monitored by TLC and all the products were identified by comparison of their physical and spectroscopic data with those reported for authentic samples. All the yields were calculated from crystallized products.

GENERAL PROCEDURES

Preparation of substituted flavones and chromones without solvent

1,3-diketone (0.7 mmol) was dissolved in catalyst (0.3 mmol), then the mixture was stirred at reflux temperature (110 °C) for different time periods (Table 1), and this mixture was extracted (via) warm toluene (3×5 mL). The extracted compounds were washed, first with 3M NaOH, then with H_2O , and dried over $MgSO_4$. The pure products were obtained by column chromatography. The residue was isolated by the chromatograph on the silica column and thus favones and chromones were obtained. The residue was chromatographed on the silica column ($CH_2Cl_2:CHCl_3=70:30$) and two components were obtained. All the solid crude products were recrystallized from methanol.

Preparation of substituted flavones and chromones in solvent

1,3-diketone (0.7 mmol) was dissolved in chloroform (5 mL), then the catalyst (0.3 mmol) was added to the solution. The reaction mixture was heated and stirred at reflux temperature (60–62°C) for different time periods (Table 2). After completion of the reaction, the catalyst was filtered off, washed with ethyl ether (3×10 mL), and the solvent was subjected to evaporation. The extracts were combined and washed with 3M NaOH, then with H_2O , and dried over $MgSO_4$. The organic solution was concentrated in the vacuum. The pure products were obtained by column chromatography. The residue was isolated by the chromatograph on the silica column and thus favones and chromones were obtained. The residue was chromatographed on the silica column ($CH_2Cl_2:CHCl_3 =70:30$) and two components were obtained. All the solid crude products were recrystallized from ethanol. All products were identified with those, reported for authentic samples, by comparison of their physical and spectroscopic data.

CONCLUSION

The Preyssler silica supported catalyst and Keggin heteropolyacid catalysts provide very good and appropriate yields in this reaction. These catalysts are reusable, recyclable, and they separate and recover easily for further use; they are green, environmentally friendly, inexpensive, non-corrosive, solid - with higher acidic strength than the mineral acid; they are of high thermal stability; they produce low waste and oxidation, and reduced effectiveness. The catalyst properties are constant. The catalysts, based on the supported tungsto-phosphoric and molybdo-phosphoric acids, showed catalytic activity for the reaction of cyclization of 1-(2-hydroxyphenyl)-3-aryl-1,3-propanediones. The conversion to flavones and substituted chromones was in general higher in homogeneous phase than that observed for the supported catalysts.

Acknowledgements: *The authors are grateful to the Agricultural Research & Service Center, Mashhad, Feyzabad, Iran and Mashhad Islamic Azad University and Chemistry Department, the University of Oslo, Norway and the National Research Council, Canada, for all the support to this work, and with special thanks from Professor Dr. J. (Hans) W. Scheeren from Organic Chemistry Department, Radboud University Nijmegen, The Netherlands.*

REFERENCES

1. S. Yano, H. Tachibana and K. Yamada, *J. Agric. Food Chem.*, **53**, 1812 (2005).
2. J. Wu, X. Wang, Y. Yi and K. Lee, *Bioorg. Med. Chem. Lett.*, **13**, 1813 (2003).
3. H. Chu, H. Wu and Y. Lee, *Tetrahedron.*, **60**, 2647 (2004).
4. M. Lee, B. JagadeesH, Manik R, Pullagurla, D. Małgorzata, L. Bryan and A. Glennon Richard. *Bioorg. Med. Chem.*, **13**, 1707 (2005).
5. S. Martens, and A. Mithöfer, *Phytochemistry.*, **66**, 2399 (2005).
6. P. Briet, J. J. Berthelon, F. Collonges and Fr. Demande Fr. FR Patent., 2, 536, 397 (1984).
7. M. Morimoto, K. Tanimoto, S. Nakano, T. Ozaki, A. Nakano and K. Komai, *J. Agric. Food Chem.*, **51**, 389 (2003).
8. D. Barton and W. Ollis, *Comprehensive Organic Chemistry. The Synthesis and Reactions of Organic Compounds*, Vol. 4, Pergamon, Oxford, 1984, p.659.
9. A. Ganguly, S. Kaur, P. Mahata, D. Biswas, B. Pramanik and T. Chan, *Tetrahedron Lett.*, **46**, 4119 (2005).
10. Y. Hoshino and N. Takeno, *Bull. Chem. Soc. Jpn.*, **60**, 1919 (1987).
11. S. Saxena, J. Makrandi and S. Grover, *Synthesis.*, 697 (1985).
12. P. T. Anastas and J. C. Warner, *Green Chemistry, Theory and Practice*, Oxford University Press, 1998.
13. I. V. Kozhevnikov, in: E. Derouane (Ed.), *Catalysts for Fine Chemical Synthesis, Catalysis by Polyoxometalates 2*, Wiley, New York, 2002.
14. M. Kimura, T. Nakato and T. Okuhara, *Appl. Catal. A Gen.*, **165**, 227 (1997).
15. T. Nakato, M. Kimura, S. Nakata and T. Okuhara, *Langmuir.*, **14**, 319 (1998).
16. I. V. Kozhevnikov, *Catal. Rev. Sci. Eng.*, **37**, 311 (1995).
17. C.L. Chill and C. M. Prosser-McCartha, *Coord. Chem. Rev.*, **143**, 407 (1995).
18. M. A. Barteau, J. E. Lyons and I. K. Song, *J. Catal.*, **216**, 236 (2003).
19. K. Eguchi, T. Seiyama, N. Yamazoe, S. Katsuki and H. Taketa, *J. Catal.*, **111**, 336 (1998).
20. M. T. Pope and Jr G. M. Varga, *Inorg. Chem.*, **5**, 1249 (1996).
21. I. K. Song and M. A. Barteau, *J. Mol. Catal. A.*, **212**, 229 (2004).
22. T. Okuhara, N. Mizuno and M. Misono, *Advances in Catalysis. Catalytic Chemistry of Heteropoly compounds.* **41**, 113 (1996).
23. N. Mizuno and M. Misono, *Heterogeneous Catalysis. Chem. Rev.*, **98**, 199 (1998).
24. G. Romanelli, J. C. Autino, G. Baronetti and H. Thomas, *Molecules.*, **6**, 1006 (2001).
25. M. H. Alizadeh, S. P. Harmalker, Y. Jeannin, J. Martin-Frere and M. T. Pope, *J. Am. Chem. Soc.*, **107**, 2662 (1958).
26. M. H. Alizadeh, H. Razavi, F. F. Bamoharram and K. Daneshvar, *J. Mol. Catal.*, **206**, 89 (2003).
27. M. H. Alizadeh, H. Razavi, F. F. Bamoharram and M. H. Hassanzadeh, *Kinet. Catal.*, **44**, 524 (2003).

ЕФЕКТИВНА СИНТЕЗА НА СУБСТИТУИРАНИ ФЛАВОНИ И ХРОМОНИ ЧРЕЗ ПРАЙСЛЕРОВИ АНИОНИ И ХЕТЕРО-ПОЛИКИСЕЛИНИ КАТО КАТАЛИЗАТОРИ

А. Гариб^{АВ}, М. Джахангир^А, М. Рошани^А, Й.(Ханс) Схеерен^В

^{А)} Департамент по химия, Ислямски университет „Азад“, Иран

^{В)} Земеделски изследователски и служебен център, Маишад, Иран

^{В)} Обединение по молекулна химия, Департамент по органична химия, Университет „Радбауд“, Наймехен, Нидерландия

Постъпила на 17 септември 2009 г., Преработена на 5 март 2010 г.

(Резюме)

Съобщава се за използването на Прайслерови аниони и хетеро-поликиселини като катализатори на получаването на флавони и хромони чрез циклизирането на 1-(2-хидроксифенил)-3-арил-1,3-пропандиони. Реакциите се извършват, като се използва хлороформ като разтворител с рецикулация или в отсъствие на разтворител при 110°C. Постигнати са отлични добиви и висока селективност. Настоящият метод е проста, чиста и съобразена с околната среда алтернатива за синтезата на субституирани флавони и хромони.

A method for catalytic synthesis of convenient thioxanthone crown ethers using Wells-Dawson, $H_6[P_2W_{18}O_{62}]$ and Preyssler $H_{14}[NaP_5W_{30}O_{110}]$, heteropolyacid catalysts

A. Gharib^{A,B*}, M. Jahangir^A, M. Roshani^A, J. (Hans) W. Scheeren^C

^ADepartment of Chemistry, Islamic Azad University, Mashhad, IRAN

^BAgricultural Research and Service Center, Mashhad, IRAN

^CCluster for Molecular Chemistry, Department of Organic Chemistry, Radboud University, Nijmegen, The Netherlands

Received September 17, 2009, Revised May 10, 2010

Heteropolyacids (HPAs) were used as an effective catalyst for the synthesis of thioxanthone crown ethers from the reaction of thiosalicylic acid and benzocrown ethers. This reaction was carried out subsequently via intramolecular electrophilic cyclization. The reaction was in mild and clean conditions, and has high selectivity with good yields.

Keywords: Heteropolyacid; Wells-Dawson; Preyssler; Thioxanthone; Crown ether; Catalyst

INTRODUCTION

The reactions, catalyzed by heteropolyacids (HPAs) and polyoxometalates (POMs) in both heterogeneous and homogeneous systems, have been reviewed by various authors [1]. HPAs have several advantages as catalysts, which make them economical and environmentally attractive in both academic and industrial points. They have a very strong Brønsted acidity, approaching the super-acid region. They have significantly higher catalytic activity than that of strong mineral or organic acids, such as H_2SO_4 , HCl, HNO_3 , TsOH, TfOH, $MeSO_3H$, and conventional catalysts, such as alumina, silica gel, zeolites, clay, and acidic Amberlyst-15 [2]. Heteropolyacids (HPAs) are strong Brønsted acids composed of heteropolyanions and protons as the counter cations and promising solid acids to replace environmentally harmful liquid acid catalysts [3-5]. Among HPAs, the Keggin-type HPAs have attracted much interest since they possess strong acidity, while a few studies have been published on the use of Preyssler's anion heteropolyacids. Even, in some cases there have been reports of no catalytic activity [6]. The important advantages of this polyanion, in comparison to the Keggin heteropolyacids

are: a) more thermal stability, b) more hydrolytic stability (pH=0–12), and c) larger number of protons. These properties are very important in catalytic processes especially in synthesis of drugs. Crown ethers have enjoyed widespread use in various areas of science and technology [7] ever since the first preparation of the ligands by Pedersen [8]. Thioxanthone derivatives are potential anti-cancer drugs and they are an important class of molecules and are a common heterocyclic scaffold in biologically active and medicinally significant compounds. Thioxanthone ring is the core structure of a wide variety of naturally occurring and synthetic compounds that exhibit extraordinary anti-tumor activity [9] and methods for the synthesis of thioxanthenes are used in concentrated sulfuric acid at room or high temperature [9].

RESULTS AND DISCUSSION

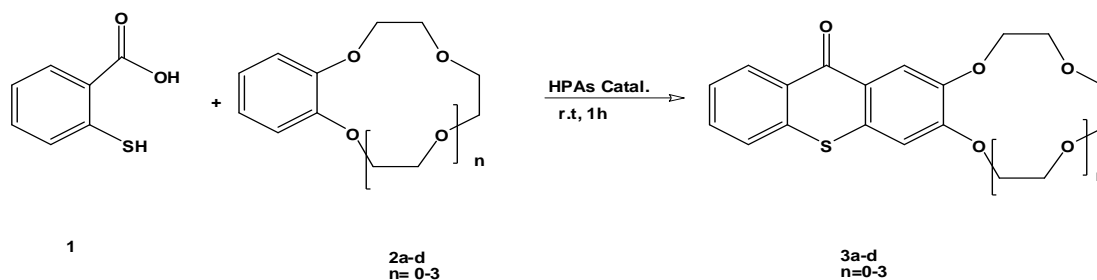
We wish to report a catalytic convenient synthesis of thioxanthone crown ether with reaction of thiosalicylic acid and benzo-15-Crown-5 (**2c**) in the presence of Wells-Dawson, various heteropolyacids, HY-zeolit, H_3PO_4 , $C_6H_5SO_3H$ and H_2SO_4 at room temperature (Scheme 1 and 2).

In the synthesis of thioxanthone crown ether, the results were compared with the yields of other catalysts types at room temperature (Table 1).

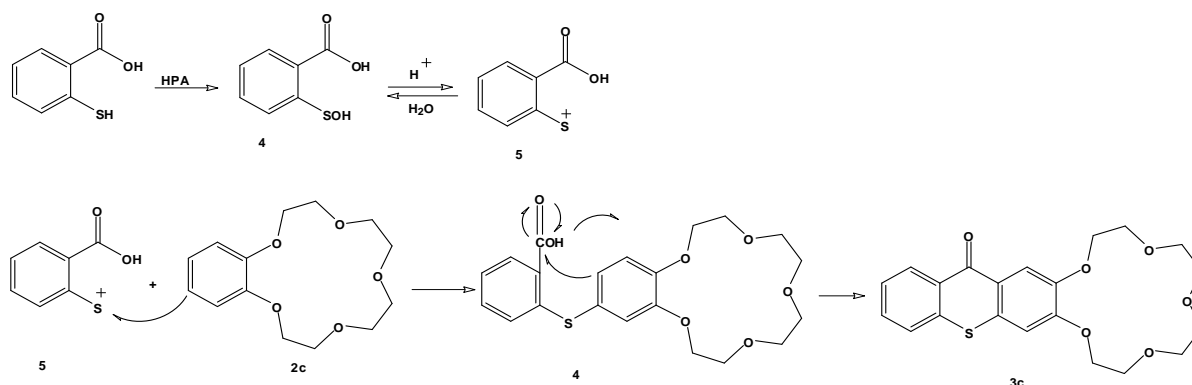
* To whom all correspondence should be sent:
E-mail: E-mail: : aligharib5@yahoo.com

We developed our researches in this synthesis and used various crown ethers with the same conditions in the synthetic reaction, and obtained

the corresponding thioxanthone crown ethers in good yields (Scheme 2) (Table 2).



Scheme 1. Synthesis of convenient thioxanthone crown ethers.



Scheme 2. The mechanism and the synthesis of convenient thioxanthone crown ethers using Wells-Dawson, $H_6[P_2W_{18}O_{62}]$ and Preyssler $H_{14}[NaP_5W_{30}O_{110}]$ heteropolyacids catalysts.

Table 1. The yields of **3a-d** (5 mmol) in the presence of Preyssler catalyst $H_{14}[NaP_5W_{30}O_{110}]$, ($H_{14}-P_5$).

Entry	n (Substrate)	Time (h)	^a Yield [%]
1	0	1.5	94
2	1	1.5	91
3	2	1.5	77.5
4	3	1.5	72

^aIsolated yield

Table 2. The yields of **3a** (5 mmol) in the presence of various catalysts.

Entry	Catalyst	Time (h)	^a Yield [%]
1	$H_3[PMo_{12}O_{40}]$	2	74
2	$H_3[PW_{12}O_{40}]$	2	82
3	$H_4[SiW_{12}O_{40}]$	2	79
4	$H_6[P_2W_{18}O_{62}]$	1.5	86
5	$H_4[SiMo_{12}O_{40}]$	2	71.5
6	HY-zeolite	3	71
7	H_3PO_4	2	55
8	H_2SO_4	2	69
9	$C_6H_5SO_3H$	2	67

^aYields are analyzed by GC and products isolated.

The Wells-Dawson heteropolyacid and various heteropolyacid catalysts have very straight acidic and oxidation properties because the thiosalicylic acid **1** is oxidized to sulfinic acid by heteropolyacid and this compound

decomposes to sulfenium ion 2,3,5,6-Tetrahydro-14*H*-thioxantheno[2,3-*b*] [1,4,7]trioxonin-14-one (**3a**), [10] and when using electrophilic substitution of sulfenium ion with the benzo-15-crown-5 (**2c**) gave intermediate thioether, and then with the cyclization of thioether gave the thioxanthone-15-crown-5 ether (**3c**) (Scheme 2). The results in Table 1 showed that the yields of the products (**3a-d**) were good and so the yields of the products with $n=0, 1$ (**3a** and **3b**) were higher than other products (entry 1, 2).

In this reaction which is used from Preyssler heteropolyacid catalyst at room temperature, and with acidic protons [11] has more straight acidic properties than other heteropolyacids and catalysts, and when Preyssler catalyst was used in this reaction, its time was 1.5 h, but when H_2SO_4 , H_3PO_4 , HY-zeolit, $C_6H_5SO_3H$ and Keggin heteropolyacids were used in the reaction, the reaction times were 2 and 3 h (Table 2, entries 1–3, 5–9) and the yield of the product (**3a**) was lower than when using Wells-Dawson heteropolyacid and Preyssler catalysts (Table 1, entry 1, Table 2, entry 4). There is a

proposed mechanism, an electrophilic substitution of sulfenium ion with the benzo-15-crown-5 (**2c**) would then give intermediate thioether and the cyclization of thioether gives the thioxanthone-15-crown-5 ether (**3c**) (Scheme 4). Thioxanthone crown ether yields depended

directly upon the sulfuric acid concentration because sulfonation of **2c** competes with the generation of sulfenium ion (**5**) and subsequent electrophilic substitution [12]. The spectral data for the compounds **3a-3d** are presented in Table 3.

Table 3. Spectral data of the compounds (**3a-3d**).

Compound	Spectral data
2,3,5,6-Tetrahydro-14H-thioxantheno [2,3- <i>b</i>][1,4,7]trioxonin-14-one (3a)	IR, $\tilde{\nu}/\text{cm}^{-1}$: 2900 (s), 1630 (s), 1590 (s), 1490 (s), 1300 (s), 1125 (s), 1045 (s), 870 (s), 740 (s) $^1\text{H NMR}$ (DMSO- d_6), δ : 3.92(m, 4H), 4.31 (m, 2H), 4.70 (m, 2H), 7.07 (s, 1H), 7.52 (m, 3H), 8.25 (s, 1H), 8.55 (d, 1H, J=7.4 Hz) MS, m/z ($I_r/\%$): 314 (M+)
2,3,5,6,8,9-Hexahydro-17H-thioxantheno[2,3- <i>b</i>][1,4,7,10]tetraoxacyclododecin-17-one (3b)	IR, $\tilde{\nu}/\text{cm}^{-1}$: 2873 (s), 1635 (s), 1593 (s), 1505 (s), 1440 (s), 1292(s), 1269 (s), 1254 (s), 1149 (s), 1115 (s) 745 (s) $^1\text{H NMR}$ (DMSO- d_6), δ : 3.78 (s,4H), 3.85 (m, 4H), 3.94 (m, 2H), 4.30 (s, 2H), 7.06 (s, 3H),7.46 (t, 1H, J=7.2 Hz), 7.58 (m, 2H), 8.20 (s, 1H), 8.59 (d, 1H J=7.4 Hz) MS, m/z ($I_r/\%$): 358 (M+)
2,3,5,6,8,9,11,12-Octahydro-20H-thioxantheno[2,3- <i>b</i>] [1,4,7,10,13]pentaoxacyclopentadecin-20-one (3c)	IR, $\tilde{\nu}/\text{cm}^{-1}$: 2875 (s), 1595 (s) ,1505 (s), 1446 (s), 1409 (s), 1261 (s), 1210 (s), 1135 (s), 1085 (s), 935 (s) 740 (s) $^1\text{H NMR}$ (DMSO- d_6), δ : 3.35 (s, 8H), 3.63 (s, 4H), 3.81 (s, 2H), 4.20 (s, 2H), 7.35 (s, 3H), 7.57 (t, 1H, J=7.5 Hz), 7.74 (t, 1H, J=7.5. Hz), 7.82 (d, 1H, J=7.9. Hz), 7.86 (s, 1H), 8.55 (d, 1H, J=7.9. Hz) MS, m/z ($I_r/\%$): 402 (M+)
2,3,5,6,8,9,11,12,14,15-Decahydro-23H-thioxantheno[2,3- <i>b</i>] [1,4,7,10,13,16]hexaoxacyclooctadecin-23-one (3d)	IR, $\tilde{\nu}/\text{cm}^{-1}$: 2925(s), 2860 (s), 1685 (s), 1589 (s), 1505 (s), 1415 (s), 1260 (s), 1120 (s), 950 (s), 740 (s) $^1\text{H NMR}$ (DMSO- d_6), δ : 3.75 (s, 8H), 3.97 (s, 2H), 4.28 (s, 2H), 6.92 (s, 1H), 7.50 (m, 2H), 7.56 (s, 1H), 8.02 (s, 1H), 8.60 (d, 1H, J=7.5. Hz) MS, m/z ($I_r/\%$): 446 (M+)

All compounds were characterized by mass, IR and $^1\text{H NMR}$ spectra.

EXPRIMENTAL

The chemical materials were purchased commercially. $^1\text{H NMR}$ spectra were recorded in CDCl_3 on a FT NMR Bruker 100 M Hz Aspect 3000 spectrometer. IR spectra were obtained with a Bruker 500 scientific spectrometer. The mass spectra were scanned on a Varian Mat. CH-7 at 70 ev.

Preparation of Preyssler catalyst, $\text{H}_{14}[\text{NaP}_5\text{W}_{30}\text{O}_{110}]$ ($\text{H}_{14}\text{-P}_5$)

$\text{H}_{14}\text{-P}_5$ was prepared by passage of a solution of the potassium salt in water through a column (50 cm×1 cm) of Dowex50W×8 in the H^+ form

and evaporation of the elute to dryness under vacuum [13].

Preparation of Wells-Dawson species $\text{H}_6[\text{P}_2\text{W}_{18}\text{O}_{62}]$

The Wells-Dawson species $\text{H}_6[\text{P}_2\text{W}_{18}\text{O}_{62}]$ was prepared as described elsewhere [11], from an aqueous solution of $\alpha/\beta \text{K}_6\text{P}_2\text{W}_{18}\text{O}_{62} \cdot 10\text{H}_2\text{O}$ salt which was treated with ether and concentrated (37%) HCl solution.

General procedure for the synthesis of thioxanthone crown ethers

A mixture of thiosalicylic acid (1 mmol), the appropriate crown ether (5 mmol) and catalyst (0.05 mmol) was added to a round-bottomed

flask, then this mixture was stirred and refluxed at room temperature for one hour. The reaction progress was monitored by TLC. After completion of the reaction, the mixture was poured onto ice and the product was filtered, washed with water and then washed with a saturated aqueous solution of sodium hydrogen carbonate until alkali-free and dried under vacuum over night at room temperature to yield product as shown in Table 2.

2,3,5,6-tetrahydro-1,4,7-benzotrioxonine (**2a**) was provided in accordance to the literature [14] and this product was known and characterized by comparison of their physical and ¹HNMR, IR and mass spectral data with those reported. The preparation of the benzo-9-crown-3 used as precursors has been described in accordance to the literature [15].

CONCLUSION

In summary, we have developed a novel, ecofriendly, and efficient method for the synthesis of thioxanthone crown ethers using HPAs as an inexpensive, green, and reusable catalyst. The advantages of the present method are simplicity of workup, high yields, short reaction times, recyclability of the catalyst.

Acknowledgments: *The authors are grateful to the Agricultural Research & Service Center, Mashhad, Feyzabad, Iran and Mashhad Islamic Azad University and Chemistry Department, the University of Oslo, Norway and the National Research Council, Canada for the support of this work and with special thanks from Professor. Dr. J. (Hans) W. Scheeren from the Organic Chemistry Department, Radboud University Nijmegen, the Netherlands.*

REFERENCES

1. T. Okuhara, N. Mizuno and M. Misono, *Advances in Catalysis. Catalytic Chemistry of Heteropoly compounds.*, **41**, 113 (1996).
2. M. Misono, N. Mizuno, K. Katamura, A. Kasai, Y. Konishi, K. Sakata, T. Okuhara and Y. Yoneda, *Bull. Chem. Soc. Jpn.*, **55**, 400 (1982).
3. I. V. Kozhevnikov, *Chem. Rev.*, **98**, 171 (1998).
4. Y. Izumi, K. Urabe, M. Onaka, *Zeolite, Clay and Heteropoly Acids in Organic Synthesis*, Vol.37, Kodansha/VCH, Tokyo, 1992, p.311.
5. I. V. Kozhevnikov, *Catal. Rev. Sci. Eng.*, **37**, 311 (1995).
6. M. A. Fox, R. Cardona, E. Gaillard, *J. Am. Chem. Soc.*, **109**, 6347 (1987).
7. S. Patai, *In The Chemistry of Ethers, Crown Ethers, Hydroxyl Groups and Their Sulphur Analogues*; John Wiley & Sons: New York, 1981.
8. C. J. Pedersen, *J. Am. Chem. Soc.*, **89**, 2495 (1967).
9. G. M. Laidlaw, J. C. Collins, S. Archer, D. Rosi and J. W. Schulenberg, *J. Org. Chem.*, **38**, 1743 (1973).
10. B. J. Foster, R. A. Wiegand, S. P. Patricia, M. Lorusso, J. Rake and T. H. Corbett, *Clin. Cancer Res.*, **3**, 2047 (1997).
11. G. Romanelli, J. C. Autino, G. Baronetti and H. Thomas, *Molecules.*, **6**, 1006 (2001).
12. R. E. Benesch, R. Benrsch., *J. Am. Chem. Soc.*, **80**, 1666 (1958).
13. F. F. Bamoharram, M. M. Heravi, M. Roshani, A. Gharib and M. Jahangir, *J. Mol. Catal.*, **252**, 90 (2006).
14. A. P. Krapcho and S. N. Haydar, *J. Heterocyclic Chem.*, **34**, 1637 (1997).
15. G. W. Buchanan, A. B. Driega, A. Moghimi, C. Bensimon and K. Bourque, *Can. J. Chem.*, **71**, 951 (1993).

МЕТОД ЗА СИНТЕЗИРАНЕ НА ПОДХОДЯЩИ ТИОКСАНТОННИ КРАУН-ЕТЕРИ ПРИ
ИЗПОЛЗВАНЕ НА УЕЛС-ДОУСЪН'ОВИ $H_6[P_2W_{18}O_{62}]$ И ПРАЙСЛЕР'ОВИ ХЕТЕРО-
ПОЛИКИСЕЛИНИ $H_{14}[NAP_5W_{30}O_{110}]$ КАТО КАТАЛИЗАТОРИ

А. Гариб^{АВ}, М. Джахангир^А, М. Рошани^А, Й.(Ханс) Схеерен^В

^{А)} Департамент по химия, Ислямски университет „Азад“, Иран

^{В)} Земеделски изследователски и служебен център, Маишад, Иран

^{В)} Обединение по молекулна химия, Департамент по органична химия, Университет „Радбауд“,
Наймехен, Нидерландия

Постъпила на 17 септември 2009 г., преработена на 10 май, 2010 г.

(Резюме)

Хетеро-поликиселините са използвани като ефикасен катализатор за синтезата на тиоксантонови краун-етери чрез реакция между тио-салицилова киселина и бензо-краун-етери. Реакцията се извършва чрез вътрешно-молекулна циклизация и протича при меки условия, с висока селективност и добри добиви.

Kinetic and mechanistic study of bromination of sulfanilic acid with *N*-bromosuccinimide in alkaline medium

P.M. Ramdas Bhandarkar, K.N. Mohana*

Department of Chemistry Studies, University of Mysore, Manasagangothri, Mysore- 570006, India

Received November 23, 2010, Revised April 22, 2010

The sulfanilic acid (*p*-amino benzene sulfonic acid) (SNA) is an important and interesting compound which finds a number of applications in the syntheses of organic dyes. The amide of sulfanilic acid (sulfanilamide) and certain related substituted amides are of considerable medicinal importance as the sulfa drugs. The kinetics of bromination of SNA with *N*-bromosuccinimide (NBS) in NaOH medium has been studied at 308 K. The experimental rate law obtained is $-d[NBS]/dt = [NBS][SNA]^x[OH^-]$ where x is less than unity. The reaction was subjected to changes in concentration of succinimide, the reduction product of NBS, concentration of added neutral salt, as well as to dielectric permittivity and ionic strength of the medium. Solvent isotope effect has been studied using D₂O. The stoichiometry of the reaction has been determined, and the products were identified and characterized. Activation parameters for the overall reactions have been computed using the Arrhenius plot. OBr⁻ has been postulated as the reactive species of NBS. The reaction fails to induce polymerization of added acrylonitrile. The proposed mechanism and the derived rate law are consistent with the observed kinetic data.

Key words: *N*-bromosuccinimide, sulfanilic acid, bromination, alkaline medium.

INTRODUCTION

The Sulfanilic acid (*p*-aminobenzene sulfonic acid) (SNA) is an important and interesting compound, which finds a number of applications in the syntheses of organic dyes [1]. The amide of sulfanilic acid (sulfanilamide) and certain related substituted amides are of considerable medicinal importance as the sulfa drugs. Although they have been supplanted to a wide extent by antibiotics such as penicillin, terramycin, chloromycetin, and aureomycin, the sulfa drugs still have their medical uses, and make up a considerable portion of the output of the pharmaceutical industry [2]. The kinetics of ruthenium (III) catalysed oxidation of sulfanilic acid by hexacyanoferrate(III) in alkaline medium has been studied [3]. In view of this, it becomes important to study sulfanilic acid because of its biological importance and reactivity towards different oxidants. *N*-bromosuccinimide (NBS) is a source of positive halogen, and this reagent has been exploited as an oxidant for a variety of substrates [4-8] in both acidic and alkaline solutions. The use of NBS as an oxidant is extensive in the determination of number of organic compounds [9-12]. However, a little information exists in the literature on NBS reactions, particularly with respect to the oxidation

kinetics of pharmaceuticals [13, 14], which may throw some light on the mechanism [15] of the metabolic conversions in the biological systems. In view of these facts, there is a considerable scope for the study of the reactions with NBS to get better insight of the speciation of NBS reaction models and to understand its redox chemistry in solutions. This paper reports for the first time on the detailed kinetics of SNA bromination with NBS in NaOH medium. The work was carried out with the intention to elucidate the mechanism of the reaction, to put forward the appropriate rate law, to identify the products of the reaction, and to ascertain the reactive species of NBS.

EXPERIMENTAL

Materials

An aqueous solution of NBS was prepared afresh each day from a G.R. Merck sample of the reagent, and its strength was checked by the iodometric method. Sulfanilic acid (Merck) is not only insoluble in organic solvents, but also nearly insoluble in water and in aqueous acids. Sulfanilic acid is soluble in aqueous bases. Therefore the solution of sulfanilic acid was prepared by dissolving an appropriate amount of the sample in warm very dilute alkaline solution. All other reagents, namely sodium hydroxide, sodium perchlorate and succinimide, were of Analar grade.

*To whom all correspondence should be sent:
E-mail: knmsvp@yahoo.com; Phone: + (91) 422 2685000

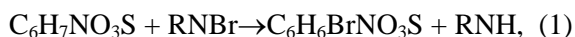
Doubly distilled water was used throughout the investigations.

Kinetic measurements

All kinetic measurements were performed in glass stoppered Pyrex boiling tubes coated black to eliminate the photochemical effects. The reactions were carried out under pseudo-first-order conditions by taking a known excess of $[SNA]_0$ over $[NBS]_0$ at 308 K. Appropriate amounts of SNA, NaOH solutions, sodium perchlorate, and water to keep the total volume constant were equilibrated at constant temperature ($\pm 0.1^\circ\text{C}$). A measured amount of NBS solution also pre-equilibrated at the same temperature was rapidly added to the mixture. The progress of the reaction was monitored by estimating the amount of unconsumed NBS at regular time intervals iodometrically. The course of reaction was studied for at least two half-lives. The pseudo-first-order rate constants (k_{obs}), calculated from the linear plots of $\log [NBS]$ vs. time were reproducible within $\pm 4\%$. Regression analysis of the experimental data to obtain regression coefficient, r was performed using MS Excel.

Stoichiometry and product analysis

Reaction mixtures, containing varying ratios of NBS and SNA in the presence of 0.01 mol dm^{-3} NaOH at 308 K, were kept aside for 48 h, so that the substrate was completely converted into products. Estimation of the unreacted NBS showed that one mole of substrate utilized one mole of NBS, confirming the following stoichiometry:



where $\text{R} = (\text{CH}_2\text{CO})_2$.

The products in the reaction mixture were extracted with ether. The combined ether extract was evaporated and subjected to column chromatography on silicagel. The reduction product of NBS, succinimide (RNH), was detected by spot tests [16] and confirmed by IR absorption bands, as follows RNH: A broad band at 3450 cm^{-1} for NH stretching mode and a sharp band at 1698 cm^{-1} for $\text{C} = \text{O}$ stretching mode. The bromination product of sulfanilic acid was found to be 4-amino 3-bromo benzene sulfonic acid and identified by its IR absorption bands: 3030 cm^{-1} (Aromatic C-H stretch), 3226 cm^{-1} (N-H stretch), 1275 cm^{-1} (C-N stretch) and 588 cm^{-1} (C-Br stretch). Further, it was confirmed by ^1H NMR spectral studies: ^1H NMR (DMSO- d_6 , 400 MHz) δ : 9.74 (s, 1H, OH), 7.85 (s, 1H, Ar-H), 7.62 (d, 1H, Ar-H), 6.63 (d, 1H, Ar-H), 7.62 (s, 2H, NH_2). IR spectrum was recorded on FT-IR spectrometer using KBr pellets. ^1H NMR

spectrum was recorded on Shimadzu AMX 400-Bruker, 400MHz spectrometer using DMSO as a solvent and TMS as internal standard.

RESULTS

The bromination of SNA with NBS was kinetically investigated at several initial concentrations of the reactants in NaOH medium at 308 K. The salient feature obtained in this medium is discussed as follows.

The effect of varying reactant concentrations on the rate

Under pseudo-first-order conditions ($[SNA] \gg [NBS]$) at constant $[\text{NaOH}]$ and temperature, the plots of $\log [NBS]$ vs. time were linear ($r \geq 0.997$), indicating a first-order dependence of the rate on $[NBS]_0$. Table 1 gives the calculated pseudo-first-order rate constants (k_{obs}). Further, the values of k_{obs} calculated from these plots are unaltered with $[NBS]_0$ variation, confirming the first-order dependence on $[NBS]_0$. The rate increased with the $[SNA]_0$ increase (Table 1). A plot of $\log k_{\text{obs}}$ vs. $\log [SNA]$ was linear (Fig. 1; $r = 0.999$) with a slope of 0.72, indicating a fractional-order dependence of the rate on $[SNA]_0$.

Table 1. The effect of varying concentrations of NBS, SNA and NaOH on the reaction rate at 308 K. Ionic strength - $\mu = 0.1 \text{ mol dm}^{-3}$; a - at $\mu = 0.15 \text{ mol dm}^{-3}$; b - at $\mu = 0.25 \text{ mol dm}^{-3}$

$[NBS] \times 10^4$ mol dm^{-3}	$[SNA] \times 10^3$ mol dm^{-3}	$[\text{NaOH}] \times 10^3$ mol dm^{-3}	$k_{\text{obs}} \times 10^4$ s^{-1}
1.0	8.0	10.0	4.15
3.0	8.0	10.0	4.18
5.0	8.0	10.0	4.10
7.0	8.0	10.0	4.12
9.0	8.0	10.0	4.17
5.0	4.0	10.0	2.42
5.0	6.0	10.0	3.31
5.0	10.0	10.0	4.68
5.0	12.0	10.0	5.49
5.0	8.0	6.0	2.29
5.0	8.0	8.0	3.22
5.0	8.0	12.0	5.02
5.0	8.0	14.0	5.86
^a 5.0	8.0	10.0	4.16
^b 5.0	8.0	10.0	4.19

The effect of varying $[\text{NaOH}]$ on the rate

The rate increased with the increase in $[\text{NaOH}]$ (Table 1). A plot of $\log k_{\text{obs}}$ vs. $\log [\text{NaOH}]$ was linear (Fig. 2; $r = 0.998$) with a slope of 1.03, indicating a first-order dependence of the rate on $[\text{NaOH}]$.

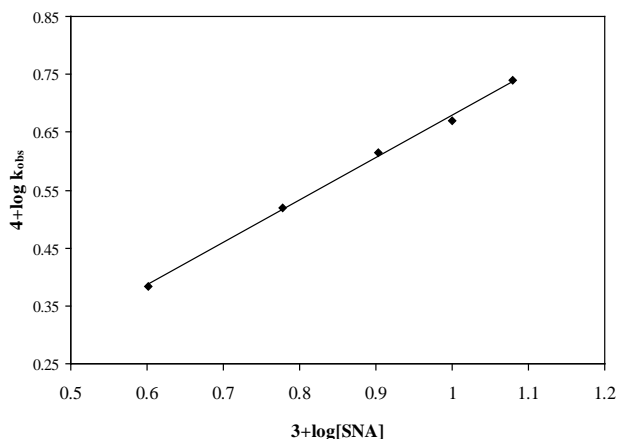


Fig. 1: Plot of $4 + \log k_{\text{obs}}$ vs. $3 + \log [\text{SNA}]$.

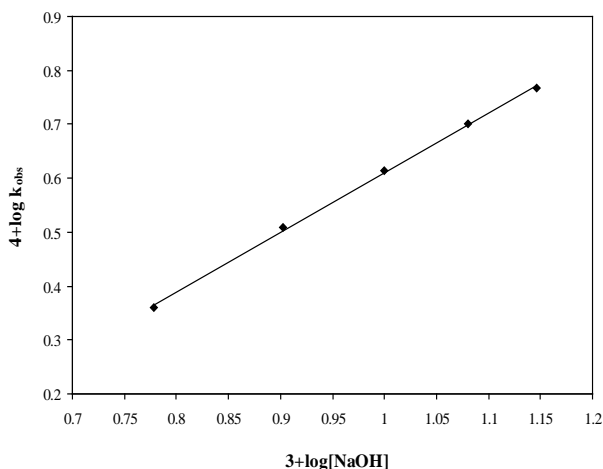


Fig. 2: Plot of $4 + \log k_{\text{obs}}$ vs. $3 + \log [\text{NaOH}]$.

The effect of added product

The effect of initially added product, succinimide (RNH) was studied in the concentration range from 0.0002 to 0.001 mol dm⁻³, keeping all other concentrations constant. It was found that the added product had no significant effect on the reaction rate.

The effect of the dielectric permittivity (D) and the ionic strength (μ) of the medium

The effect of the dielectric permittivity (D) on the reaction rate was studied by adding various proportions of CH₃CN (0 - 20 % v/v) to the reacting system. The rate decreased with increasing CH₃CN content and the results are shown in Table 2.

The plot of $\log k_{\text{obs}}$ vs. $1/D$ was linear ($r = 0.997$) with a negative slope. The values of permittivity (D) for the CH₃CN-H₂O mixtures are calculated through the equation, $D = D_w V_w + D_A V_A$ where D_w and D_A are the dielectric permittivities of pure water and acetonitrile, and V_w and V_A are the volume fractions of components, water and acetonitrile in the total mixture. Blank experiments

Table 2. The effect of varying dielectric permittivity of the medium on the reaction rate at 308 K

% CH ₃ CN (v/v)	D	$k_{\text{obs}} \times 10^4$ (s ⁻¹)
0	73.6	4.10
5	71.8	3.22
10	70.0	2.34
15	68.2	1.96
20	66.5	1.88

[NBS] = 5×10^{-4} mol dm⁻³; [SNA] = 8×10^{-3} mol dm⁻³; [NaOH] = 10×10^{-3} mol dm⁻³; $\mu = 0.1$ mol dm⁻³.

performed indicated that CH₃CN was not oxidized with NBS under the experimental conditions employed. Variation of ionic strength of the medium (0.1-0.3 mol dm⁻³) using NaClO₄ solution had no significant effect on the rate.

Solvent isotope effect and proton inventory studies

Solvent isotope study in D₂O medium was made. The value of k_{obs} (H₂O) is 4.10 and that of the k_{obs} (D₂O) is 2.33 leading to solvent isotope effect $k_{\text{obs}} (\text{H}_2\text{O}) / k_{\text{obs}} (\text{D}_2\text{O}) = 1.73$. Proton inventory studies were made in H₂O - D₂O mixtures, and the results are shown in Table 3. The corresponding proton inventory plot for the rate constant, k_{obs} in a solvent mixture containing deuterium atom fraction (n) is given in Fig. 3.

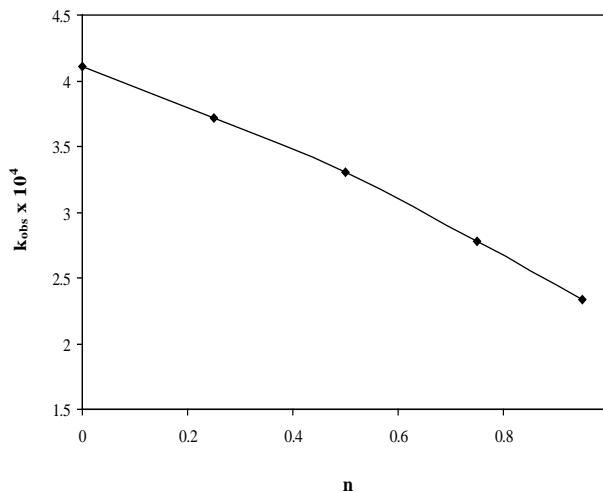


Fig. 3: Plot of k_{obs} vs. n.

Table 3. Proton inventory studies in H₂O - D₂O mixture at 308 K

Atom fraction of D ₂ O (n)	$k_{\text{obs}} \times 10^4$ (s ⁻¹)
0.00	4.10
0.25	3.71
0.50	3.30
0.75	2.78
0.95	2.33

[NBS] = 5×10^{-4} mol dm⁻³; [SNA] = 8×10^{-3} mol dm⁻³; [NaOH] = 10×10^{-3} mol dm⁻³; $\mu = 0.1$ mol dm⁻³.

The Effect of Temperature

Kinetic and thermodynamic parameters were calculated by studying the reaction at different temperatures (303 – 321 K). The results are given in Table 4. The values of activation parameters for the overall reaction were computed through the linear Arrhenius plot of $k_{\text{obs}} \log$ vs. $1/T$ (Fig. 4; $r = 0.997$). The results are compiled in Table 5.

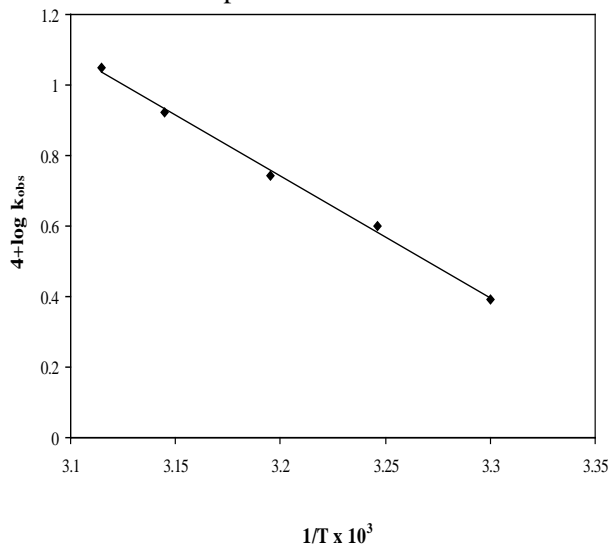


Fig. 4: Plot of $4 + \log k_{\text{obs}}$ vs. $10^3/T$.

Table 4. The effect of varying temperature on the reaction rate

Temperature, K	$k_{\text{obs}} \times 10^4, \text{s}^{-1}$
303	2.45
308	4.10
313	5.52
318	8.37
321	11.24

$[\text{NBS}] = 5 \times 10^{-4} \text{ mol dm}^{-3}$; $[\text{SNA}] = 8 \times 10^{-3} \text{ mol dm}^{-3}$; $[\text{NaOH}] = 10 \times 10^{-3} \text{ mol dm}^{-3}$; $\mu = 0.1 \text{ mol dm}^{-3}$.

Table 5. Activation parameters for the bromination of SNA

E_a kJ mol ⁻¹	ΔH^\ddagger kJ mol ⁻¹	ΔG^\ddagger kJ mol ⁻¹	ΔS^\ddagger J K ⁻¹ mol ⁻¹
57.83	55.20	96.10	-130.84

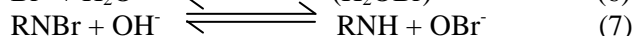
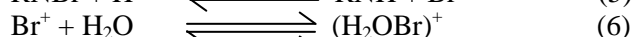
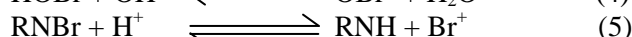
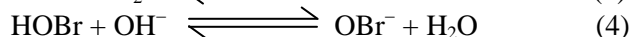
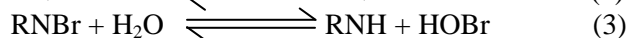
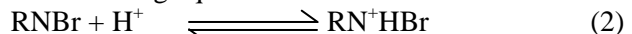
Test for Free Radicals

Addition of aqueous acrylonitrile monomer solution to the reaction mixture in an inert atmosphere did not initiate polymerization, indicating the absence of free radical species in the reaction sequence.

DISCUSSION AND MECHANISM

NBS is a two equivalent oxidant which oxidizes many substrates through NBS itself or Br^+ or RN^+HBr or hypobromite anion. The reactive species responsible for brominating character may

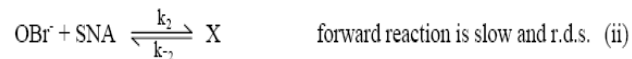
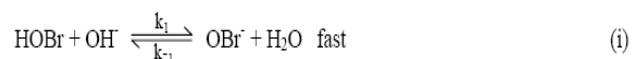
depend on the pH of the medium [6]. Depending on the pH of the medium NBS furnishes different types of reactive species in solutions [17-19] as shown in the following equilibria:



where R is $(\text{CH}_2\text{CO})_2$.

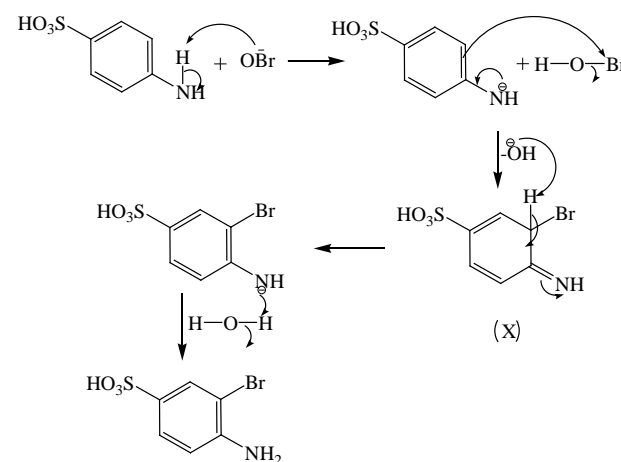
In acid medium, the probable reactive species of NBS are NBS itself or Br^+ or protonated NBS (RN^+HBr), and the reactive species in alkaline solutions are NBS itself HOBr or OBr^- .

NBS oxidizes many substrates through NBS itself, or hypobromite anion [20, 21]. In this study, the reaction exhibits 1:1 stoichiometry of SNA and NBS with unit order dependence on $[\text{NBS}]$. The increase in rate with increasing $[\text{OH}^-]$ can be well-explained [22] by the formation of OBr^- according to equilibria (4) and (7). The insignificant effect of added succinimide on the rate can be attributed to the involvement of OBr^- according to the equilibrium step (4). Hence, OBr^- reacts with the substrate to form a complex (X) in the rate determining step, which then undergoes rearrangement in the fast step to give products as shown in Scheme 1.



Scheme 1

A detailed mechanistic interpretation is shown in Scheme 2.



Scheme 2

From slow step of Scheme 1,

$$\text{rate} = k_2 [\text{OBr}^-] [\text{SNA}] \quad (8)$$

Applying steady state condition for OBr^-

$$k_1[\text{HOBr}][\text{OH}^-] - k_{-1}[\text{OBr}^-][\text{H}_2\text{O}] - k_2[\text{OBr}^-][\text{SNA}] = 0$$

$$[\text{OBr}^-] \{k_{-1}[\text{H}_2\text{O}] + k_2[\text{SNA}]\} = k_1[\text{HOBr}][\text{OH}^-]$$

$$[\text{OBr}^-] = \frac{k_1[\text{HOBr}][\text{OH}^-]}{k_{-1}[\text{H}_2\text{O}] + k_2[\text{SNA}]} \quad (9)$$

By inserting $[\text{OBr}^-]$ from Eq.(9) into Eq.(8) the following rate law (Eq.10) is obtained:

$$\text{rate} = \frac{k_1 k_2 [\text{NBS}][\text{OH}^-][\text{SNA}]}{k_{-1}[\text{H}_2\text{O}] + k_2[\text{SNA}]} \quad (10)$$

Since $\text{rate} = k_{\text{obs}} [\text{NBS}]$, Eq.(10) can be transformed into Equations (11) and (12).

$$k_{\text{obs}} = \frac{k_1 k_2 [\text{OH}^-][\text{SNA}]}{k_{-1}[\text{H}_2\text{O}] + k_2[\text{SNA}]} \quad (11)$$

$$\frac{1}{k_{\text{obs}}} = \frac{k_{-1}[\text{H}_2\text{O}]}{k_1 k_2 [\text{OH}^-][\text{SNA}]} + \frac{1}{k_1 [\text{OH}^-]} \quad (12)$$

Based on Eq. (12), a plot of $1/k_{\text{obs}}$ vs. $1/[\text{SNA}]$ was found to be linear (Fig. 5; $r = 0.998$). From the intercept and slope of the plot, the values of k_1 and k_{-1}/k_2 at standard $[\text{OH}^-]$ and $[\text{H}_2\text{O}] = 55.56 \text{ mol dm}^{-3}$, were found to be $0.1371 \text{ mol}^{-1} \text{ dm}^3 \text{ s}^{-1}$ and 3.3703×10^{-4} , respectively. The proposed Scheme 1 and the rate law are also substantiated by the experimental results, discussed below.

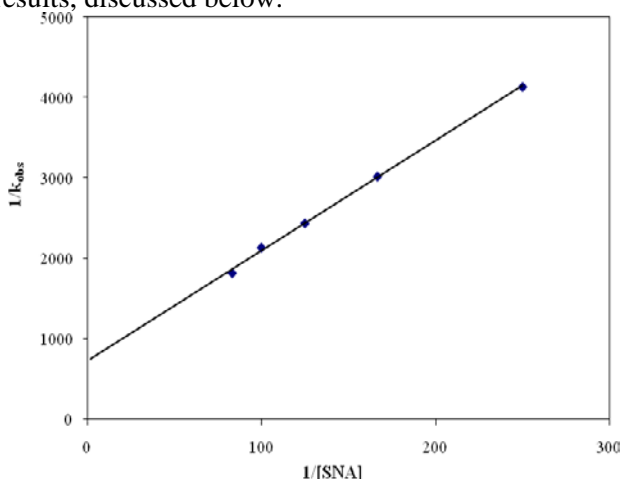


Fig. 5: Plot of $1/k_{\text{obs}}$ vs. $1/[\text{SNA}]$.

The change in solvent composition by varying the CH_3CN content into $\text{CH}_3\text{CN-H}_2\text{O}$ mixture affects the reaction rate. For a limiting case of zero angle of approach between the two dipoles or a ion - dipole system, Amis [23] showed that a plot of $\log k_{\text{obs}}$ vs. $1/D$ gives a straight line with a positive slope for a reaction between a positive ion-dipole interaction, whereas a negative slope for a reaction between a

negative ion and a dipole or between two dipoles. In this investigation, a plot of $\log k_{\text{obs}}$ vs. $1/D$ was linear with a negative slope. This observation indicates the ion-dipole nature of the rate determining step in the reaction sequence and also points to extending of charge to the transition state.

The observed solvent isotope effect supports the proposed mechanism and the derived rate law. For a reaction involving a fast equilibrium H^+ or OH^- ion transfer, the rate increases in D_2O medium, since D_3O^+ and OD^- are stronger acid and stronger base, respectively than H_3O^+ and OH^- ions [24, 25]. In the present case, the observed solvent isotope effect of $k_{\text{obs}}(\text{H}_2\text{O}) / k_{\text{obs}}(\text{D}_2\text{O}) > 1$ is due to the protonation step followed by hydrolysis involving the OH bond scission. The retardation of rate in D_2O is due to the hydrolysis step which tends to make the normal kinetic isotope effect. The proton inventory studies made in $\text{H}_2\text{O} - \text{D}_2\text{O}$ mixture could throw light on the nature of the transition state. The dependence of the rate constant, k_{obs} , on the deuterium atom fraction 'n' in the solvent mixture is given by the following form of Gross-Butler equation [26],

$$\frac{k_o^1}{k_n^1} = \frac{\pi \text{TS}(1 - n + n\phi_i)}{\pi \text{RS}(1 - n + n\phi_j)} \quad (13)$$

where ϕ_i and ϕ_j are isotope fractionation factor for isotopically exchangeable hydrogen sites in the transition state (TS) and in the ground / reactant state (RS), respectively. The Gross-Butler equation permits the evaluation of ϕ_i when the value of ϕ_j is known. However, the curvature of proton inventory plot could reflect the number of exchangeable proton in the reaction [26]. Plot of k_{obs} vs. n is a curve in this case, and this in comparison with the standard curves indicates the involvement of a single proton or H-D exchange in the reaction sequence [27]. This proton exchange is indicative of the participation of hydrogen in the formation of transition state.

The negligible influence of added succinimide and halide ions on the rate are in agreement with the proposed mechanism. The proposed mechanism is also supported by the high values of energy of activation and other thermodynamic parameters. The fairly high positive value of ΔH^\ddagger indicates that, the transition state is highly solvated.

CONCLUSIONS

In conclusion, the stoichiometry of bromination of SNA by NBS is 1:1. The bromination product of SNA was found to be 4-amino-3-bromobenzene sulfonic acid, and confirmed by IR and ^1H NMR spectral studies. OBr^- is postulated as the reactive species of NBS. Solvent isotope effect, studied using

D₂O, supports the proposed mechanism, and the derived rate law is consistent with the observed results.

Acknowledgement: The authors are thankful to the University of Mysore, Mysore, India for the financial support.

REFERENCES

1. R.Q. Brewster, W.E. McEwen, Organic Chemistry, 3rd edition, Prentice-Hall of India, NewDelhi, 1971.
2. R.T. Morrison, R.N. Boyd, Organic Chemistry, 6th edition, Prentice-Hall of India, NewDelhi, 2001, p 862.
3. R.M. Mulla, G.C. Hiremath, S.T. Nandibewoor, *Monatshefte fur Chemie.*, **135**, 1489 (2004).
4. R. Filler, *Chem. Rev.*, **63**, 21 (1963).
5. R. Surendra Kumar, A. Sharma, *J. Indian Chem. Soc.*, **85**, 71 (2008).
6. G. Gopalakrishnan, J.L. Hogg, *J. Org. Chem.*, **50**, 1206 (1985).
7. K.N. Mohana, K.R. Ramya, *J. Mol. Catal. A: Chem.*, **302**, 80 (2009).
8. C.P. Kathari, P.D. Pol, S.T. Nandibewoor, *Inorg. React. Mechanism*, **3**, 213 (2002).
9. K. Basavaiah, U.R. Anilkumar, *Bull. Chem. Soc. Ethiopia.*, **22**, 135 (2008).
10. K. Basavaiah, U.R. Anilkumar, *Proc. National. Acad. Sci.*, **77A**, 301 (2007).
11. K. Basavaiah, U.R. Anilkumar, V. Ramakrishna, *Indian J. Chem. Tech.*, **14**, 313 (2007).
12. K. Basavaiah, V. Ramakrishna, B. Somashekara, *Acta Pharma.*, **57**, 87 (2007).
13. P.M. Ramdas Bhandarkar, K.N. Mohana, *Indian J. Chem.*, **48A**, 1107 (2009).
14. K.N. Mohana, P.M. Ramdas Bhandarkar, *J. Chin. Chem. Soc.*, **54**, 1223 (2007).
15. K.J. Isselbacher, E. Braunwald, J.D. Wilson, J.B. Martin, A.S. Fauci, D.L. Kasper, Harrison's Principles of Internal Medicine, 13th edition, McGraw-Hill Inc., New York, 1994.
16. F. Feigl, V. Anger, Spot Tests in Organic Analysis, Elsevier, New York, 1975.
17. C.P. Kathari, R.M. Mulla, S.T. Nandibewoor, *Oxid. Commun.*, **28**, 579 (2005).
18. B. Singh, L. Pandey, J. Sharma, S.M. Pandey, *Tetrahedron*, **38**, 169 (1982).
19. B. Thimmegowda, J. Iswara Bhat, *Indian J. Chem.*, **28A**, 43 (1989).
20. R.B. Chougale, D.L. Kamble, S.T. Nandibewoor, *Polish J. Chem.*, **71**, 986 (1997).
21. S.K. Mavalangi, K. Surekha, Miss Nirmala, N. Halligudi, S.T. Nandibewoor, *React. Kinet. Cat. Letters*, **72**, 391 (2001).
22. D.L. Kamble, G.H. Hugar, S.T. Nandibewoor, *Indian J. Chem.*, **35A**, 144 (1996).
23. E.S. Amis, Solvent Effects on Reaction Rates and Mechanisms, Academic press, New York, 1966.
24. C.J. Collins, N.S. Bowman, Isotope Effects in the Chemical Reactions, Van Nostrand Reinhold, New York, 1970.
25. K.B. Wiberg, *Chem. Rev.*, **55**, 713 (1955); K.B. Wiberg, Physical Organic Chemistry, Wiley, New York, 1964.
26. W.J. Albery, M. H. Davies, *J. Chem. Soc. Faraday Trans.*, **68**, 167 (1972).
27. N.S. Isaacs, Physical Organic Chemistry, Wiley, New York, 1987.

КИНЕТИЧНО И МЕХАНИСТИЧНО ИЗСЛЕДВАНЕ НА БРОМИРАНЕТО НА СУЛФАНИЛОВА КИСЕЛИНА С *N*-БРОМО-СУКЦИНИМИД В АЛКАЛНА СРЕДА

П.М. Рамдас Бхаданкар, К.Н. Мохана *

Департамент по химични изследвания, Университет в Майсор, Манасаганготри, Майсор - 570006, Индия

Постъпила на 23 ноември 2009 г.; преработена на 22 април 2010 г.

(Резюме)

Сулфаниловата киселина (*p*-амино бензен-сулфонова киселина, SNA) е важно и интересно съединение, което намира редица приложения при синтезите на органични багрила. Нейният амид (сулфаниламидът) и някои подобни субституирани амиди са със значително приложение в медицината като лекарства. В настоящата работа е изследвана кинетиката на бромирането на SNA с *N*-бромосукцинимид (NBS) при 308 К в алкална среда от натриева основа. Експериментално е изведено следното кинетично уравнение: $-d[NBS]/dt = [NBS][SNA]^2[OH^-]$, от дробен порядък по отношение на SNA. Изследвани са измененията на концентрациите на сукцинимида, на продуктите на редукцията на NBS, на добавяната неутрална сол, както и диелектричната проницаемост и йонната сила на средата. Изотопният ефект на разтворителя е изследван с помощта на D₂O. Определена е стехиометрията на реакцията, а продуктите ѝ са идентифицирани и охарактеризирани. Параметрите на активация за сумарните реакции са изчислени чрез координатите на Арениус. Постулирано е, че йонът OBr⁻ е реактивоспособната частица за NBS. При добавянето на акрилонитрил не се наблюдава полимеризация. Предложеният механизъм и изведеното кинетично уравнение са в съгласие с получените кинетични данни.

EPR investigation of gamma-irradiated iminodiacetic and amino acid derivatives

M. Aydın

Faculty of Education, Adiyaman University, TR 02030-Adiyaman, Turkey

Received February 16, 2010, Revised March 23, 2010

Electron paramagnetic resonance spectroscopy was used to investigate the radiation damage in powder of iminodiacetic acid hydrobromide and methyl-DL- α -aminobutyrate hydrochloride at room temperature. It has been found that gamma-irradiation produces the $\text{HN}\dot{\text{C}}\text{HCH}_2(\text{COOH})_2$ radical in the first and the $\text{CH}_2\dot{\text{C}}(\text{NH}_2)\text{COOCH}_3$ radical in the second. The g values of the radicals and the hyperfine structure constants of the unpaired electron with the protons and ^{14}N nucleus were determined. The results were found to be in good agreement with the existing literature data.

Keywords: EPR; gamma irradiation; free radicals; amino acid derivatives

INTRODUCTION

During irradiation of solid amino and iminodiacetic acid derivatives, free radicals are formed. Due to the fact that the unpaired electron is involved in free radicals, these species are paramagnetic and the most used method for detecting free radicals is electron paramagnetic resonance (EPR) technique [1]. When an unpaired electron in a magnetic field interacts with a nuclear spin, the spectrum splits into two or more lines, which produces a hyperfine structure in the spectrum. The splitting of the spectrum is expressed in terms of a hyperfine coupling constant (a value), and the relative position of the spectrum is expressed by the spectroscopic splitting factor (g value) [2]. EPR is one of the many spectroscopy techniques that has been used for many years to study and characterize different types of materials. The biological molecules, amino and iminodiacetic acid derivatives are examples of materials that have been studied by EPR spectroscopy through detection of paramagnetic species [3-10]. Iminodiacetic acid hydrochloride and N-(2-hydroxyethyl) iminodiacetic acid powders were gamma-irradiated and studied by EPR at room temperature [11]. The radiation damage center was attributed to $\text{HN}\dot{\text{C}}\text{HCH}_2(\text{COOH})_2$ and $\text{HOCH}_2\text{CH}_2\text{N}\dot{\text{C}}\text{HCH}_2(\text{COOH})_2$ radicals, respectively. Furthermore, the investigation of gamma-irradiated powders of glycyl-L-glutamine by means of EPR revealed that the radical produced by radiation was $\text{CH}_2\dot{\text{C}}(\text{NH})\text{COOH}$ [12]. To our knowledge, iminodiacetic acid hydrobromide (IDAAHBr), $\text{HN}(\text{CH}_2\text{COOH})_2\cdot\text{HBr}$, and methyl-

DL- α -aminobutyrate hydrochloride (MDLAHCl), $\text{CH}_3\text{CH}_2\text{CH}(\text{NH}_2)\text{COOCH}_3\cdot\text{HCl}$, were not investigated. Moreover, these samples are biologically important organic substances. Therefore, the goal of this study was to investigate the defects, induced by gamma-irradiation in powders of IDAAHBr and MDLAHCl, and to determine their spin Hamiltonian parameters at room temperature.

EXPERIMENTAL

The samples, used in this study, were obtained from commercial sources. Powder samples of the compounds were exposed to gamma-irradiation from ^{60}Co gamma-ray source (Nordion-Canada, model JS 9600) at a dose rate of 2 kGy/h for a total of 10 h at room temperature. After irradiation, samples were kept in plastic bags at room temperature and in dark. Quartz tubes were used for the EPR measurements of the samples. The EPR spectroscopy was carried out in a Varian model X-band E-109C EPR spectrometer at room temperature. The modulation amplitude was below $5\cdot 10^{-2}$ mT and the microwave power was 2 mW. The g factors were found by comparison with a diphenylpicrylhydrazyl (DPPH) sample at $g = 2.0036$. The EPR spectrum of gamma-irradiated samples was monitored during a four month period in order to follow the stability of the formed species. The EPR spectra were analyzed by a computer simulation program [13].

RESULTS AND DISCUSSION

The characteristic EPR spectrum of the

*To whom all correspondence should be sent:

E-mail: maydin@adiyaman.edu.tr; Phone: (+90) 416-2232210;

Fax: (+90) 416-2231426

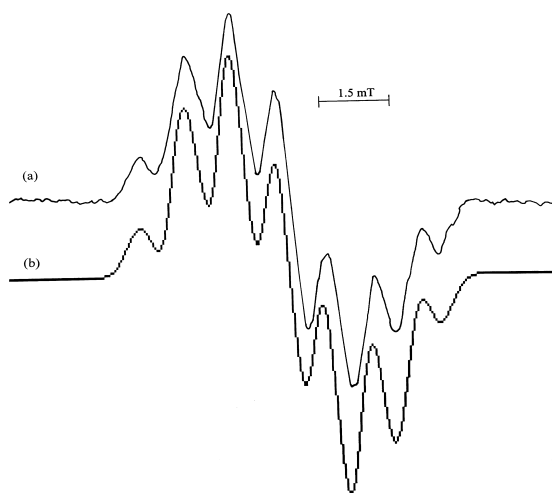


Fig. 1. (a) The EPR spectrum of gamma-irradiated IDAAHBr powder at room temperature; (b) simulation form of the spectrum using $a_{\text{CHCH}_2} = 1.03$ mT, $a_{\text{NH}} = 0.69$ mT, $a_{\text{N}} = 0.69$ mT and line width 0.36 mT.

gamma-irradiated IDAAHBr in Fig. 1a exhibits an intensity distribution of 1:5:11:14:11:5:1, and can be attributed to $\text{HN}\dot{\text{C}}\text{HCH}_2(\text{COOH})_2$ radical. Similar intensity distributions were observed in $\text{CH}_3\dot{\text{N}}\text{H}$ radical by Hadley and Volman [14]. The $\text{HN}\dot{\text{C}}\text{HCH}_2(\text{COOH})_2$ radical exhibits an intensity distribution of 1:3:3:1 because of the α -proton and the methylene protons which are all magnetically equivalent. On the other hand, the hyperfine constants of β -protons are greater than α -proton [3, 15] in some studies. But there are some studies in which the hyperfine constants of β -protons are smaller than α -proton or equivalent [11, 12, 16]. Moreover, the spectra exhibit 4 lines with the intensity distribution of 1:2:2:1 owing to NH proton and ^{14}N nucleus ($I=1$) with equal coupling constants. The binomial expansion for this spectrum is given as $1:2:2:1+3:6:6:3+3:6:6:3+1:2:2:1 = 1:5:11:14:11:5:1$.

The EPR spectrum for a larger number of inequivalent protons can be found by graphic construction which is a mathematical record of the EPR spectrum. The intensity ratio for more complicated spectra is obtained by direct addition of the line intensities of simple spectra, the lines being displaced relatively to each other by the coupling constant [17]. The hyperfine interaction of the unpaired electrons with one α -proton, two equivalent methylene protons, one NH proton, and ^{14}N nucleus can be taken as $a_{\text{CHCH}_2} = 1.03$ mT, $a_{\text{NH}} = 0.69$ mT and $a_{\text{N}} = 0.69$ mT. The spectrum, simulated with these hyperfine parameters, is presented in Fig. 1b. The paramagnetic centre has been attributed to the $\text{HN}\dot{\text{C}}\text{HCH}_2(\text{COOH})_2$ radical [16] in the gamma-irradiated powders of iminodiacetic acid at room

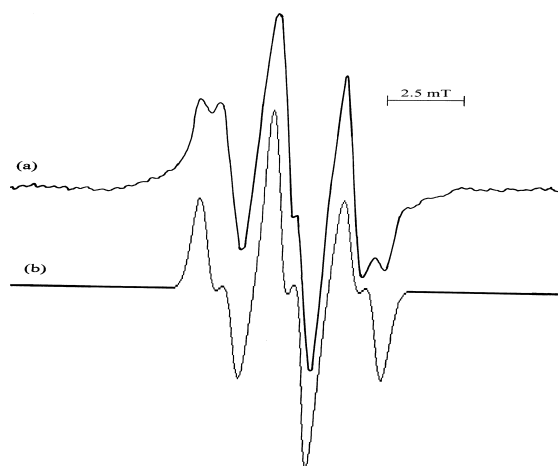


Fig.2. (a) The EPR spectrum of gamma-irradiated MDLAHCl powder at room temperature, (b) simulation form of the spectrum using $a_{\text{CH}_2} = 2.34$ mT, $a_{\text{NH}} = 0.74$ mT, $a_{\text{N}} = 0.25$ mT and line width 0.30 mT.

temperature. This is similar to our proposed radical, and the reported values of $a_{\text{CHCH}_2} = 1.40$ mT, $a_{\text{NH}} = 0.58$ mT, $a_{\text{N}} = 0.39$ mT are in good agreement with our results. Moreover, a radical similar to this has been observed in the gamma-irradiated powders of iminodiacetic acid hydrochloride [11].

The measured value of the g factor is $g = 2.0029 \pm 0.0005$. The g value of the radical, discussed here, seems to be in agreement with the literature data for their analogs and various amine radicals [18 - 20]. Consequently, it can be stated that gamma-irradiation produced free radicals in IDAAHBr by loss of the hydrogen atom bond from the carbon atom bond to the ^{14}N nucleus and COOH group.

The gamma-irradiated powder of MDLAHCl at room temperature gives the spectrum shown in Fig. 2a. This spectrum can easily be thought as consisting of 6 lines with intensity distribution of 1:1:2:2:1:1. This 6 lines in the spectra are due to the radical $\text{CH}_2\dot{\text{C}}(\text{NH}_2)\text{COOCH}_3$ in which the unpaired electron interacts significantly with two methylene protons and one NH proton. The spectrum can again be interpreted as a 1:1 doublet of a 1:2:1 triplet. In a thorough examination of the spectrum, it can be seen that it consists of a triplet with a spacing of 2.34 mT. Then each line of the triplet is further into doublet lines with spacing of 0.74 mT. A simulation of the MDLAHCl spectrum is shown in Fig. 2b, using the hyperfine coupling constants $a_{\text{CH}_2} = 2.34$ mT, $a_{\text{NH}} = 0.74$ mT and $a_{\text{N}} = 0.25$ mT. There is good agreement between the experimental and simulated EPR spectra. The line width of the spectrum is somewhat larger than the hyperfine coupling constant of the nitrogen nuclei ($a_{\text{N}} = 0.25$ mT), and therefore the hyperfine splitting of the nitrogen nuclei is not observed in the spectrum. The g value of radical is g

= 2.0030 ± 0.0005. The g value and the hyperfine constants of the radical discussed here agree well with some other literature data [12, 16, 21, 22].

Different values of the hyperfine coupling constants of the methylene protons have been found also by the other authors [17, 23 - 26]. These differences in methylene protons coupling constants can be expressed by the relation [27]

$$a_{\beta} = B_0 + B_1 \cos^2 \theta \quad (1)$$

Here, B_0 is the spin polarization contribution ($B_0 = 0 - 0.35$ mT), B_1 is hyperconjugative contribution ($B_1 = 5.00$ mT) and the dihedral angle, θ , is the angle between the p_{π} orbital of the unpaired electron and the C-H bond projections on a plane perpendicular to the $C_{\alpha}-C_{\beta}$ bond direction. Therefore, when θ varies, the hyperfine constant varies accordingly and a_{β} approaches zero [24]. According to the value of the hyperfine coupling constants of the methylene protons obtained in this study, the dihedral angle, θ , varies approximately between $47^{\circ}-50^{\circ}$. As a conclusion, we can state that gamma-irradiation produces free radicals in MDLAHCl by loss of one hydrogen atom from CH group. The hydrogen abstraction is one of the most common mechanisms of producing free radicals in aliphatic compounds [28].

CONCLUSION

The analysis of EPR spectra indicated the presence of amine type free radical in gamma-irradiated powder samples. The EPR parameters and the structure of the radicals could be determined.

Acknowledgments. I acknowledge Prof. Dr. Ali Bayri for the technical and scientific support. This work was supported by Grant No. EFBAP2009-0005 of the Research Fund of Adiyaman University (ADÜYAP).

REFERENCES

1. B. Aşık, *Radiat. Phys. Chem.*, **77**, 697 (2008).
2. G. Damian, G. Schmutzer, D. Petrisor, V. Miclaus, S. Simon, *Romanian J. Biophys.*, **15**, 23 (2005).
3. J.R. Morton, H. Horsfield, *J. Chem. Phys.*, **35**, 1142 (1961).
4. H. Shields, P. Hamrick, D. Delaigle, *J. Chem. Phys.*, **46**, 3649 (1967).
5. J. Sinclair, *J. Chem. Phys.*, **55**, 245 (1971).
6. E. Sagstuen, E. O. Hole, S. R. Haugedal, W. H. Nelson, *J. Phys. Chem. A*, **101**, 9763 (1997).
7. N.D. Yordanov, R. Mladenova *Spectrochim. Acta A*, **60**, 1395 (2004).
8. R. Mladenova, N. D. Yordanov, *Bulgarian Chem. Commun.*, **39**, 128 (2007).
9. A.L. Maniero, V. Chis, A. Zoleo, M. Brustolon, A. Mezzetti, *J. Phys. Chem.*, **B 112**, 3812 (2008).
10. N. D. Yordanov, O. Lagunov and K. Dimov, *Radiat. Phys. Chem.*, **78**, 277 (2009).
11. M. Aydın, M. H. Başkan, Y. E. Osmanoğlu, *Braz. J. Phys.*, **39**, 583 (2009).
12. M.H. Başkan, *Radiat. Eff. Defect. Solids*, **163**, 35 (2008).
13. R.D. McKelvey, *J. Chem. Educ.*, **64**, 497 (1987).
14. S.G. Hadley, D.H. Volman, *J. Am. Chem. Soc.*, **89**, 1053 (1967).
15. R. Livingston, H. Zeldes, *J. Chem. Phys.*, **44**, 1245 (1966).
16. M. Aydın, Y.E. Osmanoğlu, M.H. Başkan, *Radiat. Eff. Defects Solids*, **163**, 47 (2008).
17. M. Birey, *Z. Naturforsch.*, **57a**, 36 (2001).
18. R. Köseoğlu, E. Köseoğlu, F. Köksal, *App. Radiat. Isot.*, **58**, 63 (2003).
19. P. Neta and R. W. Fessenden, *J. Phys. Chem.*, **75**, 738 (1971).
20. D.E. Wood, D.V. Lloyd, *J. Chem. Phys.* **53**, 3932 (1970).
21. M. Ogawa, K. Ishigure, K. Oshima, *Radiat. Phys. Chem.*, **16**, 289 (1980).
22. M. Aydın, M. H. Başkan, S. Yakar, F. Ş. Ulak, M. Aydınol, B. Aydınol, M. Büyüm, *Radiat. Eff. Defect. Solids*, **163**, 41 (2008).
23. Ş. Osmanoğlu, *J. Mol. Struct.* **877**, 7 (2008).
24. Ş. Osmanoğlu, F. Köksal, *Radiat. Phys. Chem.*, **49**, 445 (1997).
25. F. Köksal, Ş. Osmanoğlu, I. Kartal, F. Uzun, *Radiat. Phys. Chem.*, **49**, 537 (1997).
26. Ş. Osmanoğlu, M. Aydın, M. H. Başkan, *Z. Naturforsch.*, **60a**, 549 (2005).
27. J. R. Morton, *Chem. Rev.*, **64**, 453 (1964).
28. M.D. Sevilla, C. V. Paemel, G. Zorman, *J. Phys. Chem.*, **76**, 3577 (1972).

ИЗСЛЕДВАНЕ НА ГАМА-ОБЛЪЧЕНИ ИМИНО-ДИОЦЕТНИ И АМИНОКИСЕЛИННИ
ПРОИЗВОДНИ ЧРЕЗ ЕЛЕКТРОННО-ПАРАМАГНИТЕН РЕЗОНАНС

М. Айдын

Факултет по образование, Университет в Адияман, 02030 Адияман, Турция

Постъпила на 16 февруари 2010 г.; Преработена на 23 март 2010 г.

(Резюме)

Използвана е електронно-парамагнитна спектроскопия за изследване на промените в прахове от хидробромида на имино-диоцетната киселина и хидрохлорида на метил- DL- α -маслената киселина при стайна температура. Установено е, че облъчването с гама-лъчи води до получаването на $\text{HN}\dot{\text{C}}\text{HCH}_2(\text{COOH})_2$ – радикали при първия и $\text{CH}_2\dot{\text{C}}(\text{NH}_2)\text{COOCH}_3$ – радикали при втория изследван образец. Определени са g -стойностите за радикалите и константите за свръх-фината структура на не-сдвоения електрон с протоните и ^{14}N -ядрата. Получените резултати са в добро съгласие с съществуващите литературни данни.

Theoretical study on the structure, stability and vibrational spectra of the hydrogen-bonded phenoxides, containing strong short hydrogen bonds

Y. Dimitrova*

Institute of Organic Chemistry with Center of Phytochemistry, Bulgarian Academy of Sciences, Acad. G. Bonchev St., Bl. 9, 1113, Sofia, Bulgaria

Received November 18, 2009; Revised May 18, 2010

The structure, stability, and the vibrational spectra of the 3.5-(CF₃)₂C₆H₄O and 3.5-(CF₃)₂C₆H₃O⁻ hydrogen-bonded system, containing a strong, short hydrogen bond (SSHB), have been studied by means of *ab initio* and DFT calculations at different basis sets. Full geometry optimization of the hydrogen-bonded system has been performed through HF/6-31G(d,p) *ab initio* and BLYP/6-31+G(d,p) calculations. The calculations show that a strong, almost symmetrical O-H...O⁻ bond is observed. The calculated O-H...O⁻ distance (1.235 Å) and the OH...O⁻ = 179.60° angle are in agreement with the SSHB classification. The corrected values of the dissociation energy (-29.31 - 35.95 kcal.mol⁻¹), calculated through HF/6-31G(d,p) and BLYP calculations, confirm the ionic structure of the hydrogen-bonded system. The calculations show that formation of a hydrogen bond of 3.5-(CF₃)₂C₆H₄O and 3.5-(CF₃)₂C₆H₃O⁻ leads a considerable charge rearrangement in the monomers. The changes of the atomic charges, (Δq_i), in the complex, resulted from the hydrogen bonding, show large proton polarizability of the SSHB within this complex, i.e. a hydrogen-bonded system of ionic nature is formed. The formation of SSHB leads to significant changes in the vibrational characteristics for most of the vibrational modes. This phenomenon could be explained with the considerable charge rearrangement, occurring under the action of the hydrogen bonding.

Keywords: SSHB; structure; stability; vibrational spectra; *ab initio*; DFT.

INTRODUCTION

Hydrogen bonding is of fundamental importance in the chemistry, physics and biology. The hydrogen bonding, for example, is the key to understand how molecules align themselves, both in crystals and in the gas phase. The hydrogen bonds, in which either the donor or the acceptor is ion, play an important role in the aqueous chemistry and in the biological systems. It is therefore not surprising that these systems have often been studied through theoretical and experimental methods [1-7].

Recently, there has been much interest in a special class of hydrogen bonds called “strong, short hydrogen bonds” (SSHBs) or “low-barrier hydrogen bonds (LBHBs). The SSHBs are an important factor in enzyme catalysis [8-14]. Notable features of such hydrogen bonds are the short distances between hydrogen donor and acceptor atoms, the strong hydrogen bond energy, the low isotopic fractional factor, the Hadzi type II IR spectra [15]. SSHBs in D...H...A systems are characterized by short D...A distances of 2.2 – 2.5 Å [16]. These bonds are important in biological

catalysis [17,18] and are quantitatively different, in most of their properties, from the molecule or weak bonds. When D is an exceedingly electronegative atom, and A has an exceptionally large excess of electronic charge, strong hydrogen bonds are formed. Strong, almost symmetrical, hydrogen bonds are also observed when the donor group is a cation or the acceptor group is an anion, as O⁺ - H...O or O-H...O⁻. Most often these hydrogen bonds are formed from carboxylates and carboxylic acid [19,20].

The SSHBs between phenoxides are less observed and are less studied than other systems [21]. They have important relevance in the enzyme active sites that use tyrosine [22-26].

The aim of this study is to investigate, through using *ab initio* and DFT calculations at different basis sets, the structure, stability, and the vibrational spectra of the 3.5-(CF₃)₂C₆H₄O and 3.5-(CF₃)₂C₆H₃O⁻ hydrogen-bonded system which contains SSHB.

METHODOLOGY

The structure, stability, and vibrational characteristics of the 3.5-(CF₃)₂C₆H₄O and

*To whom all correspondence should be sent:
E-mail: dimj@orgchm.bas.bg

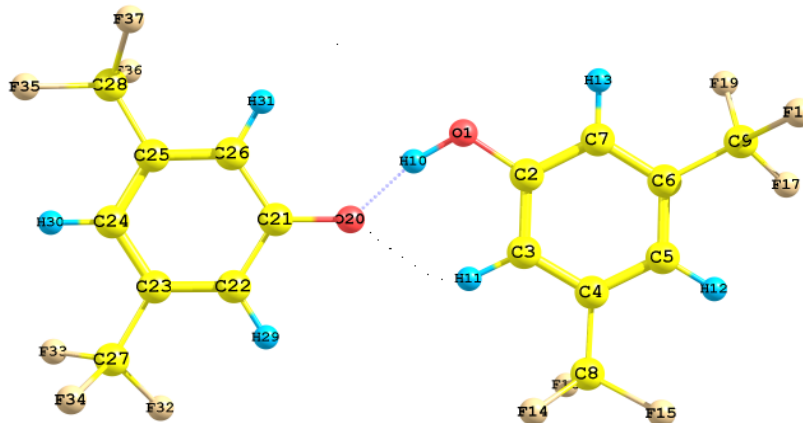


Fig. 1. Optimized structure with BLYP/6-31+G(d,p) calculations for the hydrogen-bonded system: $[(Ar'O)_2H]^-$, where $Ar' = 3,5-(CF_3)_2C_6H_3$:
 $R_{O_{20}\dots H_{10}}=1.235\text{\AA}$; $R_{O_{20}\dots H_{11}}=2.571\text{\AA}$; $R_{O_1-H_{10}}=1.208\text{\AA}$; $R_{O_1-C_2}=1.322\text{\AA}$; $R_{O_{20}-C_{21}}=1.321$;
 Angles ($^\circ$): $H_{10}\dots O_{20}\dots H_{11}=64.8$; $O_{20}\dots H_{11}C_3=119.9$; $C_{21}O_{20}\dots H_{11}=114.0$; $C_3H_{11}\dots O_{20}=119.9$; $H_{10}O_1C_2=113.7$;
 $O_1H_{10}\dots O_{20}=179.5$.

3.5- $(CF_3)_2C_6H_3O^-$ hydrogen-bonded system which contain SSHB, have been calculated through *ab initio* and DFT calculations at different basis sets, using the GAUSSIAN 03 series of programs [27]. All calculations were performed on a Pentium IV PC.

The density functional calculations in this work have been carried out in the framework of Kohn-Sham density-functional theory [28] (DFT) with the non-local gradient-corrected exchange-correlation functional of Becke and Lee, Yang and Parr, including partially exact HF-exchange (BLYP) [29]. The density functional methods for electronic structure calculations [28,30,31] contain semi-empirical elements based on the properties of atoms and simple molecules. Prior to routine application in a given field such as the hydrogen bonding [32-34], they have to be checked through experiments and established quantum chemical approaches, applied for some prototype systems [35]. In combination with *ab initio* calculations and experimental data, the semi-empirical character of the density functional methods might be turned into advantage.

The dissociation energy, calculated using the *ab initio* and DFT calculations, can be used for estimation of the stability of the hydrogen-bonded systems of two and more partners. The supermolecular variation method determines dissociation energy (ΔE) as a difference between the energy of the complex and the energies of the isolated molecules. For the complex, studied here and shown in Figure 1, the dissociation energy is calculated by the equation (1):

$$\Delta E = E_{\text{com.}} - [E(3.5-(CF_3)_2C_6H_4O) + E(3.5-(CF_3)_2C_6H_3O^-)] \quad (1)$$

where $E(3.5-(CF_3)_2C_6H_4O)$ and $E(3.5-(CF_3)_2C_6H_3O^-)$ are the energies of the isolated monomers in their own basis set, and $E_{\text{com.}}$ is the energy of the complex.

To compare the calculated results of the dissociation energy with the respective experimental energy, the effect of the zero-point energy (ZPE) should be taken into account. *Ab initio* calculations yield the total molecular electronic energy of the hypothetical vibrationless state at 0 K. The conversion of this energy (U_0^0) into enthalpy at 298.15 K requires correction of the zero-point energy ($E_{\text{zp vib}}$) using the enthalpy function, ($H_{298}^0 - H_0^0$):

$$\Delta H_{298}^0 = (U_0^0) + \Delta(E_{\text{zpvib}}) + \Delta(H_{298}^0 - H_0^0) \quad (2)$$

$$E_{\text{zpvib}} = 0.5h \sum \nu_i \quad (3)$$

The zero-point energy is calculated through Eq. (3), and the enthalpy function is obtained through standard statistical thermodynamic procedures using the optimized geometries to provide structural constants.

The zero-point vibrational energy correction for the studied complex can be defined as a difference between the calculated zero-point vibrational energy of the complex and the zero-point energies of the monomers:

$$\Delta E_{\text{zpvib}} = E_{\text{zp vib. (com.)}} - (E_{\text{zp vib. (3.5-(CF_3)_2C_6H_4O)}} + E_{\text{zp vib. (3.5-(CF_3)_2C_6H_3O^-)}}) \quad (4)$$

Table 1. Calculated selected geometrical parameters for free and complexed 3,5-(CF₃)₂C₆H₄O and 3,5-(CF₃)₂C₆H₃O⁻ and changes in the parameters from monomers to a complex obtained from HF/6-31G(d,p) and BLYP/6-31+G(d,p) calculations.

Parameters ^a	Monomers		Complex		Change of the parameters	
	HF	BLYP	HF	BLYP	HF	BLYP
Bond length ^b						
C ₂ -O ₁	1.3454	1.3750	1.3174	1.3225	-0.028	-0.0525
C ₃ -C ₂	1.3894	1.4079	1.3983	1.4329	0.0089	0.0250
C ₄ -C ₃	1.3803	1.4064	1.3815	1.4026	0.0012	-0.0038
C ₅ -C ₄	1.3866	1.4042	1.3865	1.4096	-0.0001	0.0054
C ₆ -C ₅	1.3806	1.4075	1.3834	1.4084	0.0028	0.0009
C ₇ -C ₆	1.3854	1.4028	1.3825	1.4028	-0.0029	0
C ₈ -C ₄	1.5056	1.5158	1.5033	1.5096	-0.0023	-0.0062
C ₉ -C ₆	1.5059	1.5167	1.5017	1.5084	-0.0042	-0.0083
H ₁₀ -O ₁	0.9429	0.9776	0.9896	1.2060	0.0467	0.2284
H ₁₁ -C ₃	1.0744	1.0927	1.0739	1.0909	-0.0005	-0.0018
H ₁₂ -C ₅	1.0722	1.0889	1.0714	1.0884	-0.0008	-0.0005
H ₁₃ -C ₇	1.0738	1.0900	1.0736	1.0912	-0.0002	0.0012
F ₁₄ -C ₈	1.3223	1.3711	1.3217	1.3709	-0.0006	-0.0002
F ₁₅ -C ₈	1.3228	1.3672	1.3290	1.3788	0.0062	0.0116
F ₁₆ -C ₈	1.3228	1.3712	1.3280	1.3790	0.0052	0.0078
F ₁₇ -C ₉	1.3207	1.3686	1.3268	1.3762	0.0061	0.0076
F ₁₈ -C ₉	1.3232	1.3688	1.3286	1.3799	0.0054	0.0111
F ₁₉ -C ₉	1.3233	1.3711	1.3257	1.3746	0.0024	0.0035
O ₂₀ ...H ₁₀	-	-	1.5651	1.2353	-	-
O ₂₀ ...H ₁₁	-	-	2.3474	2.5710	-	-
C ₂₁ -O ₂₀	1.2386	1.2708	1.2666	1.3201	0.028	0.0493
C ₂₂ -C ₂₁	1.4440	1.4635	1.4208	1.4319	-0.0232	-0.0316
C ₂₃ -C ₂₂	1.3689	1.4003	1.3757	1.4012	0.0068	0.0009
C ₂₄ -C ₂₃	1.3980	1.4152	1.3901	1.4104	-0.0079	-0.0048
C ₂₅ -C ₂₄	1.3864	1.4152	1.3862	1.4081	-0.0002	-0.0071
C ₂₆ -C ₂₅	1.3780	1.4003	1.3795	1.4038	0.0015	0.0035
C ₂₇ -C ₂₃	1.5005	1.5043	1.5018	1.5083	0.0013	0.004
C ₂₈ -C ₂₅	1.5019	1.5043	1.5021	1.5097	0.0002	0.0054
H ₂₉ -C ₂₂	1.0739	1.0929	1.0741	1.0908	0.0002	-0.0021
H ₃₀ -C ₂₄	1.0714	1.0884	1.0709	1.0885	-0.0005	0.0001
H ₃₁ -C ₂₆	1.0760	1.0929	1.0750	1.0912	-0.001	-0.0017
F ₃₂ -C ₂₇	1.3269	1.3782	1.3297	1.3729	0.0028	-0.0053
F ₃₃ -C ₂₇	1.3336	1.3829	1.3311	1.3778	-0.0025	-0.0051
F ₃₄ -C ₂₇	1.3337	1.3863	1.3293	1.3805	-0.0044	-0.0058
F ₃₅ -C ₂₈	1.3307	1.3829	1.3306	1.3775	-0.0001	-0.0054
F ₃₆ -C ₂₈	1.3316	1.3782	1.3270	1.3721	-0.0046	-0.0061
F ₃₇ -C ₂₈	1.3317	1.3863	1.3270	1.3796	-0.0047	-0.0067
Angle ^c						
C ₃ C ₂ O ₁	122.45	122.91	122.85	123.30	0.4	0.39
H ₁₀ O ₁ C ₂	111.70	108.86	112.27	113.68	0.57	4.82
H ₁₁ C ₃ C ₂	120.24	120.57	118.52	118.51	-1.72	-2.06
C ₄ C ₃ H ₁₁	120.21	119.80	121.75	120.79	1.54	0.99
C ₄ C ₃ C ₂	120.21	119.63	121.75	120.70	1.54	1.07
C ₇ C ₂ O ₁	117.52	117.00	118.38	119.61	0.86	2.61
C ₇ C ₂ C ₃	120.03	120.10	117.77	117.10	-2.26	-3.00
C ₅ C ₄ C ₃	121.08	120.85	121.83	121.68	0.75	0.83
C ₂₆ C ₂₁ C ₂₂	113.79	113.44	115.43	116.91	1.64	3.47
C ₂₅ C ₂₆ C ₂₁	122.19	122.66	121.56	120.82	-0.63	-1.84
C ₂₃ C ₂₂ C ₂₁	122.24	122.66	121.69	121.23	-0.55	-1.43
C ₂₄ C ₂₃ C ₂₂	122.57	122.00	122.07	121.35	-0.5	-0.65
C ₂₂ C ₂₁ O ₂₀	122.54	123.28	121.41	119.66	-1.13	-3.62
C ₂₆ C ₂₁ O ₂₀	123.67	123.28	123.16	123.42	-0.51	0.14
C ₂₁ O ₂₀ ...H ₁₀	-	-	129.40	114.02	-	-
H ₁₀ ...O ₂₀ ...H ₁₁	-	-	67.89	64.86	-	-
C ₂₁ O ₂₀ ...H ₁₁	-	-	162.71	127.09	-	-

$C_3H_{11}...O_{20}$	-	-	126.32	119.97	-	-
$O_1H_{10}...O_{20}$	-	-	172.14	179.60	-	-
$O_{20}...H_{11}C_3$	-	-	126.32	119.97	-	-
E^{tot} (a.u.)	-976.81128	-981.36639	-1953.10876	-1962.24081		
	-976.24838	-980.81541				

The dissociation energies, uncorrected and corrected with zero-point energy differences, are calculated through *ab initio* and DFT calculations with different basis sets.

The shifts in the vibrational frequencies (Δv_i), occurring upon formation of the 3.5-(CF₃)₂C₆H₄O and 3.5-(CF₃)₂C₆H₃O⁻ hydrogen-bonded complex, have been calculated through *ab initio* and DFT (BLYP) calculations. The predicted frequency shift for each vibration is defined as follows:

$$\Delta v_i = v_i^{\text{complex}} - v_i^{\text{monomer}} \quad (5)$$

The changes in the infrared intensities (ΔA_i) upon hydrogen bond formation are also estimated using *ab initio* and DFT calculations:

$$\Delta A_i = A_i^{\text{complex}} - A_i^{\text{monomer}} \quad (6)$$

RESULTS AND DISCUSSION

Structure and stability

The first objective of this work is to establish the most stable structure of the complex, studied here. Full geometry optimization of the hydrogen-bonded system, formed by 3.5-(CF₃)₂C₆H₄O and 3.5-(CF₃)₂C₆H₃O⁻, was made with GAUSSIAN 03 series of programs [27]. Fig. 1 shows the optimized structure, calculated through BLYP/6-31+G(d,p) calculations. It can be seen that the optimized structure for the studied ionic hydrogen-bonded system is cyclic. Table 1 shows the optimum values of the total energy and the equilibrium geometries for the monomers (3.5-(CF₃)₂C₆H₄O and 3.5-(CF₃)₂C₆H₃O⁻), and for the complex. These optimum values were obtained through BLYP/6-31+G(d,p) and HF/6-31G(d,p) calculations.

The complex has an optimum geometry when H₁₀...O₂₀ distance is 1.235 Å, and the H₁₁...O₂₀ distance is 2.571 between 3.5-(CF₃)₂C₆H₄O and 3.5-(CF₃)₂C₆H₃O⁻ molecules. It was noted that SSHBs in the D...H...A systems are characterized by short D...A distances of 2.2 – 2.5 Å [16]. The O₁...O₂₀ distance at optimum geometry, calculated through BLYP/6-31+G(d,p) calculations, is 2.441 Å. It is in agreement with the results from the X-ray diffraction studies (2.436 Å) of this hydrogen-bonded system [36]. The calculations

show that a strong, almost symmetrical O-H...O bond is observed. The structure of the bond is of III type according to the Valence Bond analysis [37]. The calculated H₁₀...O₂₀ distance (1.235 Å) and the angle O₁H₁₀...O₂₀ = 179.60° are in agreement with the SSHB classification, given from Suksangpanya [38] (H...A is within 1.2 to 1.5 Å, and the D-H...A ≅ 180°). The second hydrogen bond distance, H₁₁...O₂₀, is estimated to be in the range between 2.35-2.57 Å. This hydrogen bond is longer and weaker than the H₁₀...O₂₀ bond.

The changes of the geometrical parameters of the complex are defined to investigate the influence of the hydrogen bonding over the structural parameters of the (3.5-(CF₃)₂C₆H₄O and 3.5-(CF₃)₂C₆H₃O⁻) monomers. Table 1 presents the selected optimized geometrical parameters for free and complexed 3.5-(CF₃)₂C₆H₄O and 3.5-(CF₃)₂C₆H₃O⁻. These parameters were obtained through BLYP/6-31+G(d,p) and HF/6-31G(d,p) calculations. It is seen that the bond lengths and angles for the complex studied, shown on Fig. 1, are perturbed from their values in the monomers. The most sensitive to the complexation are the bonds, taking part in the C₂-O₁, O₁-H₁₀, C₂₁-O₂₀, C₂₂-C₂₁ and C₃-C₂ hydrogen bonding. The O₁-H₁₀, C₂₁-O₂₀ and C₃-C₂ bonds are lengthened in the complex, while the C₂-O₁ and C₂₂-C₂₁ bonds are shorted in the formation of the hydrogen bonds.

The changes in the angles of the monomers in the hydrogen bond formation are also estimated. The data in Table 1 evidence that the most sensitive to complexation are the H₁₀-O₁-C₂ and O₂₀-C₂₁-C₂₂ angles which take part in the hydrogen bonding. Their values change significantly in the complex. The calculations show that the changes in the remaining geometrical parameters in the hydrogen bonding are smaller, and in some cases are negligible.

The next step in the study is to establish the stability of the ionic 3.5-(CF₃)₂C₆H₄O and 3.5-(CF₃)₂C₆H₃O⁻ hydrogen-bonded system. The dissociation energies, uncorrected and corrected with zero-point energy differences, are calculated through *ab initio* and DFT calculations at different basis sets. The calculation results are presented in Table 2. The corrected values of the dissociation energy (-29.31 - 35.95 kcal.mol⁻¹), calculated through HF/6-31G(d,p) and BLYP calculations, are in agreement with the SSHB classification, given in

the ‘Theoretical Treatment of Hydrogen Bonding’ hydrogen-bonded system. [1], and confirm the ionic structure of the studied

Table 2. Dissociation energies ΔE (uncorrected and corrected), zero-point energy differences ΔE_{zpe} in kcal/mol and interatomic distances in Å for the hydrogen-bonded complex between 3,5-(CF₃)₂C₆H₄O and 3,5-(CF₃)₂C₆H₃O⁻.

Basis set	ΔE^{uncorr}	$\Delta E^{zpe\ vib}$	ΔE^{corr}	$R_{O...H}$
HF/6-31G(d,p)	-30.8149	1.0103	-29.8046	H ¹⁰ ...O ²⁰ = 1.5651 H ¹¹ ...O ²⁰ = 2.3474
BLYP/6-31+G(d,p)	-37.0222	1.0753	-35.9469	H ¹⁰ ...O ²⁰ = 1.2353 H ¹¹ ...O ²⁰ = 2.5691
BLYP/6-311++G(d,p)	-30.5486	1.2345	-29.3141	H ¹⁰ ...O ²⁰ = 1.4022 H ¹¹ ...O ²⁰ = 2.4820

Charge distribution in the hydrogen bonding

It is known from the previous studies [39,40] that the hydrogen bonding leads to charge rearrangement of the monomers forming a complex. The aim of this study is to determine the influence of the hydrogen bonding on the charge distribution in the studied hydrogen-bonded complex. In this connection, the atomic charges (q_i) for the monomers (3,5-(CF₃)₂C₆H₄O and 3,5-(CF₃)₂C₆H₃O⁻) and for the complex, have been calculated through BLYP/6-31+G(d,p) calculations using the Mulliken population analysis and the Natural Bond Orbital analysis [41-48]. The data are shown in Table 3. Table 3 also contains the changes of the atomic charges (Δq_i) in hydrogen bonding:

$$\Delta q_i = q_i^{complex} - q_i^{monomer} \quad (5)$$

The data in Table 3 show that the atomic charges (q_i) in the monomers and in the complex, calculated through the Mulliken population and the Natural Bond Orbital analyses, are different by value in all cases, even by sign sometimes. However, the atomic charges (Δq_i) in the hydrogen bonding in most cases are similar, both by value and by sign. In view of this result, the conclusion could be that both population analyses are suitable for the estimation of the changes of the atomic charges in the hydrogen bonding.

The calculations show that the most sensitive to complexation are the atoms, taking part in the hydrogen bonding. The oxygen O(1) atom acts as acceptor of electric charge in the studied complex. The negativity of this atom increases significantly in the complex compared to the corresponding negativity in the monomer. In the same time the H(10) and H(11) hydrogen atoms (from OH group), the C(2), C(27), C(28) carbon atoms, and the H(29)- H(31) hydrogen atoms become more positive in the complex. The calculated changes of the atomic charges, (Δq_i), of the remaining atoms are smaller.

The calculation results show that the 3,5-(CF₃)₂C₆H₄O and 3,5-(CF₃)₂C₆H₃O⁻ hydrogen bond

formation leads considerable charge rearrangement in the monomers. The changes of the atomic

charges, (Δq_i), in the complex, resulted from the hydrogen bonding, show large proton polarizability of the SSHB within this complex, i.e. a hydrogen-bonded system of ionic nature is formed.

Changes in the vibrational characteristics in SSHB formation

The prediction of vibrational characteristics (vibrational frequencies and infrared intensities) of the hydrogen-bonded systems through *ab initio* and DFT calculations at different levels [39,40, 49-55] has become widely employed in order to elucidate the influence of the hydrogen bonding on the vibrational spectra of the monomers, forming a complex. The geometrical symmetry of the monomers often changes under perturbation [56] in the hydrogen-bonded system. The vibrational mixing, derived by a perturbation approach, is the counterpart of the orbital mixing.

The infrared (IR) spectroscopic signature of the hydrogen bond formation is the shift to the lower frequency and the increase in intensity of the stretching vibrations of the monomer bonds involving in hydrogen bonding. It is known that the *ab initio* and DFT predicted values of the vibrational frequencies depend on the method and the basis set used for the calculations. The calculated frequencies with a larger basis set give reasonable agreement with the experimental values if the vibrations have small anharmonicity.

In order to estimate the influence of the SSHB on the vibrational characteristics of the 3,5-(CF₃)₂C₆H₄O; 3,5-(CF₃)₂C₆H₃O⁻ monomers, forming a complex, the monomer and complex vibrational spectrum were predicted through (HF/6-31G(d,p)) *ab initio* and DFT (BLYP/6-31+G(d,p)) calculations. Table 4 shows the calculation results.. Table 4 also contains a detailed description of the normal modes based on the potential energy distribution (PED), obtained through HF/6-31G(d,p) calculations. The changes in the vibrational frequencies and the

infrared intensities ($\Delta\nu_i$; ΔA_i) in the hydrogen bond formation are calculated through Equations 5 and 6 using *ab initio* and DFT calculations.

Table 3. NBO and Mulliken charges (q_i) for free and complexed 3,5-(CF₃)₂C₆H₄O and 3,5-(CF₃)₂C₆H₃O⁻, obtained from BLYP/6-31+G(d,p) calculations.

No.	Atom	q_i (NBO)		Δq_i (NBO)	q_i		Δq_i
		Monomers	Complex		Monomers	Complex	
1	O	-0.6593	-0.7068	-0.0475	-0.5157	-0.6327	-0.1170
2	C	0.3242	0.3543	0.0301	0.3171	0.3470	0.0299
3	C	-0.2802	0.2780	-0.0022	-0.1197	-0.1569	-0.0372
4	C	-0.1443	-0.1729	-0.0286	0.0000	0.0099	0.0099
5	C	-0.2177	-0.2571	-0.0394	-0.1140	-0.1445	-0.0305
6	C	-0.1449	-0.1772	-0.0323	-0.0016	0.0101	0.0117
7	C	-0.2465	-0.2654	-0.0189	-0.0901	-0.1217	-0.0316
8	C	1.0798	1.0763	-0.0035	0.6889	0.6683	-0.0206
9	C	1.0803	1.0757	-0.0046	0.6905	0.6650	-0.0255
10	H	0.4924	0.4930	0.0006	0.3110	0.4050	0.0940
11	H	0.2487	0.2586	0.0099	0.0748	0.0836	0.0088
12	H	0.2658	0.2450	-0.0208	0.0943	0.0526	-0.0417
13	H	0.2660	0.2430	-0.0230	0.0943	0.0512	-0.0431
14	F	-0.3479	-0.3509	-0.0030	-0.2450	-0.2500	-0.0050
15	F	-0.3430	-0.3601	-0.0171	-0.2390	-0.2621	-0.0231
16	F	-0.3418	-0.3550	-0.0132	-0.2315	-0.2487	-0.0172
17	F	-0.3447	-0.3578	-0.0131	-0.2410	-0.2593	-0.0183
18	F	-0.3452	-0.3564	-0.0111	-0.2416	-0.2505	-0.0089
19	F	-0.3418	-0.3547	-0.0129	-0.2317	-0.2552	-0.0235
20	O	-0.6890	-0.7089	-0.0200	-0.6390	-0.6394	-0.0004
21	C	0.3619	0.3555	-0.0064	0.3742	0.3505	-0.0237
22	C	-0.3014	-0.2671	0.0343	-0.1764	-0.1258	0.0506
23	C	-0.1992	-0.1783	0.0209	0.0250	0.0119	-0.0131
24	C	-0.3020	-0.2591	0.0	-0.1779	-0.1459	0.0320
25	C	-0.1992	-0.1731	0.0261	0.0250	0.0101	-0.0149
26	C	-0.3014	-0.2812	0.0202	-0.1764	-0.1577	0.0187
27	C	1.0719	1.0752	0.0033	0.6481	0.6650	0.0169
28	C	1.0719	1.0758	0.0039	0.6481	0.6678	0.0197
29	H	0.2225	0.2437	0.0212	0.0131	0.0503	0.0372
30	H	0.2306	0.2443	0.0137	0.0232	0.0516	0.0284
31	H	0.2225	0.2560	0.0335	0.0131	0.0798	0.0667
32	F	-0.3622	-0.3542	0.008	-0.2656	-0.2548	0.0108
33	F	-0.3664	-0.3582	0.0082	-0.2714	-0.2601	0.0113
34	F	-0.3658	-0.3570	0.0088	-0.2631	-0.2522	0.0109
35	F	-0.3664	-0.3593	0.0071	-0.2714	-0.2613	0.0101
36	F	-0.3622	-0.3515	0.0107	-0.2656	-0.2505	0.0151
37	F	-0.3658	-0.3558	0.0100	-0.2631	-0.2504	0.0127

Table 4 shows that the C-H stretching vibrations are predicted to be in the range between 3100 and 3400 cm⁻¹. Their vibrational characteristics are changed negligibly in the hydrogen bonding.

The $\nu(\text{O}_1\text{-H}_{10})$ stretching vibration of the hydrogen-bonded O-H group is shifted to lower frequencies and its IR intensity increases considerably in the hydrogen bonding. This result confirms the optimized stable structure of the studied complex (see Figure 1) and shows the formation of the O⁻...H⁺...O⁻ SSHB with proton transfer, i.e. of the polar structure. The changes in the vibrational characteristics of the stretching

$\nu(\text{C}_{21} - \text{O}_{20})$ vibration confirm also the polar structures of the studied hydrogen-bonded system. The vibrational frequencies of $\nu(\text{C}_{21} - \text{O}_{20})$ in the complex are shifted to lower wavenumbers indicating that the electron density at the C₂₁ - O₂₀ group is decreased due to the formation of the O⁻...H⁺ hydrogen bonds.

The calculations show that the $\delta(\text{HOC})$ deformation is also very sensitive to the hydrogen bonding. Its vibrational frequency is shifted to higher frequencies, and its infrared intensity decreases in the hydrogen bonding. The stretching C-C(F) vibrations are also shifted to higher

frequencies and their IR intensities increase significantly in the complex.

The data in Table 4 show that the formation of the SSHB leads to significant changes in the

Table 4. Calculated vibrational characteristics (ν in cm^{-1} and A in km mol^{-1}) for the hydrogen-bonded systems between 3,5-(CF_3) $_2$ $\text{C}_6\text{H}_4\text{O}$ and 3,5-(CF_3) $_2$ $\text{C}_6\text{H}_3\text{O}^-$.

Approximate description (PED) ^a	HF/6-31G(d,p)		BLYP/6-31+G(d,p)	
	$\nu_i/\Delta\nu_i$	$A_i/\Delta A_i$	$\nu_i/\Delta\nu_i$	$A_i/\Delta A_i$
100v(C ₂₄ -H ₃₀)	3431/11	0.67/-1.03	3161/7	1.09/-2.13
100v(C ₇ -H ₁₃)	3408/9	2.79/2.59	3159/4	1.26/0.84
100v(C ₃ -H ₁₁)	3402/41	45.17/41.85	3141/23	0.36/-5.01
100v(C ₅ -H ₁₂)	3394/-33	1.01/0.47	3138/-26	6.04/5.81
100v(C ₂₆ -H ₃₁)	3374/13	8.20/-12.58	3136/27	0.08/-17.17
100v(C ₂₂ -H ₂₉)	3361/-2	8.81/-3.40	3133/25	6.38/-18.53
100v(O ₁ -H ₁₀)	3164/-1005	3989.86/3880.84	2832/-831	3042.51/3001.26
51v(C-C) + 34 δ (CCC)	1830/16	4.06/0.11	1563/38	0.23/-2.05
45 δ (CCC) + 32v(C-C)	1804/-15	32.42/-23.24	1555/-35	15.98/-54.70
48v(C-C) + 30 δ (CCC)	1785/120	7.84/-13.91	1746/138	24.07/11.14
45v(C-C) + 18 δ (CCC)	1768/136	603.80/-98.42	1631/103	127.92/-82.85
31 δ (HOC) + 15v(C-C)	1739/695	88.69/-54.08	1645/188	75.34/-20.11
40v(O ₂₀ -C ₂₁) + 18v(C-C)	1664/-127	579.70/167.09	1605/-98	275.75/86.06
38v(C-C) + 21 δ (HCC)	1637/267	399.15/194.73	1648/303	195.31/104.25
51v(C-C) + 15 δ (HCC)	1604/3	50.17/-98.08	1595/-5	29.61/-37.97
43v(C-C) + 22v(C-C(F))	1584/5	266.22/162.19	1540/18	138.43/95.14
45v(C-C) + 11v(C-C(F))	1574/217	30.69/-20.04	1512/139	34.82/-17.52
32v(C-C(F)) + 20v(C ₂ -O ₁)	1559/198	1121.92/549.82	1486/173	1006.42/468.63
71 δ (HCC)	1438/201	170.82/159.01	1423/168	161.91/132.20
48v(C-C(F))	1434/115	527.27/76.51	1399/108	201.50/64.31
32v(C-C(F)) + 18 δ (HCC)	1433/123	421.55/228.01	1384/119	360.28/144.15
62v(C-F)	1342/10	510.60/192.05	1285/18	660.09/101.77
68v(C-F)	1334/15	223.88/-226.88	1263/18	210.83/52.38
65v(C-F)	1331/21	371.87/178.35	1258/42	106.00/48.76
89v(C-C)	1260/119	57.20/32.10	1176/95	44.75/26.60
42 δ (CCC) + 18v(C-C)	1218/132	62.24/58.10	1116/108	131.40/29.48
58v(C-C)	1199/19	49.05/-7.86	1061/35	28.30/18.95
41v(C-C) + 22 δ (CCC)	1192/-15	82.15/68.27	1059/-28	72.40/56.12
81 δ (CCC)	1082/1	5.90/-28.64	1058/-7	3.54/2.83
66 τ (HCCO)	1076/46	301.94/163.90	926/11	200.90/93.08
78 δ (CCC)	1047/9	83.17/-15.62	886/6	73.14/-32.11
48 τ (HCCO) + 15 τ (CO...HO)	1037/62	53.41/28.03	878/50	37.40/18.26
48 δ (CCC)	1032/33	11.64/7.88	850/42	3.20/2.45
66 τ (HCCC)	1001/60	20.92/-33.59	846/21	22.57/-5.50
71 τ (HCCO)	989/14	9.04/-16.34	828/0	11.21/-17.28
51 τ (CCCC)	966/82	41.82/21.49	818/62	46.51/15.37
60 τ (CCCC)	792/40	14.36/13.18	796/78	20.88/11.85
85 τ (CCCC)	791/95	12.14/12.13	791/78	16.70/15.12
53 τ (HCCC)	750/-38	3.55/-12.08	691/-29	2.61/-1.82
33 τ (CCCO) + 32 τ (CCCC)	730/0	2.89/-0.03	689/16	1.16/-5.39
31 δ (CCC) + 30 τ (FCCC)	627/49	6.83/2.68	578/32	7.78/3.87
42 τ (FCCC) + 18 δ (CCC)	624/44	1.40/-0.85	542/35	9.77/-4.55
21 δ (CCO) + 20 δ (CCC)	560/32	10.90/4.95	459/24	10.83/5.88
75 τ (FCCC)	557/-66	0.12/-0.07	423/-50	0.21/-0.22
68 τ (FCCC)	556/-26	0.05/-4.36	422/-31	0.85/-2.78
58 δ (FCC)	410/16	0.23/0.19	358/22	0.07/-1.23
51 δ (FCC)	377/164	0.54/0.1	306/122	0.26/-0.02
54 δ (FCC)	388/62	1.11/-0.22	305/55	4.39/3.29

56 τ (CCCO) + 43 τ (CCCC)	255/1	1.19/-1.46	271/18	5.45/4.43
54 τ (CCCO) + 40 τ (CCCC)	236/19	2.46/-1.37	193/14	2.94/-1.97
50 ν (O...H)	89	9.18	102	29.63
62 δ (O...HO)	52	1.41	63	0.87

^aPEDs elements lower than 10% are not included. PEDs elements obtained with HF/6-31G(d,p) are given.

vibrational characteristics of most of the vibrational modes. This phenomenon could be explained with the charge rearrangement in the hydrogen bonding, namely the 3,5-(CF₃)₂C₆H₄O and 3,5-(CF₃)₂C₆H₃O⁻ hydrogen bond formations lead more considerable charge rearrangement in the monomers.

The 3,5-(CF₃)₂C₆H₄O and 3,5-(CF₃)₂C₆H₃O⁻ hydrogen bonding leads to arising of two intermolecular vibrations the $\nu(\text{O}_1^- \dots \text{H}_{10}^+)$ and the $\nu(\text{O}_{20}^- \dots \text{H}_{11})$. The predicted frequency of the $\nu(\text{O}_1^- \dots \text{H}_{10}^+)$ vibration is at 89 – 102 cm⁻¹. The calculated IR intensity of this vibration is low. The $\delta(\text{O} \dots \text{HO})$ vibration is predicted at lower frequency (52 – 63 cm⁻¹), and its IR intensity is lower.

CONCLUSION

The structure, stability and vibrational spectra of the 3,5-(CF₃)₂C₆H₄O and 3,5-(CF₃)₂C₆H₃O⁻ hydrogen-bonded system, containing SSHB, have been investigated using *ab initio* and DFT calculations at different basis sets. The main results of the study are:

- The calculations show that a strong, almost symmetrical, O-H...O bond is formed. The calculated H₁₀...O₂₀ distance (1.235 Å) and O₁H₁₀...O₂₀ = 179.60° angle are in agreement with the SSHB classification (H...A is within 1.2 to 1.5 Å and D-H...A \cong 180°).

- The corrected values of the dissociation energy (-29.31 - 35.95 kcal.mol⁻¹), calculated through HF/6-31G(d,p) and BLYP calculations, confirm the SSHB formation as well as the ionic structure of the studied hydrogen-bonded system.

- The changes of the atomic charges (Δq_i) in the hydrogen bonding show large proton polarizability of the SSHB within this complex, i.e. hydrogen-bonded system of ionic nature is formed.

- The stretching $\nu(\text{O}_1-\text{H}_{10})$ vibration of the hydrogen-bonded O-H group is shifted to lower frequencies and its IR intensity increases considerably in the hydrogen bonding. This result confirms the optimized stable structure of the complex, and shows the formation of the O⁻ ...H⁺ ...O⁻ SSHBs with proton transfer, i.e. the polar structure.

Acknowledgements: The research is supported by the Bulgarian National Science Fund, contract X-1510. This financial support is gratefully acknowledged.

REFERENCES

1. D. Hadzi, Theoretical Treatment of Hydrogen Bonding, John Wiley and Sons, New York, 1997.
2. Y. Dimitrova, *J.Mol.Struct. (Theochem)*, **334**, 215 (1995).
3. Y. Dimitrova, *J.Mol.Struct. (Theochem)*, **343**, 25 (1995).
4. M.C. Buzzeo, L.N. Zakharov, A.L. Rheingold, L.H. Doerrer, *J.Mol.Struct.*, **657**, 19 (2003).
5. J.P.Castaneda, G.S. Denisov, S.Yu. Kucherov, V.M. Scheiber, A.V. Shurukhina, *J.Mol.Struct.*, **660**, 25 (2003).
6. R. Maiti, K. Nagarajan, S. Sarkar, *J.Mol.Struct.*, **656**, 169 (2003).
7. K. Mierzwicki, Z. Latajka, *Chemical Physics*, **265**, 30 (2001).
8. W.W. Cleland, M.M. Kreevoy, *Science*, **264**, 1887 (1994).
9. P.A. Frey, S.A. White, J.B. Tobin, *Science*, **264**, 1927 (1994).
10. J.A. Gerlt, P.J. Gassman, *J.Am.Chem.Soc.*, **115**, 11552 (1993).
11. K.S. Kim, K.S. Oh, J.Y. Lee, *Proc.Natl.Acad.Sci. USA*, **97**, 6373 (2000).
12. K.S. Kim, D. Kim, J.Y. Lee, P. Tarakeshwar, K.S. Oh, *Biochem.*, **41**, 5300 (2002).
13. K.S. Oh, S.-S. Cha, D.-H. Kim, H.-S. Cho, N.-C. Ha, G. Choi, J.Y. Lee, P. Tarakeshwar, H.S. Son, K.Y. Choi, B.-H. Oh, K.S. Kim, *Biochem.*, **39**, 13891 (2000).
14. B.H. Hong, C.-W. Lee, J.C. Kim, K.S. Kim, *J.Am.Chem.Soc.*, **123**, 10748 (2001).
15. D. Hadzi, *Pure Appl.Chem.*, **11**, 435 (1965).
16. T. Steiner, *Angew.Chem.Int. Ed.*, **41**, 48 (2002).
17. Y. Wei, A.E. McDermott, *ACS Symp. Ser.*, **732**, 177 (1999).
18. S. Shan, S. Loh, D. Herschlag, *Science*, **272**, 97 (1996).
19. Y. Pan, M.A. McAllister, *J.Am.Chem.Soc.*, **120**, 166 (1998).
20. Y. Kato, L.M. Toledo, J. Rebek, *J.Am.Chem.Soc.*, **118**, 8575 (1996).
21. H.-F. Klein, A. Dal, T. Jung, U. Flörke, H.J. Haupt, *Eur.J.Inorg.Chem.*, 2027 (1998).
22. C. Gerdemann, C. Eicken, B. Krebs, *Acc.Chem.Res.*,

- 35, 183 (2002).
23. D.M. Williams, P.A. Cole, *J.Am.Chem.Soc.*, **124**, 5956 (2002).
24. J.A. Gerlt, M.M. Kreevoy, W.W. Cleland, P.A. Frey, *Chem.Biol.*, **4**, 259 (1997).
25. A.S. Mildvan, M.A. Massian, T.K. Harris, G.T. Marks, D.H.T. Harrison, C. Viragh, P.M. Reddy, I.M. Kovach, *J.Mol.Struct.*, **615**, 163 (2002).
26. K.S. Kim, D. Kim, J.Y. Lee, P. Tarakeshwar, K.S. Oh, *Biochemistry*, **41**, 5300 (2002).
27. M. J. Frisch, G. W. Trucks, H. B. Schlegel, G. E. Scuseria, M. A. Robb, J. R. Cheeseman, J. A. Montgomery, Jr., T. Vreven, K. N. Kudin, J. C. Burant, J. M. Millam, S. S. Iyengar, J. Tomasi, V. Barone, B. Mennucci, M. Cossi, G. Scalmani, N. Rega, G. A. Petersson, H. Nakatsuji, M. Hada, M. Ehara, K. Toyota, R. Fukuda, J. Hasegawa, M. Ishida, T. Nakajima, Y. Honda, O. Kitao, H. Nakai, M. Klene, X. Li, J. E. Knox, H. P. Hratchian, J. B. Cross, C. Adamo, J. Jaramillo, R. Gomperts, R. E. Stratmann, O. Yazyev, A. J. Austin, R. Cammi, C. Pomelli, J. W. Ochterski, P. Y. Ayala, K. Morokuma, G. A. Voth, P. Salvador, J. J. Dannenberg, V. G. Zakrzewski, S. Dapprich, A. D. Daniels, M. C. Strain, O. Farkas, D. K. Malick, A. D. Rabuck, K. Raghavachari, J. B. Foresman, J. V. Ortiz, Q. Cui, A. G. Baboul, S. Clifford, J. Cioslowski, B. B. Stefanov, G. Liu, A. Liashenko, P. Piskorz, I. Komaromi, R. L. Martin, D. J. Fox, T. Keith, M. A. Al-Laham, C. Y. Peng, A. Nanayakkara, M. Challacombe, P. M. W. Gill, B. Johnson, W. Chen, M. W. Wong, C. Gonzalez, and J. A. Pople, Gaussian 03, Revision B.04, Gaussian, Inc., Pittsburgh PA, 2003.
28. R.G. Parr, W. Yang, *Density-Functional Theory of Atoms and Molecules*, Oxford University Press, Oxford, 1989.
29. A.D. Becke, *J.Chem.Phys.* **98**, 5648 (1993).
30. R.G. Parr, W. Yang, *Annu.Rev.Phys.Chem.* **46**, 701 (1995).
31. J.K. Labanowski, J.W. Andzelm, *Density Functional Methods in Chemistry*, Springer, Berlin, 1991.
32. P. Schuster, Ed., *Hydrogen Bonds, Topics in Current Chemistry Vol. 120*, Springer, Berlin, 1984.
33. G.A. Jeffrey and W. Saenger, *Hydrogen Bonding in Biological Structures*, Springer, Berlin, 1991.
34. R. Ludwig, F. Weinhold and T.C. Farrar, *J.Chem.Phys.*, **102**, 5118 (1995).
35. M.C. Holthausen, C. Heinemann, H.H. Cornehl, W. Koch and H. Schwartz, *J.Chem.Phys.*, **102**, 4931 (1995).
36. M.C. Buzzeo, L.N. Zakharov, A.L. Rheingold, L.H. Doerrer, *J.Mol.Struct.*, **657**, 19 (2003).
37. S. Humbel, *J.Phys.Chem. A*, **106**, 5517 (2002).
38. U. Suksangpanya, *KKU Sci. J.*, **32**, 1 (2004).
39. Y. Dimitrova, *Recent Research Development, Phys. Chem.*, **3**, 133 (1999).
40. Y. Dimitrova, *Recent Research Development, Phys. Chem.*, **6**, 127 (2002).
41. J.E. Carpenter and F. Weinhold, *J.Mol.Struct.(Theochem)*, **169**, 41 (1988).
42. J.E. Carpenter, PhD thesis, University of Wisconsin (Madison, WI), 1987.
43. J.P. Foster and F. Weinhold, *J.Am.Chem.Soc.*, **102**, 7211 (1980).
44. A.E. Reed and F. Weinhold, *J.Chem.Phys.*, **78**, 4066 (1983).
45. A.E. Reed and F. Weinhold, *J.Chem.Phys.*, **76**, 1736 (1983).
46. A.E. Reed, R.B. Weinstock and F. Weinhold, *J.Chem.Phys.*, **83**, 735 (1985).
47. A.E. Reed, L.A. Curtiss and F. Weinhold, *Chem.Rev.*, **88**, 899 (1988).
48. F. Weinhold and J.E. Carpenter, "The structure of Small Molecules and Ions", Plenum (1988) 277.
49. T. Bürgi, M. Schütz, S. Leutwyler, *J.Chem.Phys.*, **103**, 6350 (1995).
50. M. Gerhards, K. Kleinermanns, *J.Chem.Phys.*, **103**, 7392 (1995).
51. Ch. Jacoby, W. Roth, M. Schmitt, Ch. Janzen, D. Spangenberg,
52. K. Kleinermanns, *J. Phys. Chem. A*, **102**, 4471 (1998).
53. J.E. Del Bene, M.J.T. Jordan, *Intern. Rev. Phys. Chem.*, **18**, 119 (1999).
54. J. Smets, W. McCarthy, G. Maes, L. Adamowicz, *J.Mol.Struct.*, **476**, 27 (1999).
55. Y. Dimitrova, *Spectrochim.Acta, Part A*, **60**, 2457 (2004).
56. Y. Dimitrova, *Spectrochim.Acta, Part A*, **60**, 3049 (2004).
57. T. Hirano, T. Taketsugu, Y. Kurita, *J.Phys.Chem.*, **98**, 6936 (1994).

ТЕОРЕТИЧНО ИЗСЛЕДВАНЕ НА СТРУКТУРИ, СТАБИЛНОСТ И ВИБРАЦИОННИ СПЕКТРИ
НА ВОДОРОДНО-СВЪРЗАНИ ФЕНОКСИДИ СЪДЪРЖАЩИ СИЛНИ, КЪСИ ВОДОРОДНИ
ВРЪЗКИ

Й. Димитрова

Институт по органична химия с Център по фитохимия, Българска академия на науките, ул. "Акад. Г. Бончев"
бл. 9, 1113 София

Постъпила на 18 ноември 2009 г.; Преработена на 18 май 2010 г.

(Резюме)

Структурата, стабилността и вибрационните спектри на водородно-свързаната система между 3,5-(CF₃)₂C₆H₄O и 3,5-(CF₃)₂C₆H₃O⁻, съдържаща силна, къса водородна връзка са изследвани посредством *ab initio* и ТФП пресмятания с различни базисни набори. Проведена е пълна геометрична оптимизация на водородно-свързаната система с *ab initio* HF/6-31G(d,p) и BLYP/6-31+G(d,p) пресмятания. Пресмятанията показват, че се наблюдава силна, почти симетрична О-Н...О⁻ връзка. Изчисленото О-Н...О⁻ разстояние (1.235 Å) и ъгълът ОН...О⁻ = 179.60° са в съгласие с класификацията за силни, къси водородни връзки. Коригираните стойности на дисоциационната енергия (-29.31 - 35.95 kcal.mol⁻¹) изчислени с HF/6-31G(d,p) и BLYP пресмятанията потвърждават йонната структура на водородно-свързаната система. Пресмятанията показват, че образуването на водородна връзка между 3,5-(CF₃)₂C₆H₄O и 3,5-(CF₃)₂C₆H₃O⁻ води до значително преразпределение на зарядите при мономерите. Промените на атомните заряди (Δq_i) за комплекса в резултат на водородното свързване показват значителна протонна поляризуемост за силната, къса водородна връзка, т.е. образува се водородно-свързана система с йонен характер. Образуването на силна, къса водородна връзка води до значителни промени на вибрационните характеристики на повечето трептения. Това явление би могло да се обясни със значителното преразпределение на зарядите под действие на водородното свързване.

Kinetics of oxidation of adenosine by *tert*-butoxyl radicals – protection and repair by rosmarinic acid

G. Vijayalakshmi, M. Adinarayana* and P. Jayaprakash Rao

Department of Chemistry, Osmania University, Hyderabad, 500 007, India

*Post Graduate College of Science, Saifabad, Osmania University, Hyderabad, 500 004, India

Received February 3, 2010; Revised February 17, 2010

The rates of oxidation of adenosine and rosmarinic acid by *tert*-butoxyl radicals have been studied by measuring the absorbance of adenosine at 260 nm and rosmarinic acid at 324 nm spectrophotometrically. *Tert*-butoxyl radicals are generated by photolysis of *tert*-butyl hydroperoxide in presence of *tert*-butyl alcohol to scavenge OH• radicals. The rates and the quantum yields (ϕ) of oxidation of rosmarinic acid by *t*-BuO• radicals have been determined in the absence and presence of varying concentrations of adenosine. An increase in the concentration of adenosine has been found to decrease the rate of oxidation of rosmarinic acid suggesting that adenosine and rosmarinic acid compete for *t*-BuO• radicals. From competition kinetics, the rate constant of rosmarinic acid reaction with *t*-BuO• radicals has been calculated to be $2.51 \times 10^9 \text{ dm}^3 \text{ mol}^{-1} \text{ s}^{-1}$. The quantum yields (ϕ_{expt}) have been calculated from the experimentally determined initial rates of oxidation of rosmarinic acid under different experimental conditions. Assuming that rosmarinic acid acts as a scavenger of *t*-butoxyl radicals only, quantum yields (ϕ_{cal}) have been theoretically calculated. The values of ϕ_{expt} and ϕ_{cal} suggest that rosmarinic acid not only protects adenosine from *t*-BuO• radicals but also repairs adenosine radicals formed by the reaction of adenosine with *t*-BuO• radicals.

Keywords: Rosmarinic acid, adenosine, oxidation, protection, repair, *tert*-butoxyl radicals.

INTRODUCTION

Reactive oxygen species (ROS) are generated in biological systems as by-product of normal cellular processes [1], exposure to UV radiation, and in the presence of transition metal ions [2]. In the presence of oxygen, these species react rapidly with biological targets such as lipids, carbohydrates, proteins, nucleic acids, etc. to form alkyl hydroperoxides [3, 4]. Metabolic degradation of endogenous and exogenous peroxides is thought to play a role in the etiology of several diseases including cancer [5, 6]. DNA is one of the main molecular targets of toxic effects of free radicals formed in mammalian cells during respiration, metabolism and phagocytosis. The lethal effects of the hydroxyl radicals on DNA and its constituents have been extensively studied but relatively little is known about the biological effects of alkoxy radicals and the key cellular targets for these species. Recent studies have demonstrated that the exposure of cultured cells to alkoxy radicals resulted in the generation of DNA strand breaks [7–9], though the mechanism of damage has not been elucidated. Previous studies on the reactivity of

tertiary butoxyl radicals suggest that these species might be expected to attack both the sugar and the base moieties of DNA [10]. The experimental evidence indicates that base radicals also contribute to strand breaks by transfer of their radical sites from base moiety to sugar moiety. Strand breaks are considered to be a very serious kind of damage to DNA [11, 12].

Antioxidants are substances, when present in small quantities prevent the oxidation of cellular organelles by minimizing the damaging effects of oxidative stress [13, 14]. Antioxidants such as phenolics are widely distributed in the plant kingdom and are therefore an integral part of the diet, with significant amounts being reported in fruits, vegetables and beverages [15]. Chemical, biochemical, clinical and epidemiological evidence has supported the role that dietary antioxidants play an important role in the prevention of several chronic diseases including cardiovascular diseases, cancer, ageing and diabetes [16,17]. The pharmacological actions of phenolic antioxidants stem mainly from their free radical scavenging and metal chelating properties as well as their effects on cell signaling pathway and on gene expression [18]. From our laboratory, caffeic acid has been reported [19, 20] to repair adenosine radicals in addition to

* To whom all correspondence should be sent:
E-mail: E-mail: adinarayana_mundra@live.com

efficiently scavenging of $\text{SO}_4\cdot$ and tert-butoxyl radicals. In this context, studies involving rosmarinic acid assume importance due to its presence in many dietary phytochemicals in higher concentrations.

The t-BuO \cdot radicals have been generated by steady state photolysis of tert-butyl hydroperoxide in the presence of t-BuOH to scavenge the hydroxyl radicals in aqueous solution [21]. The reactions of t-BuO \cdot radicals with adenosine have been studied in the presence of rosmarinic acid with a view to assess the protection by rosmarinic acid towards oxidation of adenosine by t-BuO \cdot radicals and also repair, if any, offered by rosmarinic acid towards adenosine radicals.

MATERIALS AND METHODS

Adenosine and rosmarinic acid were purchased from Sigma and used as received. All solutions were prepared afresh using double distilled water. tert-Butyl hydroperoxide (t-BuOOH) was used as received from Merck-Schuchardt of Germany. There was no contamination of other peroxides in the assay of the sample. t-BuOOH was estimated by the iodometric method [22]. The irradiations were carried out at room temperature in a quantum yield reactor model QYR-20, supplied by Photophysics, England, and attached with 400 W medium pressure mercury lamp. The quartz cuvette, containing the sample, was irradiated and the irradiations were interrupted at definite intervals of time and the absorbance was noted. The light intensity corresponding to the irradiating wavelength (254 nm) was measured using peroxydisulphate chemical actinometry [23]. On photolysis, t-BuOOH is activated at 254 nm to generate $\cdot\text{OH}$ and t-BuO \cdot radicals by homolytic cleavage of -O-O-bond [24]. The $\cdot\text{OH}$ radicals produced have been scavenged using sufficient concentration of t-BuOH [21]. In a typical kinetic run the aqueous reaction mixture of adenosine, t-BuOOH and t-BuOH was taken in a specially designed one-centimeter path length quartz cuvette, suitable for both irradiations and absorbance measurements. The absorbance measurements were made at the λ_{max} of adenosine (260 nm) on a Chemito UV-Visible spectrophotometer (model 2100).

The photochemical reaction of rosmarinic acid in the presence of t-BuOOH and other additives, viz., t-BuOH and adenosine, has been followed by measuring the absorbance of rosmarinic acid at 324 nm at which adenosine is totally transparent. It is known that t-BuOOH is activated

to radical reaction by the absorption of light at 254 nm [20]. However, the substrates used in the present work, viz., rosmarinic acid and adenosine have strong absorption in this region. But in the absence of t-BuOOH, rosmarinic acid, adenosine or rosmarinic acid-adenosine mixtures have not undergone any observable chemical change on shining the light. Even though a small fraction of the total light intensity is absorbed by t-BuOOH directly in the presence of adenosine and/or rosmarinic acid, a considerable chemical change has been observed with adenosine as well as with rosmarinic acid. If adenosine and rosmarinic acid act as only inner filters, the rates of the reaction of adenosine or rosmarinic acid with t-BuO \cdot would have been decreased with increase in concentration of adenosine or rosmarinic acid. But the results in Table 1 and Table 2 are contrary to this. Another

Table 1. Effect of t-BuOOH and adenosine on the rate and quantum yield of photooxidation of adenosine by t-BuOOH in the presence of light in aqueous neutral medium.

$10^5 \times$ [adenosine] (mol dm $^{-3}$)	$10^3 \times$ [t-BuOOH] (mol dm $^{-3}$)	$10^{10} \times$ Rate (mol dm $^{-3}$ s $^{-1}$)	ϕ_{expt}
1.0	5.0	2.2183	0.000147
2.0	5.0	2.5866	0.000172
4.0	5.0	3.4362	0.000228
5.0	5.0	4.1222	0.000274
5.0	8.0	5.3467	0.000356
5.0	10.0	6.5324	0.000434

Light Intensity = 2.7168×10^{15} quanta s $^{-1}$, $\lambda_{\text{max}} = 260$ nm, pH ~ 7.5 ; temperature = 298 K, [t-BuOH] = 1.0 mol dm $^{-3}$.

Table 2. Effect of t-BuOOH and rosmarinic acid on the rate and quantum yield of photooxidation of rosmarinic acid by t-BuOOH in the presence of light and t-BuOH in an aqueous solution.

$10^5 \times$ [rosmarinic acid] (mol dm $^{-3}$)	$10^3 \times$ [t-BuOOH] (mol dm $^{-3}$)	$10^9 \times$ Rate (mol dm $^{-3}$ s $^{-1}$)	ϕ_{expt}
2.0	1.0	1.6476	0.00109
2.0	2.0	2.3428	0.00155
2.0	5.0	3.4190	0.00227
0.5	5.0	0.7334	0.00049
0.8	5.0	1.1428	0.00076
1.0	5.0	1.3809	0.00092
3.0	5.0	4.8476	0.00346
4.0	5.0	7.4857	0.00695

Light Intensity = 2.7168×10^{15} quanta s $^{-1}$, $\lambda_{\text{max}} = 324$ nm, pH ~ 7.5 ; temperature = 298 K, [t-BuOH] = 1.0 mol dm $^{-3}$.

fact against the inner filter concept is that the rate of oxidation of rosmarinic acid in the presence of adenosine would have been much less than the

experimentally observed values (Table 4). Hence, we propose that the excited states of rosmarinic acid and adenosine act as sensitizers to transfer energy to *t*-BuOOH to produce radical species. This type of sensitizing effect has been proposed in similar systems earlier [19, 25]. Therefore, the light intensity at 254 nm has been used to calculate the quantum yields of oxidation of adenosine as well as rosmarinic acid under different experimental conditions.

RESULTS AND DISCUSSION

The oxidation of adenosine by *t*-BuO• radicals has been carried out by irradiating the reaction mixture containing known concentrations of adenosine and *t*-BuOOH in the presence of sufficient amount of *t*-BuOH to scavenge OH radicals completely [20]. The reaction was followed by measuring the absorbance of adenosine at 260 nm (λ_{max} of adenosine) with time. The reported [20] initial rates and quantum yields of oxidation of adenosine by *t*-BuO• are presented in Table 1. UV-visible absorption spectra of rosmarinic acid in presence of *t*-BuOOH and *t*-BuOH at different irradiation times were recorded (Fig.1). The initial rates of photooxidation of rosmarinic acid by *t*-BuOOH in presence of *t*-BuOH have been calculated from the plots of absorbance of rosmarinic acid at 324 nm vs. time using microcal origin computer program on a personal computer (Table 2). In order to find the protection, offered to adenosine by rosmarinic acid towards oxidation by *t*-BuO•, the reaction mixture, containing known

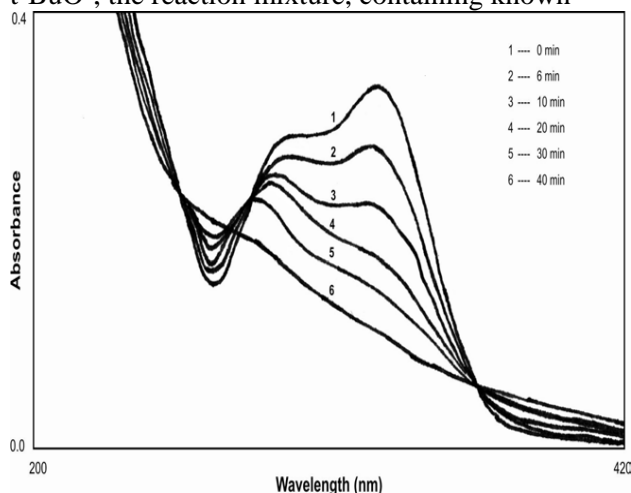


Fig. 1. Absorption spectra of photooxidation of rosmarinic acid in the presence of tert-butylhydroperoxide at different irradiation times; [rosmarinic acid] = 2×10^{-5} mol dm⁻³, [*t*-BuOOH] = 5×10^{-3} mol dm⁻³, Light Intensity = 2.7168×10^{15} quanta s⁻¹, λ_{max} = 324 nm, pH ~ 7.5, temperature = 298K, [*t*-BuOH] = 1.0 M

concentrations of adenosine, *t*-BuOOH and *t*-BuOH, was irradiated in presence of varying concentrations of rosmarinic acid. The reactions were followed by measuring the absorbance of rosmarinic acid at 324 nm (Fig.2) at which adenosine is transparent and the rate data are presented in Table 3.

Table 3. Effect of varying [rosmarinic acid] on the rate and quantum yield of photooxidation of rosmarinic acid by *t*-BuOOH in the absence and presence of adenosine in aqueous solution

$10^5 \times$ [rosmarinic acid] (mol dm ⁻³)	$10^4 \times$ [adenosine] (mol dm ⁻³)	$10^9 \times$ Rate (mol dm ⁻³ s ⁻¹)	Φ_{expt}
0.5	0.0	0.7334	0.00049
0.8	0.0	1.1428	0.00076
1.0	0.0	1.3809	0.00092
2.0	0.0	3.4190	0.00227
0.5	5.0	0.3162	0.00021
0.8	5.0	0.8384	0.00056
1.0	5.0	0.9714	0.00065
2.0	5.0	2.1619	0.00144

[*t*-BuOOH] = 5×10^{-3} mol dm⁻³, Light Intensity = 2.7168×10^{15} quanta s⁻¹, λ_{max} = 324 nm, pH ~ 7.5, temperature = 298 K, [*t*-BuOH] = 1.0 M.

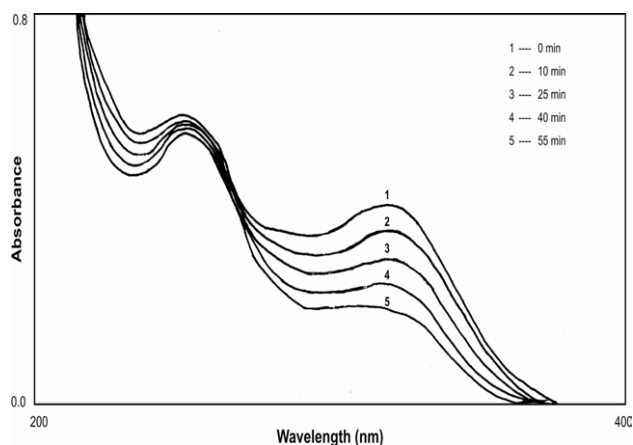


Fig. 2. Absorption spectra of photooxidation of rosmarinic acid in the presence of tertbutyl hydroperoxide and adenosine at different irradiation times; [rosmarinic acid] = 2×10^{-5} mol dm⁻³, [*t*-BuOOH] = 5×10^{-3} mol dm⁻³, [adenosine] = 2×10^{-5} mol dm⁻³, Light Intensity = 2.7168×10^{15} quanta s⁻¹, λ_{max} = 324 nm, pH ~ 7.5, temperature = 298K, [*t*-BuOH] = 1.0 M

The photooxidation of rosmarinic acid by *t*-BuO• at different concentrations of adenosine was also studied (Fig.3) and the data is presented in Table 4. The oxidation rate of adenosine in the presence of *t*-BuOH refers exclusively to the reaction of *t*-BuO• with adenosine [20]. These rates have been found to increase with increase in concentration of adenosine as well as *t*-BuOOH. The quantum yield values are also found to increase

Table 4. Effect of varying [adenosine] on the rate and quantum yield of photooxidation of rosmarinic acid in the presence of *t*-BuOOH, *t*-BuOH and light in aqueous solution.

$10^5 \times$ adenosine (mol dm ⁻³)	$10^9 \times$ Rate (mol dm ⁻³ s ⁻¹)	ϕ_{expt}	ϕ_{cal}	p	ϕ'	% scavenging	% repair
0.00	3.41	0.00227	0.00227	1.0000	0.00227	100.0	0.00
5.00	3.14	0.00209	0.00201	0.8876	0.00235	88.76	3.73
8.00	2.97	0.00198	0.00185	0.8178	0.00242	81.78	6.45
10.0	2.94	0.00196	0.00177	0.7819	0.00250	78.19	10.37
20.0	2.69	0.00179	0.00146	0.6419	0.00279	64.19	22.73
50.0	2.16	0.00144	0.00095	0.4176	0.00344	41.76	51.68
100.0	1.64	0.00109	0.00060	0.2639	0.00413	26.39	81.78

[rosmarinic acid] = 2.0×10^{-5} mol dm⁻³, [*t*-BuOOH] = 5.0×10^{-3} mol dm⁻³, [*t*-BuOH] = 1.0M, Light Intensity = 2.7168×10^{15} quanta s⁻¹, λ_{max} = 324 nm, pH~7.5, temperature = 298 K.

with increase in [adenosine] as well as [*t*-BuOOH] (Table 1).

The rate of oxidation of rosmarinic acid has been found to increase with increase in concentration of rosmarinic acid (Table 2). The quantum yields of oxidation of rosmarinic acid have been calculated from the initial rates and the light intensity at 324 nm. These values are also found to increase with increase in concentration of rosmarinic acid (Table 2). Having known the rates of *t*-BuO• radical reactions with adenosine as well as with rosmarinic acid under varying experimental conditions, both adenosine and rosmarinic acid are introduced for the competitive studies with *t*-BuO• radical. Aqueous solutions of reaction mixture containing rosmarinic acid *t*-BuOOH and *t*-BuOH were irradiated in the presence of varying concentrations of adenosine (Fig.3). The initial rates and quantum yields of oxidation of rosmarinic acid by *t*-BuO• radicals were found to decrease with the increase in concentration of adenosine (Table 4). Comparison of the initial rates and quantum yields of oxidation of rosmarinic acid in the presence and absence of adenosine clearly indicate that the initial rates and quantum yields of oxidation of rosmarinic acid are substantially decreased in the presence of

adenosine (Table 4). These observations clearly demonstrate that adenosine and rosmarinic acid are in competition for *t*-BuO• radicals.

The rate constant of the reaction of *t*-BuO• with adenosine has been reported [12] to be 1.40×10^8 dm³ mol⁻¹s⁻¹ under similar experimental conditions of the present work. The rate constant for the reaction of *t*-BuO• with rosmarinic acid has been calculated by the adenosine competition method, which is very similar to the one chosen to determine the rate constant for the reaction of •OH radicals with polyhydric alcohols in competition with KSCN [26]. In the present study, solutions containing rosmarinic acid and varying amounts of adenosine in presence of *t*-BuOOH and *t*-BuOH were irradiated for two minutes and the decrease in absorbance of rosmarinic acid was measured. The decrease in absorbance of rosmarinic acid reflects the extent of *t*-BuO• radicals reacted with rosmarinic acid. From the known rate constant of the reaction of adenosine with *t*-BuO• radical under similar experimental conditions of the present work ($k_{\text{adenosine}} = 1.40 \times 10^8$ dm³ mol⁻¹ s⁻¹), the rate constant of *t*-BuO• radical reaction with rosmarinic acid ($k_{\text{rosmarinic acid}}$) is calculated using Eq. (1).

$$\frac{[\text{Absorbance of rosmarinic acid}]_0}{[\text{Absorbance of rosmarinic acid}]_{\text{adenosine}}} = 1 + \frac{k_{\text{adenosine}} [\text{adenosine}]}{k_{\text{rosmarinic acid}} [\text{rosmarinic acid}]} \quad (1)$$

$$P(t\text{-BuO}^\bullet + \text{rosmarinic acid}) = \frac{k_{\text{rosmarinic acid}} [\text{rosmarinic acid}]}{k_{\text{adenosine}} [\text{adenosine}] + k_{\text{rosmarinic acid}} [\text{rosmarinic acid}]} \quad (2)$$

In Eq.(1), $[\text{Absorbance of rosmarinic acid}]_0$ and $[\text{Absorbance of rosmarinic acid}]_{\text{adenosine}}$ are the absorbance values of rosmarinic acid in the absence

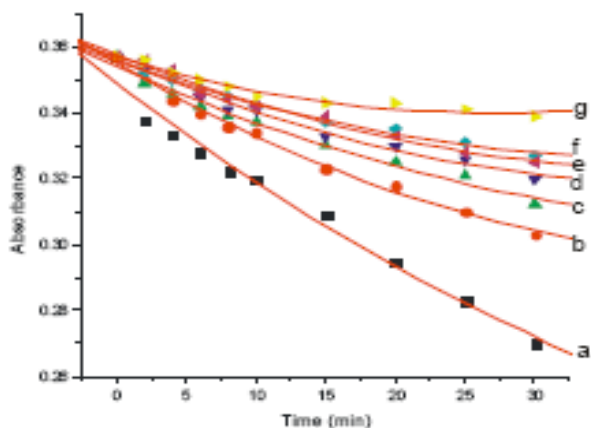


Fig. 3. Effect of varying concentrations of adenosine on the photooxidation of rosmarinic acid ($2.0 \times 10^{-5} \text{ mol dm}^{-3}$) in the presence of $t\text{-BuOOH}$ ($5 \times 10^{-3} \text{ mol dm}^{-3}$) at 298 K. $[\text{adenosine}] =$ (a) 0.0, (b) $5 \times 10^{-5} \text{ mol dm}^{-3}$, (c) $8 \times 10^{-5} \text{ mol dm}^{-3}$, (d) $1 \times 10^{-4} \text{ mol dm}^{-3}$, (e) $2 \times 10^{-4} \text{ mol dm}^{-3}$, (f) $5 \times 10^{-4} \text{ mol dm}^{-3}$, (g) $1 \times 10^{-3} \text{ mol dm}^{-3}$, $[t\text{-BuOH}] = 1.0 \text{ M}$.

and presence of adenosine respectively, at the same interval of time. Experiments of this kind can be carried out with great accuracy. Using Eq.(1) the rate constant for the reaction of $t\text{-BuO}^\bullet$ radical with rosmarinic acid ($k_{\text{rosmarinic acid}}$) has been calculated at different concentrations of rosmarinic acid and adenosine and the average of these values is found to be $2.51 \times 10^9 \text{ dm}^3 \text{ mol}^{-1} \text{ s}^{-1}$. As rosmarinic acid has strong absorption at 260 nm, it is not possible for the direct determination of protection and repair offered to adenosine by rosmarinic acid at this wavelength. However, one can calculate indirectly the extent of protection offered to adenosine by rosmarinic acid from competition kinetic studies measured at 324 nm, λ_{max} of rosmarinic acid. When the system containing adenosine, rosmarinic acid and $t\text{-BuOOH}$ in the presence of $t\text{-BuOH}$ is irradiated, the probability of $t\text{-BuO}^\bullet$ radicals reacting with rosmarinic acid $\{p(t\text{-BuO}^\bullet + \text{rosmarinic acid})\}$ is calculated using Eq. (2).

If rosmarinic acid scavenges only $t\text{-BuO}^\bullet$ radicals and does not give rise to any other reaction (e.g. reaction with adenosine radicals), the quantum yield of oxidation of rosmarinic acid (ϕ_{cal}) at each concentration of adenosine may be given by Eq. (3):

$$\phi_{\text{cal}} = \phi_{\text{expt}}^0 \cdot P \quad (3)$$

where ϕ_{expt}^0 is the quantum yield of oxidation of rosmarinic acid in the absence of adenosine, and p is the probability given by Eqn. 2.

The calculated quantum yield (ϕ_{cal}) values at different adenosine concentrations are presented in Table 4. The data show that ϕ_{cal} values are lower than experimentally measured quantum yield (ϕ_{expt}) values. This indicates that more of rosmarinic acid is consumed in the system than theoretically expected. The most likely route for this is H atom donation by rosmarinic acid to adenosine radicals, generated during competition reactions. Table 4 presents the fraction of $t\text{-BuO}^\bullet$ radicals scavenged by rosmarinic acid at different concentrations of adenosine. These values refer to the measure of protection, offered to adenosine due to scavenging of $t\text{-BuO}^\bullet$ radicals by rosmarinic acid. Using the ϕ_{expt} values, a set of values, viz., ' ϕ' values, have been calculated from Eq. (4) and are presented in Table 4:

$$\phi' = \frac{\phi_{\text{expt}}}{p} \quad (4)$$

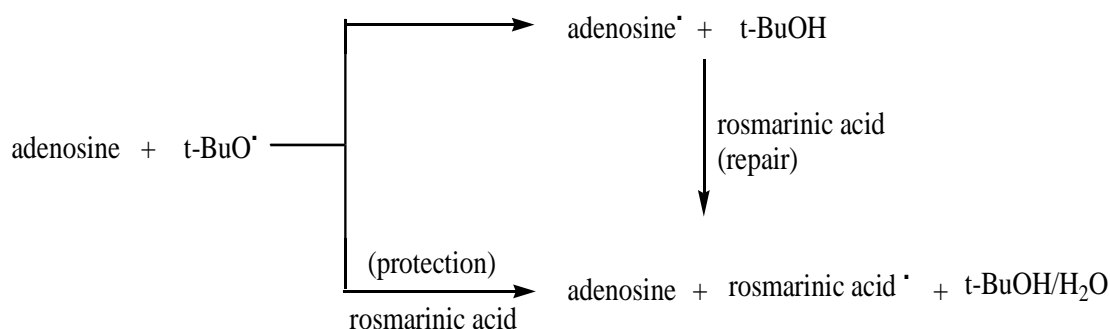
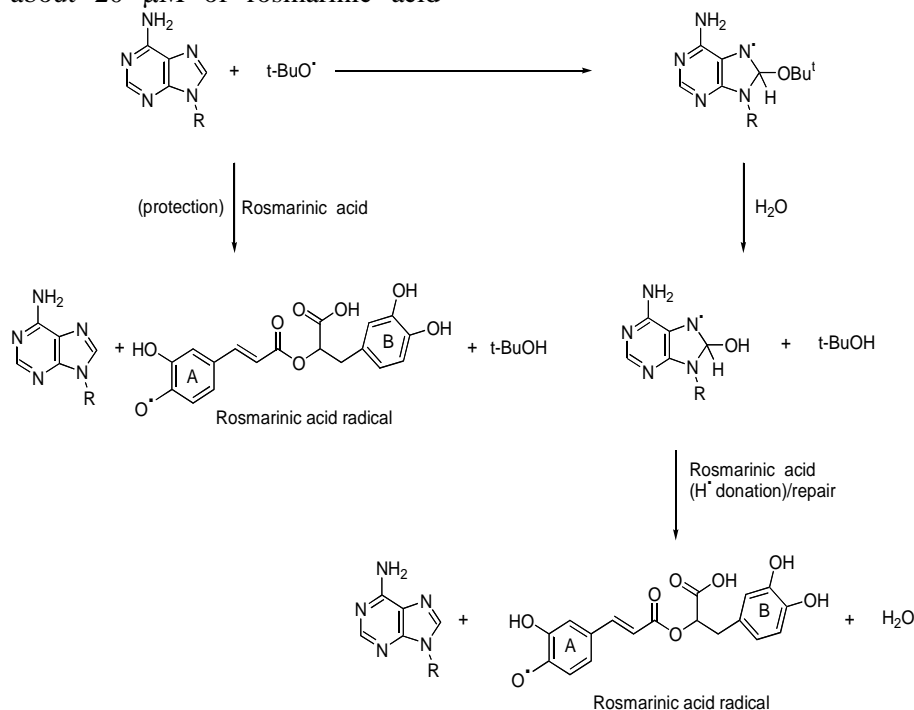
where ϕ' represents experimentally found quantum yield values if no scavenging of adenosine radicals by rosmarinic acid occurs. In the absence of any "repair" of adenosine radicals by rosmarinic acid, ϕ' values should all be equal to ϕ_{expt}^0 . The observed increase ϕ' with increasing adenosine concentration (Table 4) clearly indicates that repair of adenosine radicals does occur. The extent of repair may be quantified by the following equation:

$$\% \text{ Repair} = \frac{\phi' - \phi_{\text{expt}}^0}{\phi_{\text{expt}}^0} \cdot 100 \quad (5)$$

The data on percentage repair is presented in Table 4. The experimentally determined quantum yield (ϕ_{expt}) values are higher than the quantum yield (ϕ_{cal}) values, calculated using Eq.(3) under the assumption that rosmarinic acid acts only as a $t\text{-BuO}^\bullet$ radical scavenger. This shows that rosmarinic acid acts not only as an efficient scavenger of $t\text{-BuO}^\bullet$ radicals but also as an agent for the repair of adenosine radicals. The repair reaction of rosmarinic acid is explained in terms of H donation as shown below in Scheme 1.

The results obtained in the present study (Table 4) indicate that adenosine radicals are efficiently repaired by rosmarinic acid to the extent of ~82 % at about 20 μ M of rosmarinic acid

concentration. The protection of adenosine and repair of adenosine radicals are summarized in Scheme 2.



The electron density calculations show that C8 in adenosine is more electron rich compared to C4 or C5 [27]. The bulkiness of the $t\text{-BuO}\cdot$ radical is another reason that it prefers C8 position where no steric hindrance is present. The attack of $t\text{-BuO}\cdot$ radical at C8 leads to the formation of N7-centered radical, the nature of which has been reported to be oxidizing. Caffeic acid is known to react with oxidizing transient radicals very efficiently. This has been realized in the competition studies of caffeic acid with adenosine radicals [20]. The rosmarinic acid, which is very similar in nature to caffeic acid, is expected to repair the transient oxidizing radicals of adenosine in a similar way.

The obtained percentage of repair, in this study by rosmarinic acid (~82%, cf. Table 4),

supports our contention that rosmarinic acid repairs, oxidizing the adenosine transient radicals.

Acknowledgements: The authors would like to thank to the Head of the Department of Chemistry, Osmania University for providing the facilities to carry out the research work.

REFERENCES

1. J. D. West, L. Marnett, *J. Chem Res. Toxicol.*, **19**, 173 (2006).
2. B. Halliwell, J. M. C. Gutteridge, *Free Radic. Biol. Med.*, 2nd Edition Clarendon Press, Oxford, 1989.
3. C. Von Sonntag, *The Chemical Basis of Radiation Biology*, Taylor & Francis, London, 1987.
4. M.J. Davies, R. T. Dean, *Radical Mediated Protein Oxidation: from Chemistry to Medicine*, Oxford University Press, Oxford, 1997.

5. M. A. Trush, T. W. Kensler, *Free Radic. Biol. Med.*, **10**, 201 (1991).
6. P. A. Cerutti, *Science*, **227**, 375 (1985).
7. J. A. Hartley, N. W. Gibson, A. Kilkenny, S. H. Yuspa, *Carcinogenesis*, **8**, 1821 (1987).
8. J. A. Hartley, N. W. Gibson, L. A. Zwelling, S. H. Yuspa, *Cancer Res.*, **45**, 4864 (1985).
9. J. E. Swanger, P. M. Dolar, J. L. Zweier, P. Kuppusamy, T. W. Kensler, *Chem. Res. Toxicol.*, **4**, 223 (1991).
10. M. Erben-Russ, C. Michel, W. Bors, M. Saran, *J. Phys. Chem.*, **91**, 2362 (1987).
11. M. Adinarayana, E. Bothe, D. Schulte-Frohlinde, *Int. J. Radiat. Biol.*, **54**, 723 (1988).
12. D. G. E. Lemaire, E. Bothe, D. Schulte-Frohlinde, *Int. J. Radiat. Biol.*, **45**, 351 (1984).
13. A. T. Diplok, in: C. Rice-Evans, R. H. A. Burdon, *Free radical damage and its control, new comprehensive biochemistry*, Elsevier, Amsterdam, The Netherlands, 1994.
14. R. A. Larson, 'Naturally Occurring Antioxidants', Lewis Publisher, CRC Press, LLC, Boca Raton, FL, 1997.
15. C. J. Dillard, J. B. German, *J. Sci. Food. Agric.*, **80**, 1744 (2000).
16. J. B. Harborne, C. A. Williams, *Phytochemistry*, **55**, 481 (2000).
17. C. K. B. Ferrari, E. A. F. S. Torres, *Biomed. Pharmacother.*, **57**, 251 (2003).
18. W. Adam, G. N. Grimm, C. R. Saha Moller, *Free Radic. Biol. Med.*, **24**, 234 (1997/8).
19. M. Sudha Swaraga, M. Adinarayana, *Indian J. Biochem. Biophys.*, **40**, 27 (2003).
20. L. Charitha, M. Adinarayana, *Int. J. Chem. Kinetics*, **37**, 515 (2005).
21. K. D. Asmus, H. Mockel, A. Henglein, *J. Phys. Chem.*, **77**, 1218 (1973).
22. J. A. Howard, K. U. Ingold, *Can. J. Chem.*, **45**, 793 (1967).
23. M. Ravi Kumar, M. Adinarayana, *Proc. Indian Acad. Sci.*, **112**, 551 (1984).
24. W. Bors, C. Michel, M. Saran, *Biochem. Biophys. Acta.*, **796**, 312 (1984).
25. M. S. Akhalaq, S. Al-Baghdad, C. Von Sonntag, *Carbohydrate Res.*, **164**, 71 (1987).
26. M. Sudha Swaraga, L. Charitha, M. Adinarayana, *J. Chem. Sci. Indian Acad. Sci.*, **117**, 345 (2005).
27. B. Pullman, *J. Chem. Soc.*, 1621 (1959).

КИНЕТИКА НА ОКИСЛЕНИЕТО НА АДЕНОЗИН ОТ *tert*-БУТОКСИЛОВИ РАДИКАЛИ - ЗАЩИТА И ВЪЗСТАНОВЯВАНЕ С РОЗМАРИНОВА КИСЕЛИНА

Г. Виджаялакшми, М. Адинараяна*, П. Джаяпракаш Рао

Департамент по химия, Университет Османия, Хайдарабад 500 007

*Докторантски колеж за наука, Сайфабад, Университет Османия Хайдарабад 500 004, Индия

Постъпила на 3 февруари 2010 г.; преработена на 17 февруари 2010 г.

(Резюме)

Изследвана е скоростта на окисление на аденозин и розмаринова киселина с *tert*-бутоксидови радикали. Спектрофотометрично е определяна абсорбцията на аденозина при 260 nm и на розмариновата киселина при 324 nm. Третичните бутоксилови радикали се генерират чрез фотолиза на третичен бутилов хидропероксид в присъствие на третичен бутанол за улавянето на $\text{OH}\cdot$ - радикалите. Скоростите и квантовите добиви (ϕ) на окислението на розмариновата киселина от *t*-BuO \cdot - радикалите са определяни в отсъствие и при различни концентрации на аденозин. Повишаването на концентрацията на аденозина води до понижаване скоростта на окисление на розмариновата киселина, което се обяснява с конкуренцията на двата реагента за *t*-BuO \cdot - радикалите. Скоростната константа на реакцията на розмариновата киселина, отчитайки конкуренцията на аденозина е определена на $2.51 \times 10^9 \text{ dm}^3 \text{ mol}^{-1} \text{ s}^{-1}$. Пресметнати са квантовите добиви (ϕ_{expt}) от опитно определените начални скорости на окисление на розмариновата киселина при различни експериментални условия. Приемайки, че розмариновата киселина улавя само *t*-бутоксидовите радикали е изчислен "теоретичния" квантов добив (ϕ_{cal}). Сравняването на двата квантови добива показва, че розмариновата киселина не само защитава аденозина от *t*-BuO \cdot -радикалите, но и възстановява аденозиновите радикали, образувани при реакцията на аденозина с *t*-BuO \cdot - радикалите.

Physicochemical and optical properties of glasses from the Cu-S-Se system

V.S. Vassilev¹, T.K. Hristova-Vasileva¹, E. Fidancevska², M.N. Koleva³, A.I. Zheglova³

¹Department of Non-Ferrous Metals and Semiconductor Technologies, University of Chemical Technology and Metallurgy, 8 “Kl. Ohridski” Blvd., 1756 Sofia, Bulgaria,

²Faculty of Technology and Metallurgy, 16 Ruger Boshkovic, Skopje, Macedonia

³Technical University of Gabrovo, 4 Hadji Dimitar St., 5300 Gabrovo, Bulgaria

Received October 9, 2009, Revised April 22, 2010

Based on the results of the micro-hardness, HV, density, d , and the glass-transition temperature, T_g measurements, the thermo-mechanical characteristics (micro-voids volume, V_h , and the energy for micro-void formation, E_h), the compactness, C , and the elasticity modulus, E , of glasses from the Cu-S-Se system are calculated. The mean values of the overall bond energy, $\langle E \rangle$, coordination number, $\langle Z \rangle$, bond energy of the average cross-linking/atom, \bar{E}_c , and that of the “remaining matrix”, \bar{E}_{rm} , are determined using the known formalism. The average heteropolar bond energy, E_{hb} , and the degree of “cross-linking/atom”, P , are also calculated employing the same experimental finding. The dependence between T_g and $\langle E \rangle$ is linear: $T_g = 314(0.004\langle E \rangle + 0.88)$. The optical band gap, $E_{g,o}$, of as-deposited thin films with composition $Cu_5Se_{95-y}S_y$ ($0 \leq y \leq 30$) is determined using the Tauc’s power law. The $E_{g,o}(y)$ dependence is linear: $E_{g,o}^{opt} = 0.0057y + 1.797$. Correlations between the investigated properties and the glass composition are established.

Keywords: chalcogenide glasses; physicochemical properties, bond energy, optical band gap.

INTRODUCTION

During the last years the chalcogenide glassy semiconductors are widely investigated due to their various properties (switching and memory effects, photosensitivity and transparency in the IR spectral region, chemical and radiation stability, ionic conductivity, etc.), which determine multiple possibilities for their application [1–4].

On the one hand, the investigations referred are focused on already familiar chalcogenide glasses, and on the other hand, on the development of new ones. The experimental investigations include the outlining of glass-forming regions in new systems, and complex investigation on the structure, properties and application areas of the chalcogenide glasses.

When the component number in a given system is increased, the glass-forming ability grows due to the increased probability of formation of new structural units which impede crystal nucleation [5]. Most often two-component systems are used, one of them usually being the glass-forming elements, and the other being the modifier. The S-Se system is very suitable as a base binary system due to the presence of large glass-forming area and it spreads

from 50 to 100 at.% Se [6]. Liquid selenium and sulphur form equilibrium melts, built by linear polymer molecules and 8-ring monomers.

The unarranged interweaving of Se and S chains with rings is stimulated by structure amorphization and by the fact that both S and Se are glass-formers. For example, about 60 at.% As [7] and 30 at.% Ge [8] can be introduced in the S-Se system.

The region of glass-formation in the Cu-S-Se system is outlined by V. Vassilev *et al.* [9] on the basis of the results from visual, X-ray diffraction and electron-microscopic analyses (see Figure 1 below).

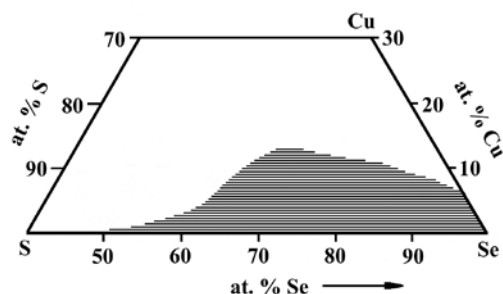


Fig. 1. Region of glass-formation in the Cu-S-Se system [9].

* To whom all correspondence should be sent:
E-mail: E-mail: venciv@uctm.edu

The aim of the present paper is the investigation of the main physicochemical and optical properties of glasses with composition $Cu_xS_ySe_z$ ($x+y+z=1$), and the analysis of the respective composition-property diagrams.

EXPERIMENTAL

The glassy samples, used for the investigations, were synthesized applying the method, described in [9]: direct monotemperature synthesis in evacuated and vacuum sealed quartz ampoules; maximum synthesis temperature of 1100 ± 5 °C; synthesis duration – 24 h, and subsequent quenching of the smelter in water+ice+NaCl mixture.

The microhardness, HV, was measured by the Vickers' method using a metallographic MIM-7 microscope with built in microhardness meter, PMT-3, at loading of 10 g (accuracy ± 4 %). The density, d, is measured by hydrostatic method in toluene as immersion fluid (accuracy ± 4 %). The glass-transition temperature, T_g , is determined by differential-thermal analysis (accuracy ± 5 °C) at heating rate of 16 °C min^{-1} and with $\alpha-Al_2O_3$ as reference substance.

Using the results of these measurements, the thermomechanical characteristics (micro-voids volume, V_h , and energy for micro-voids formation, E_h), the elasticity modulus, E, and the compactness, C, are calculated.

Based on a free volume approach in calculating cohesion glasses, Sanditov [10] proposed to determine microhardness as $HV = E_h/V_h$. Using this concept we derived in [11] the following expressions for the quantities E, V_h , and E_h :

$$V_h = 5.04 \cdot 10^{-3} \cdot \frac{T_g}{HV} [nm^3]; E_h = 29.75 \cdot T_g [J mol^{-1}];$$

$$E = 0.147 \cdot HV [GPa], \quad (1)$$

where HV – micro-hardness [$kgf mm^{-2}$]; T_g – glass-transition temperature [K].

The compactness, C, expresses, in arbitrary units, the deviation in the glass density from that of a corresponding crystal with the same composition ($C = \Delta/d_i$; $\Delta = d_i - d$). It is calculated using the equation [13]:

$$C = d \left\{ \sum_i^n \frac{M_i x_i}{d_i} - \sum_i^n \frac{M_i x_i}{d} \right\} \left[\sum_i^n M_i x_i \right]^{-1}, \quad (2)$$

where d – density of the sample; d_i , M_i and x_i are the density, the molar (atomic) mass and molar (atomic) part of the i^{th} component, respectively. The

compactness can acquire both positive and negative values. The negative ones respond to looser structure, and the positive to a denser structure, compared to a crystal with the same composition.

The properties of the chalcogenide glasses are directly related to the overall mean bond energy, which is a function of the mean coordination number and the type and the energy of the chemical bonds between the atoms, building the glasses.

The mean coordination number $\langle Z \rangle$ of the glasses is calculated by an equation (3), proposed by Tanaka [13]. The following values of the atom coordination numbers are used for the investigated system: $Z_{Se} = Z_S = 2$ [14] and $Z_{Cu} = 2$ [15].

$$\langle Z \rangle = x \cdot Z_{Cu} + y \cdot Z_S + z \cdot Z_{Se} \quad (3)$$

where x, y and z are the atomic parts of Cu, S and Se, respectively.

The overall mean bond energy $\langle E \rangle$ is calculated using Tichy's equation [16] for complex chalcogenide systems:

$$\langle E \rangle = \bar{E}_c + \bar{E}_{rm}, \quad (4)$$

where \bar{E}_c is the average bond energy of cross-linking/atom and \bar{E}_{rm} is the average bond energy per atom of the “remaining matrix”.

The value of \bar{E}_c is calculated by the equation:

$$\bar{E}_c = P \cdot E_{hb}, \quad (5)$$

where P is the degree of cross-linking/atom; E_{hb} – average heteropolar bond energy. For glasses with composition $Cu_xS_ySe_z$, the E_{hb} is calculated by the equation (6):

$$E_{hb} = (x \cdot Z_{Cu} \cdot E_{Cu-S} + x \cdot Z_{Cu} \cdot E_{Cu-Se}) / (x \cdot Z_{Cu}), \quad (6)$$

where: E_{Cu-S} and E_{Cu-Se} are the heteropolar bond energies of Cu-S and Cu-Se – Table 1.

Table 1. Energy of chemical bonding in the Cu-S-Se system.

Bond	Se-Se	S-S	Cu-Cu	Se-S	Se-Cu	S-Cu
Bond energy, eV	1.90	2.20	1.83	3.85	2.60	2.86
Reference	[16]	[16]	[17]	[18]	[19]	[19]

The coefficient R is used for determination of the chalcogen content in the glasses:

$$R = (y \cdot Z_S + z \cdot Z_{Se}) / (x \cdot Z_{Cu}). \quad (7)$$

At $R > 1$ the system is chalcogen rich and heteropolar chalcogen-chalcogen bonds are present. In this case $P = P_r$, and

$$P_r = x \cdot Z_{Cu} / (x+y+z) \quad (8)$$

At R=1 the system is with stoichiometric composition thus there are only heteropolar bonds to be expected.

At R<1 the system is chalcogen poor and heteropolar metal-metal bonds are present. In this case P=P_p.

$$P_p = z \cdot Z_{Se} / (x+y+z) \quad (9)$$

The average bond energy per atom of the “remaining matrix” is defined by:

$$\bar{E}_{rm} = 2(0.5 \cdot \langle Z \rangle - P_r) E_{<>} / \langle Z \rangle, R > 1 \quad (10)$$

$$\bar{E}_{rm} = 2(0.5 \cdot \langle Z \rangle - P_p) E_{A-A} / \langle Z \rangle, R < 1, \quad (11)$$

where E_{<>} - average bond energy between the S and Se atoms:

$$E_{<>} = \frac{1}{3} \cdot (E_{S-S} + E_{Se-Se} + E_{S-Se}) \quad (12)$$

The measurement of the optical absorption (at $\alpha < 10^4 \text{ cm}^{-1}$) gives information about the density of the states in the tail area. Since in amorphous semiconductors the doubled value of the electrical conductivity activation energy corresponding to a frequency, equivalent to $= 10^4 \text{ cm}^{-1}$, Stuke [20] suggested the optical band gap, E_g^{opt} to be defined at this α value. According to Tauc [21] in the $\alpha \geq 10^4 \text{ cm}^{-1}$ area the optical absorption is due to transitions

of electrons from the delocalized states in the valence band ($E < E_v$) to the delocalized states in the conductivity band ($E > E_c$), as the value of α increases with the photon energy (hv) according the equation:

$$\alpha hv = A [hv - (E_c - E_v)]^n, \quad (13)$$

A is a constant, characteristic for the material, and n is another constant, characterizing the transition type (for direct transitions n=1/2 and for indirect – n = 2).

The absorption coefficient is calculated from the transmission spectra using the equation

$$\alpha = -\frac{1}{d} \ln T, \quad (14)$$

where T=I/I₀ (I and I₀ are the intensities of the transmitted and incident light, respectively).

RESULTS AND DISCUSSION

1. Physical and thermo-mechanical characteristics

The T_g, d, and HV values, needed for calculation of the thermo-mechanical characteristics of glasses from the Cu-S-Se system, are shown in Table 2, as well as the obtained results for E, E_h, V_h, and C, derived using equations (1) and (2).

Table 2. Physical and thermo-mechanical properties of glassy phases with composition Cu_xS_ySe_z ((x+y+z)=1; m=z/(y+z)).

№	Composition, at. parts			m	T _g , K	d, g cm ⁻³	HV, kgf mm ⁻²	E, GPa	E _h , kJ mol ⁻¹	V _h 10 ⁻³ , nm ³	C
1	0.00	0.00	1.00	1.000	315	4.25	40	5.88	9.37	39.69	-0.1127
2	0.00	0.05	0.95	0.950	310	4.15	35	5.15	9.22	44.64	-0.1124
3	0.00	0.15	0.85	0.850	305	3.92	31	4.56	9.07	49.59	-0.1335
4	0.00	0.25	0.75	0.750	300	3.67	28	4.12	8.93	54.00	-0.1272
5	0.05	0.00	0.95	1.000	330	4.18	36	5.29	9.82	46.20	-0.1438
6	0.05	0.05	0.90	0.947	325	4.03	32	4.70	9.67	51.19	-0.1542
7	0.05	0.10	0.85	0.895	318	3.88	30	4.41	9.46	53.42	-0.1649
8	0.05	0.15	0.80	0.842	312	3.81	28	4.12	9.28	56.16	-0.1848
9	0.05	0.20	0.75	0.789	307	3.61	27	3.97	9.13	57.31	-0.1804
10	0.05	0.30	0.65	0.684	305	3.40	25	3.68	9.07	61.49	-0.2006
11	0.10	0.10	0.80	0.889	325	3.80	27	3.97	9.67	60.67	-0.1515
12	0.10	0.15	0.75	0.833	317	3.69	25	3.68	9.43	63.91	-0.2047
13	0.10	0.20	0.70	0.778	310	3.58	24	3.53	9.22	65.10	-0.2027
14	0.10	0.25	0.65	0.722	305	3.43	23	3.38	9.07	66.83	-0.2047

The increase of the glass-transition temperature, T_g, at raising the Se content at constant copper concentration (x=const) is expected since in this case the concentration of the glass-former increases

as seen from Table 2. The influence of copper on the T_g-value of the glasses seems “unusual”. It rises

with the increase of the Cu-content (at m=const) (Table 2). It has to be noticed that up to a certain concentration copper breaks the (-S-S-), (-Se-Se-),

and (–S–Se–) bonds and participates equally in the linear chains formed by the S and Se atoms in the chalcogenide glass. At Cu-content higher than a critical value, defined by the glass-forming boundaries in the Cu-S-Se system, a crystalline phase of composition Cu, Cu₂S and/or Cu₂Se is formed. The T_g-value decreases quickly in this case.

The density, d, increases noticeably with the raise of the Se-content (i.e. m increases) at a constant value of Cu (x=const) which is related to the great difference between the densities of the elements S and Se (d_{Se}=4.25>>d_S=2.09 g cm⁻³) – Table 2. In spite of the great difference between the density values (d_{Cu}=8.93 g cm⁻³), the density of the chalcogenide glasses lightly increases with the raise of the Cu content at m=const (Table 2) which is connected to the circumstance that with the inclusion of Cu the total micro-pore volume increases V_{μp}. This increase compensates the glass mass increase m_g (d=m_g/(V_g+V_{μp}), where V_g is the glass volume without the pores. This assumption is confirmed by the HV(x) dependencies at m=const (Table 2). HV decreases with the x raise since the glass structure becomes looser, i.e. the V_{μp} increases.

The elasticity modulus, E, follows the path of the microhardness.

The minimum micro-void volume, V_h, decreases with the increase of the Se-content (at x=const), and increases with the addition of Cu (at m=const) since both dependencies are almost linear. This change of the V_h of the chalcogenide glass composition is caused, on the one hand, by the fact that the atomic

radius of Se is larger than this of the S and with the gradual substitution of S- with Se-atoms (at x=const) the structure becomes denser. On the other hand, the Cu-atoms are built into the structure, formed by (–S–Se–)-chains (at m=const), as a result of which it becomes looser.

The E_n(x;m) dependencies go over the path of the T_g(x;m) dependencies. In the cases when m increases (the Se replaces the S) at x=const, as it was shown above, the structure of the glasses is denser. This process opposes the further substitution of S with Se, which by its side requires higher E_n values. The introduction of Cu in the glasses at m=const does not lead to substitution of S and/or Se but breaks their chains at different places (–S–S–; –Se–Se– и –S–Se–), builds into them, and forms fragments form the type: –S–Cu–S–; –Se–Cu–Se– и –S–Cu–Se–. Additional amount of energy is needed for these processes to take place and this is why E_n increases with the increase of the Cu content (at m=const).

The compactness of the investigated glasses has negative values and depending on the composition changes in very narrow limits (the experimental values of C are from – 0.21 to – 0.10).

2. Energy of the Chemical Bond

Based on the model shown in the Experimental Part, the average parameters (<Z>, R, P, E_{hb}, \bar{E}_c , E_{<>}, \bar{E}_{rm} , and <E>) of the chemical bond are calculated. Their values are shown in Table 3.

Table 3. Physicochemical properties of the samples with composition Cu_xS_ySe_z.

№	Composition, at. parts			m	T _g , K	Z	R	P _r	E _{hb}	\bar{E}_c , eV	E _{<>} , eV	\bar{E}_{rm} , eV	<E>, eV
1	0.00	0.00	1.00	1.000	315	2	∞	0	0	0	2.65	2.650	2.650
2	0.00	0.05	0.95	0.950	310	2	∞	0	0	0	2.65	2.650	2.650
3	0.00	0.15	0.85	0.850	305	2	∞	0	0	0	2.65	2.650	2.650
4	0.00	0.25	0.75	0.750	300	2	∞	0	0	0	2.65	2.650	2.650
5	0.05	0.00	0.95	1.000	330	2	19	0.1	5.46	0.546	2.65	2.385	2.931
6	0.05	0.05	0.90	0.947	325	2	19	0.1	5.46	0.546	2.65	2.385	2.931
7	0.05	0.10	0.85	0.895	318	2	19	0.1	5.46	0.546	2.65	2.385	2.931
8	0.05	0.15	0.80	0.842	312	2	19	0.1	5.46	0.546	2.65	2.385	2.931
9	0.05	0.20	0.75	0.789	307	2	19	0.1	5.46	0.546	2.65	2.385	2.931
10	0.05	0.30	0.65	0.684	305	2	19	0.1	5.46	0.546	2.65	2.385	2.931
11	0.10	0.10	0.80	0.889	325	2	9	0.2	5.46	1.092	2.65	2.120	3.212
12	0.10	0.15	0.75	0.833	317	2	9	0.2	5.46	1.092	2.65	2.120	3.212
13	0.10	0.20	0.70	0.778	310	2	9	0.2	5.46	1.092	2.65	2.120	3.212
14	0.10	0.25	0.65	0.722	305	2	9	0.2	5.46	1.092	2.65	2.120	3.212

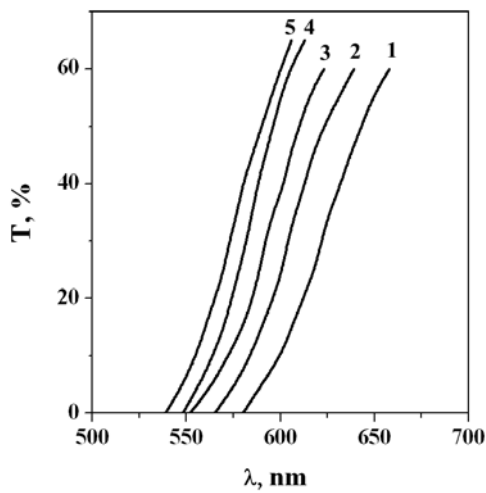
For description of the temperature dependence on the viscosity, equation (15) is used:

The investigated system is rich of chalcogen, since R>1 [R=(0.05.2+0.9.2)/(0.05.2)=19>1] - Table 3.

$$\mu(T) = \mu_0 \exp(E_\mu / kT). \quad (15)$$

It is known that at T_g the value of $\mu = 10^{13}$ dPa.s [22]. Tanaka [13] assumes that $\mu_0 = 10^0 - 10^{-5}$ dPa.s. If one puts $\mu_0 = 10^{-3}$ dPa.s the following dependence will be obtained: $T_g = 314E_\mu$

Taking into consideration the above dependence, we determined that between T_g and $\langle E \rangle$ exists a linear dependence of the type: $T_g = 314(0.004\langle E \rangle + 0.88)$. It guarantees accuracy not worse than $\pm 0.1T_g$ which is fully acceptable. The obtained value of the straight line slope (314 K/eV) is in full conformance with the theoretically expected one.



3. Optical Characteristics

For determination of the optical band gap the compositions lying on the $Cu_5Se_{95-y}S_y$ section ($0 \leq y \leq 30$) are used, since in this section the S/Se proportion varies in wide limits for the tri-component system. The thin films are deposited using vacuum-thermal evaporation ($P \approx 0.01$ Pa) on Na-Ca substrates. The film thickness varies from 0.2 to 0.4 μm . The optical transmittance spectra are recorded in the range of 200–900 nm. The dependence between the absorption edge on the film composition is shown in Fig. 2a where it can be seen that with the increase of the sulphur content, the optical edge shifts towards shorter wave lengths, i.e. the material band gap value increases – Fig. 2b.

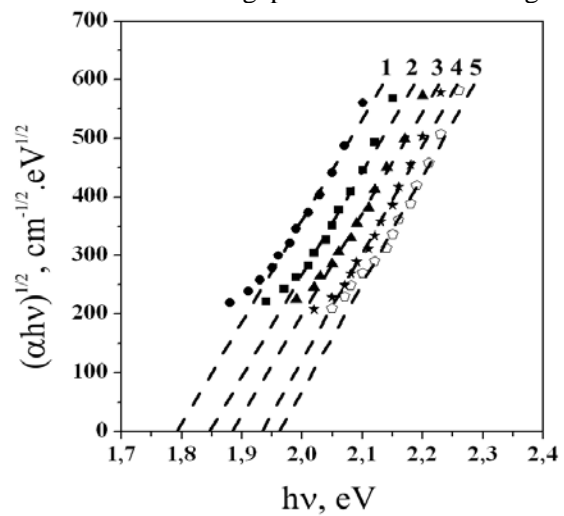


Fig. 2. Optical characteristics of thin films from the Se-S-Cu system
(1 - x = 0 %; 2 - x = 10 %; 3 - x = 15 %; 4 - x = 20 %; 5 - x = 30 %):
a – transmission spectra; b – dependence $(\alpha hv)^{1/2} = f(hv)$

Since the obtained values for α are higher than 10^4 cm^{-1} , Tauc's power law is applicable. E_g^{opt} is determined by extrapolation of the linear part of the $(\alpha hv)^{1/2} = f(hv)$ dependence at $\alpha = 0$ - Fig. 2b.

A linear dependence between the optical band gap and the S-content in the $Cu_5Se_{95-y}S_y$ glasses is observed: $E_g^{opt} = 0.0057x + 1.797$ – Fig. 3.

With the increase of the sulphur at constant Cu content, the E_g^{opt} increases, since

$$E_g^{opt}(\text{Se}) < E_g^{opt}(\text{S}) \quad (E_g^{opt}(\text{Se}) = 1.7 \div 1.9 \text{ eV} \text{ [23]})$$

$$E_g^{opt}(\text{S}) = 2.4 \text{ eV} \quad (24).$$

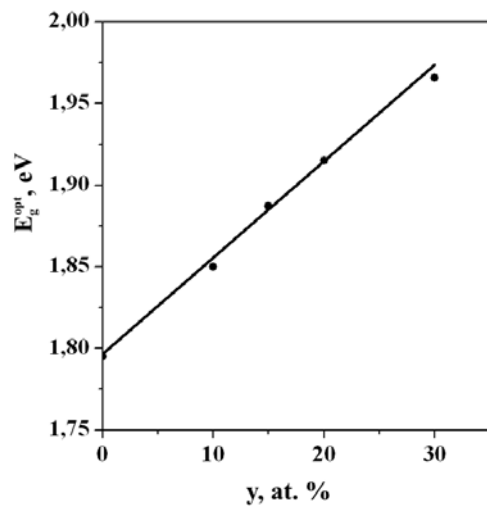


Fig. 3. Dependence of the optical band gap $\Delta E_{g,0}$ from the sulphur content in the film.

CONCLUSIONS

1. The glass-transition temperatures, density and microhardness of glasses from the Cu-S-Se system are determined. Based on the obtained results, the compactness, elasticity modulus, and the main thermo-mechanical properties of the investigated systems are calculated. A correlation between the composition and these properties is found.

2. Linear dependence between the glass-transition temperature and the overall mean bond energy is found ($T_g = 314 (0.004\langle E \rangle + 0.88)$).

3. Transmittance spectra of the synthesized glasses are recorded in the wave length range of 200-900 nm, and are used to calculate the optical band gap $\Delta E_{g,0}$. A linear dependence between $\Delta E_{g,0}$ and the sulphur content in the film is observed ($\Delta E_{g,0} = 0.0057x + 1.797$).

REFERENCES

- 1 X. Zhang, H. Ma, J. Lucas, *J. Optoelect. Adv. Mat.*, **5**, 5, 1327 (2003).
- 2 Y. Tani, Y. Shirikawa, A. Shimosaka, J. Hidaka, *J. Non-Cryst. Sol.*, **293-295**, 779 (2001).
- 3 M. Wakkad, *J. Therm. Anal. Cal.*, **63**, 533 (2001).
- 4 V. Vassilev, *J. Univ. Chem. Technol. Met.*, **41**, 3, 257 (2006).
- 5 Z.U. Borissova, Chalcogenide semiconducting glasses, Leningr. Univ., Leningrad, 1983.
- 6 M.B. Mayers, E.J. Felty, *Mater. Res. Bull.*, **2**, 7, 535 (1967).
- 7 S.S. Flaschen, A.D. Pearson, W.R. Northover, *J. Amer. Ceram. Soc.*, **43**, 274 (1960).
- 8 I.V. Alekseeva, A.A. Obrasov, Z.U. Borissova, M.D. Balmakov, *Soviet J. Glass Phys. Chem.*, **4**, 4, 411 (1978).
- 9 V. Vassilev, Z. Boncheva-Mladenova, N. Dishovsky, Glass formation in the Se-S-Cu, Proc. II Symp. Solid State Chemistry, Pardubice, Czechoslovakia, June 26-30, 1989, p. 365.
- 10 D.S. Sanditov, *Novoe v oblasti ispitaniy na mikrotverdost*, Nauka, Moskva, 1974 (in Russian).
- 11 V. Vassilev, G. Vassilev, E. Fidancevska, *Chalcogenide Letters*, **5**, 12, 415 (2008).
- 12 V. Vassilev, K. Tomova, V. Parvanova, S. Parvanov, *Mater. Chem. Phys.*, **103**, 312 (2007).
- 13 K. Tanaka, *Phys. Rev. B.*, **39**, 1270 (1989).
- 14 M. Hansen, K. Anderko, *Struktura dvojnih splavov: B 2-x*, Metalurgizdat, Moskva, 1962 (in Russian).
- 15 L. Genov, M. Maneva-Petrova, *Neorganichna himia*, part II, Nauka i izkustvo, Sofia, 1990 (in Bulgarian).
- 16 L. Tichy, H. Ticha, *J. Non-Cryst. Solids*, **189**, 141 (1995).
- 17 E.A. Rohlifing, J.J. Valentine, *J. Chem. Phys.*, **84**, 6560 (1986).
- 18 J. Drowart, S. Smoes, *J. Chem. Soc. Faraday Trans.*, **2**, 73, 1755 (1977).
- 19 S. Smoes, F. Mandy, A. Vander Auwera-Mahieu, J. Drowart, *J. Bull. Soc. Chim. Belg.*, **81**, 45 (1972).
- 20 J. Stuke, *J. Non-Cryst. Solids*, **4**, 1 (1970).
- 21 J. Tauc, *Optical properties of Solids*, F. Abeles (ed.), North-Holland, Amsterdam, 1970.
- 22 A. Feltz, *Amorphe und glasartige anorganische Festkörper*, Akademie-Verlag, Berlin, 1983.
- 23 Z. Boncheva-Mladenova, V. Vassilev, *Himia i fizikohimia na poluprovodnikovite materialii*, MON, Sofia, 1991 (in Bulgarian).
- 24 Ya.A. Ugai, *Vvedenie v himiu poluprovodnikov, Visshaia shkola*, Moskva, 1965, (in Russian).

ФИЗИКО-ХИМИЧНИ И ОПТИЧНИ СВОЙСТВА НА СЪТЪКЛА ОТ СИСТЕМАТА Cu-S-Se

В.С. Василев¹, Т.К. Христова-Василева¹, Е. Фиданчевска², М.Н. Колева³, А.И. Жеглова³

¹Катедра по металургия на цветните метали и полупроводниковите технологии, Химикотехнологичен и металургичен университет, бул. Св. Кл. Охридски, 8, 1756 София, България

²Факултет за технология и металургия, ул. Руджер Бошкович 16, Скопие, Република Македония

³Технически университет-Габрово, ул. Х. Димитър 4, 5300 Габрово, България

Постъпила на 9 октомври, 2009 г.; преработена на 22 април, 2010 г.

(Резюме)

На базата на резултатите от измерването на микротвърдостта (HV), плътността (d) и температурата на размекване (T_g) са изчислени термомеханичните характеристики обем (V_h) и енергия за образуване на микропразнина (E_h); компактността (C) и модула на еластичност (E) на стъкла от системата Cu-S-Se. По позната методика са изчислени още средните стойности на пълната енергия на връзките ($\langle E \rangle$), координационното число ($\langle Z \rangle$), енергията на средно омрежване за атом (\bar{E}_c) и тази на „останалата матрица“ ($\bar{E}_{(m)}$), средната енергия на хетерополярната връзка (E_{hb}) и степента на омрежване за атом (P). Зависимостта между T_g и $\langle E \rangle$ е линейна: $T_g = 314(0.004\langle E \rangle + 0.88)$. Оптичната ширина на забранената зона (E_g^{opt}) на свежо отложени тънки слоеве със състав $Cu_5Se_{95-y}S_y$ ($0 \leq y \leq 30$) е определена от закона на Тауц. Зависимостта $E_g^{opt}(y)$ е линейна: $E_g^{opt} = 0.0057y + 1.797$. Установени са закономерности между изследваните свойства и състава на стъклата.

CONTENTS

<i>K. Petrov, Iv. Nikolov, T. Vitanov, V. Ognyanov</i> , Pyrolysed Co-phtalocyanine as a catalyst for the oxidation of sulphur dioxide.....	189
<i>K. Semkov, S. Darakchiev</i> , Influence of small scale maldistribution in the vapor phase on the efficiency of rectification in packed columns.....	194
<i>S. Sathiyar, M. Rangarajan, S. Ramachandran</i> , An experimental study of spiral-plate heat exchanger for nitrobenzene-water two-phase system	205
<i>A. Gharib, M. Jahangir, M. Roshani, J. W. Scheeren</i> , Catalytic effective synthesis of substituted flavones and chromones using Preyssler and heteropolyacids (HPAs) as catalyst.....	210
<i>A. Gharib, M. Jahangir, M. Roshani, J. (Hans) W. Scheeren</i> , A method of catalytic synthesis of convenient thioxanthone crown ethers using Wells-Dawson $H_6[P_2W_{18}O_{62}]$ and Preyssler $H_{14}[NaP_5W_{30}O_{110}]$ heteropolyacid catalysts.....	217
<i>P. M. Ramdas Bhandarkar, K. N. Mohana</i> , Kinetic and mechanistic study of bromination of sulfanilic acid with <i>N</i> -bromosuccin-imide in alkaline medium	222
<i>M. Aydin</i> , EPR investigation of gamma-irradiated iminodiacetic and amino acid derivatives.....	232
<i>Y. Dimitrova</i> , Theoretical study of structures, stability and vibrational spectra of the hydrogen-bonded phenoxides containing strong, short hydrogen bonds	236
<i>G. Vijayalakshmi, M. Adinarayana, P. Jayaprakash Rao</i> , Kinetics of oxidation of adenosine by <i>tert</i> -butoxyl radicals – protection and repair by rosmarinic acid.....	246
<i>V.S. Vassilev, T.K. Hristova-Vasileva, E. Fidancevska, M.N. Koleva, A.I. Zheglova</i> , Physicochemical and optical properties of glasses from the Cu-S-Se system.....	253

СЪДЪРЖАНИЕ

<i>К. Петров, Ив. Николов, Т. Витанов, Д. Узун, В. Огнянов</i> , Пиролизиран Со-фталоцианин като катализатор за окислението на серен диоксид.....	193
<i>К. Семков, С. Даракчиев</i> , Отчитане влиянието на дребно-машабната неравномерност в паровата фаза при ректификация с модерни високо-ефективни ненаредени пълнежи.....	204
<i>С. Сатиян, М. Рангараджан, С. Рамачандран</i> , Експериментално изследване на работата на топлообменник със спирални пластини при дву-фазната система вода-нитробензен.....	209
<i>А. Гариб, М. Джахангир, М. Рошани, Й.(Ханс) Схеерен</i> , Ефективна синтеза на субституирани флаволи и хромони чрез Прайслерови аниони и хетеро-поликиселини като катализатори.....	216
<i>А. Гариб, М. Джахангир, М. Рошани, Й.(Ханс) Схеерен</i> , Кинетично и механистично изследване на бромирането на сулфанилова киселина с <i>N</i> -бромо-сукцинимид в алкална среда	221
<i>П.М. Рамдас Бхаданкар, К.Н Мохана</i> , Кинетично и механистично изследване на бромирането на сулфанилова киселина с <i>N</i> -бромо-сукцинимид в алкална среда	231
<i>М. Айдън</i> , Изследване на гама-облъчени имино-диоцетни и аминокиселинни производни чрез електронно-парамагнитен резонанс.....	235
<i>Й. Димитрова</i> , Теоретично изследване на структури, стабилност и вибрационни спектри на водородно-свързани феноксили, съдържащи силни, къси водородни връзки	245
<i>Г. Виджаялакшми, М. Адинараяна, П. Джаяпракаш Рао</i> , Кинетика на окислението на аденозин от <i>tert</i> -бутоксидови радикали - защита и възстановяване с розмаринова киселина.....	252
<i>В.С. Василев, Т.К. Христова-Василева, Е. Фиданчевска, М.Н. Колева, А.И. Жеглова</i> , Физико-химични и оптични свойства на стъкла от системата Cu-S-Se	259